Aus dem

Institut für Kardiovaskuläre Physiologie und Pathophysiologie im Walter-Brendel-Zentrum für Experimentelle Medizin

Institut der Ludwig-Maximilians-Universität München

Integration and interaction of cardiac progenitor cells with human failing myocardium: An ex-vivo study modeling regenerative therapy in long-term tissue culture

Dissertation
zum Erwerb des Doctor of Philosophy (Ph.D.)
an der Medizinischen Fakultät
der Ludwig-Maximilians-Universität München

vorgelegt von
Zhengwu Sun

aus
Nei Mongol / China

Jahr
2025

Mit Genehmigung der Medizinischen Fakultät der
Ludwig-Maximilians-Universität München

Erstes Gutachten:	Prof. Dr. Andreas Dendorfer
Zweites Gutachten:	Prof. Dr. Christian Schulz
Drittes Gutachten:	Priv. Doz. Dr. Sebastian Clauß
Viertes Gutachten:	Priv. Doz. Dr. Stefanie Fenske

Dekan: Prof. Dr. med. Thomas Gudermann

Tag der mündlichen Prüfung: 21.03.2025

Table of content

Abstract (English):

Background: Regenerative therapy is currently getting attention as one of the most promising treatments for heart failure. However, the survival and quality of integration of stem cell-derived cardiomyocytes with human failing myocardium is still unclear. Human cardiac progenitor cells (CPCs) have the potential to differentiate into ventricular myocytes, and their engraftment in the human failing myocardium may contribute to the enhancement of myocardial contractility and improve myocardial plasticity.

Methods: CPCs were derived from embryonic stem cells with a cardiac directed differentiation protocol and were purified with magnetic-activated cell sorting (MACS) to remove potentially remaining undifferentiated stem cells. Human myocardium was acquired from explanted hearts of transplant recipients, and was cultured as living thin slices under biomimetic conditions, enabling continuous stimulation and force measurements. CPCs were seeded on the surface of myocardial slices and were cocultured for 5 weeks. Real-time contractility was monitored and cardiac functional assessments were performed daily. Morphological maturation and integration of CPCs were characterized by no-stain labeling (eGFP and second-harmonic generation) and immunohistology. Cell-to-cell interaction and CPCs maturation in cocultured myocardial slices were investigated by single-nucleus RNA sequencing.

Results: After 5 weeks of coculture, we observed that CPCs have autonomously migrated, and were uniformly distributed into deep layers of the myocardium. They expressed morphological characteristics of cardiomyocytes (elongated and t-tubule-like structure, α-actinin positive myofibrils) during coculture. Tissue connective proteins (connexin-43 and N-cadherin) have been formed between CPC-derived cardiomyocytes and host failing cardiomyocytes. In comparison to plain myocardial slices, functional changes were detected in coculture, including enhanced force development, synchronized kinetics of contraction and intracellular calcium, more positive response to rapid pacing, and tight electrical coupling. Single-nucleus RNA sequencing demonstrates dedifferentiation-redifferentiation of host failing cardiomyocytes and advanced maturation of CPC-derived cardiomyocytes during coculture. Cell-cell communication and interaction were identified between CPC-derived and host failing cardiomyocytes, which are associated

with improved contractility and cardiac development of the failing cardiomyocytes in coculture.

Conclusion: CPCs differentiate into cardiomyocytes and self-integrate with human failing myocardium during long-term coculture. Integration promotes contractility and affects excitation-contraction coupling. Moreover, cross-talk between CPCs and host failing myocardium develops, leading to mutual adaptation and functional synchronization.

List of figures

List of tables

List of abbreviations

CPCs	Human cardiac progenitor cells
CPC-CMs	Human cardiac progenitor cells-derived cardiomyocytes
hfCMs	Host failing cardiomyocytes
FHF/SHF	First/second heart field
ISL-1	Insulin gene enhancer protein ISL-1
ESCs	Embryonic stem cells
iPSCs	Induced pluripotent stem cells
BMCCs	Biomimetic cultivation chambers
FFR	Force-frequency relationship
FDAR	Frequency-dependent acceleration of relaxation
MCR	Maximum capture rate on stimulation frequency
PPP	Post-pause potentiation on contractility
STP	Time of stimulation to peak
Tau	τ , decay constant
CD_{50}	Half time of contraction or calcium duration, also referred to as full width at half maximum (FWHM)
T_{50off}	Time of half decay (50%)
SEM	Standard error of mean
Ctrl/Cocu	Control/Coculture
2D/3D	Two/three dimension
snRNA-seq	Single-nucleus RNA sequencing
WGA	Wheat germ agglutinin
ISO	Isoprenaline
APD	Action potential duration
eGFP	Enhanced green fluorescence protein
MLC2a	Myosin Light Chain 2, atrial isoform

GEMs	Gel beads-in-emulsion
GO	Gene Ontology
GSEA	Gene set enrichment analysis
UMAP	Uniform Manifold Approximation and Projection
EVs	Extracellular vesicles
ECC	Excitation-contraction coupling
DEGs	Differentially expressed genes
Log_2FC	Log_2Fold change
SCENIC	Single-cell regulatory network inference and clustering
TFs	Transcription factors
GRN	Gene regulatory network
KIF26B	Kinesin Family Member 26B
SLIT3	Slit Guidance Ligand 3
RYR2	Ryanodine Receptor 2
TTN	Titin
XIST	X Inactive Specific Transcript
UTY	Ubiquitously Transcribed Tetratricopeptide Repeat Containing, Y-Linked
CACNA1C/A2D3/A1G	Calcium Voltage-Gated Channel Subunit Alpha1 C/ Alpha2 Delta 3/ Alpha1 G (T-type)
CACNA2D1/B2	Calcium Voltage-Gated Channel Auxiliary Subunit Alpha2delta 1/ Beta 2
MYL2/4/7	Myosin Light Chain 2/4/7
MYH6/7	Myosin Heavy Chain 6/7
HCN4	Hyperpolarization Activated Cyclic Nucleotide Gated Potassium Channel 4
PLN	Phospholamban
ACTC1	Actin Alpha Cardiac Muscle 1
TNNT2	Troponin T2, Cardiac Type

TNNI1	Troponin I1
TPM1	Tropomyosin 1 (Alpha)
MYBPC3	Myosin Binding Protein C3
ATP2A2	ATPase Sarcoplasmic/Endoplasmic Reticulum Ca2+ Transporting 2 (SERCA2)
CAMK2D	Calcium/Calmodulin Dependent Protein Kinase II Delta
SLC8A1	Solute Carrier Family 8 Member A1 (Sodium/Calcium Exchanger 1)
CDH2	Cadherin 2 (N-cadherin)
NCAM1	Neural Cell Adhesion Molecule 1
PTPRM	Protein Tyrosine Phosphatase Receptor Type M
SEMA3C	Semaphorin 3C
NRP1	Neuropilin 1
PLXNA4	Plexin A4
NRG3	Neuregulin 3
ERBB4	Erb-B2 Receptor Tyrosine Kinase 4
BMP5	Bone Morphogenetic Protein 5
BMPR1A/2	Bone Morphogenetic Protein Receptor Type 1A/2
MEF2A/2C	Myocyte Enhancer Factor 2A/2C
LAMA2	Laminin Subunit Alpha 2
ZFPM2	Zinc Finger Protein, FOG Family Member 2
SMAD2/5	SMAD Family Member 2/5
FHL2	Four and a Half LIM Domains 2
SCN5A	Sodium Voltage-Gated Channel Alpha Subunit 5
CORIN	Corin, Cardiac Prohormone
G0S2	G0/G1 Switch 2
TBX5/20	T-Box Transcription Factor 5/20
FGF12	Fibroblast Growth Factor 12

MYLK3	Myosin Light Chain Kinase 3
PDE4D	Phosphodiesterase 4D
NFIA/NFIB	Nuclear Factor IA/IB
ZBTB20	Zinc Finger and BTB Domain Containing 20
GATA6	GATA Binding Protein 6
FOXP1	Forkhead Box P1
IGF1R	Insulin Like Growth Factor 1 Receptor

1. Introduction

1.1 Background

Heart failure is the end-stage of cardiovascular disease and remains one of the predominant causes of mortality and disabilities worldwide [1, 2]. However, current treatments primarily focus on symptom management and fail to fundamentally address myocardial dysfunction. Although existing treatment strategies alleviate symptoms by improving circulation and assisting cardiac pumping, pharmacological therapies and mechanical assist devices (e.g., left ventricular assist devices, LVADs) rarely achieve long-term improvements in cardiac function, and require lifelong maintenance [3, 4]. Prospective heart transplants have also failed to be widespread due to shortage of matching donor hearts, immuno-rejection and high susceptibility to infections [5, 6]. Thus, patients with severe heart failure have limited benefit from pharmacological therapies, mechanical assist devices and transplantation.

Restricted self-repair and limited proliferative capacity of adult myocardium will direct any myocardial injury to irreversible fibrosis and ventricular remodeling [7, 8]. These chronic alterations of structure and function of the myocardium present a major challenge in the treatment of heart failure [9, 10]. As alternative strategies to conventional treatments are explored, stem cell transplantation is an attractive option, which promises to replace damaged host failing cardiomyocytes and improve cardiac function through intercellular communication. Despite the regenerative treatment for heart failure being in its infancy over the past few decades, significant progress has been made in understanding the molecular mechanisms of cardiac regeneration [11]. Exogenous myocardial regeneration derived from embryonic stem cells (ESCs) or induced pluripotent stem cells (iPSCs) has shown great potential for the treatment of heart failure in numerous experimental animal models and several clinical trials [12, 13].

1.2 Regenerative therapeutic potential of cardiac progenitor cells (CPCs) in heart failure

As a highly specialized organ, the functional heart is composed of various cardiomyocyte and non-cardiomyocyte lineages. These cells have been identified

to originate from three types of precursor embryonic cardiac progenitor cell populations: cardiogenic mesoderm cells, proepicardium, and cardiac neural crest cells. Cardiogenic mesoderm cells give rise to the first heart field (FHF, comprising left ventricle and atria) and the second heart field (SHF, comprising right ventricle and outflow tract), eventually differentiating into principal cell populations of heart. These include cardiomyocytes, vascular smooth muscle cells, arterial and venous endothelial cells, fibroblasts, and cells of cardiac conduction system [14]. Among the key factors in this differentiation process, ISL-1 emerges as one of the earliest and most crucial transcription factors, serving as a critical marker of cardiac lineage progenitor cells [15]. Unlike progenitor cells of FHF, which are restricted to early stages of heart development, ISL-1$^+$ cardiac progenitor cells of SHF exhibit a broader spectrum of lineage differentiation capabilities, including the potential to differentiate into primary types of cardiomyocytes (ventricular and atrial myocytes, and pacemaker cells), and have the capability of targeted migration prior to differentiation [16]. In this stage, cells will be defined as cardiac progenitor cells (CPCs) and are utilized in cardiac regenerative therapies. Currently, CPCs are predominantly derived from ESCs and iPSCs. ESC-derived CPCs typically manifest superior differentiation efficiency and genomic stability compared to iPSC-derived CPCs, demonstrating higher differentiation potential and functional maturity, which facilitates more effective integration with host myocardium [17, 18].

Taking advantage of high differentiation plasticity of CPCs in human heart development, CPCs are considered one of the most promising stem cells for cardiac regeneration and repair in heart failure. The current hypothesis is that cells differentiated along the cardiac lineage are more effective than non-cardiac lineage cells in the structural repair of failing myocardium and preventing severe arrhythmias [19, 20]. Compared to already differentiated cardiomyocytes, committed cardiac lineage progenitor cells still retain a limited proliferative activity, and have extensive differentiation plasticity and intrinsic properties of directed migration and autonomous integration without extra matrix or support. CPCs have already partially differentiated in the cardiac lineage, making them more efficient and specific in differentiating into functional cardiomyocytes. Unlike pluripotent stem cells with high differentiation potential, cardiac-committed CPCs have a lower tumorigenic risk and offer greater safety for clinical applications. Furthermore, CPCs

naturally exist in cardiac tissue and possess inherent reparative abilities, they are more likely to survive, integrate, and function within the myocardial microenvironment [21].

1.3 Advances of CPCs-based therapy for heart failure

To date, the first clinical trial of ESC-derived CPCs (known as ESCORT) reported on the feasibility and safety of cell patch transplantation in the patient with severe heart failure. CPCs were embedded in a fibrin scaffold to create a cellular patch, which was then applied to the infarcted region of patient's heart. The patient showed improvement in symptoms, and there were no occurrences of arrhythmias, tumor formation, or adverse events related to immunosuppression [22, 23]. Compared to solid tissue patches, the intramyocardial injection of CPCs suspension may constitute a superior approach for stem cell therapy, as the capacity of targeted migration may enable CPCs to improve tissue integration. CPCs have the potential to differentiate into ventricular myocytes, to target migration to specific requirements, and to seamlessly integrate with host heart tissue. Injections of CPCs have been shown to improve cardiac functions in hearts of mouse and pigs [24, 25].

However, the mechanisms of CPCs-based therapy remain controversial, with two potential explanations currently proposed. The direct mechanism suggests that CPCs integrate into host myocardium through electromechanical coupling and contribute to contractile force. ESC-derived CPCs have shown the potential to differentiate into functional cardiomyocytes and to integrate with host cardiac tissue in multiple preclinical studies [26, 27]. These CPCs not only contribute to the repair of myocardial structure, but also support functional recovery by improving myocardial contractility and electrical conduction [28]. However, the low survival of CPCs after in-vivo myocardial injection raised doubts about the contribution of CPC-derived cardiomyocytes (CPC-CMs) to overall contractile force. Additionally, retention and immune rejection after stem cell transplantation into the host myocardium affect therapeutic effectiveness of CPCs-based therapy [29, 30].

In recent years, evidence has accumulated that cardio-protective effects of CPCs are mainly mediated through paracrine secretion, which stimulates the release of cytokines related to endogenous regeneration and repair pathways,

thereby alleviating myocardial damage and promoting myocardial repair [31-33]. As carriers of cytokines for intercellular communication, the significance of extracellular vesicles (EVs) has been proposed. These particles comprise cells-secreted lipid bilayer nanoparticles, such as exosomes and micro-vesicles, which present extracellular transport regulatory factors (RNA, proteins, and lipids) to recipient cells, and are thus involved in intercellular communication and multiple pathophysiological processes [34, 35]. Several animal studies have indicated that CPCs-released EVs improve cardiac function and reduce fibrosis formation in myocardial ischemia-reperfusion and infarction and even heart failure [31, 33, 36, 37]. It may be related to EVs-carried miRNAs and proteins modulating distinct cardio-protective pathways to induce cardiomyocyte proliferation, to inhibit cardiomyocyte apoptosis, to stimulate angiogenesis, and to prevent myocardial fibrosis in chronic heart failure [38-40].

1.4 Importance of CPCs integration and communication with host myocardium for cardiac regeneration

CPCs may achieve short-term improvements of cardiac function by secretion of paracrine factors, but the attenuation of these effects due to CPCs maturation within host myocardium is inevitable [41, 42]. Long-term improvements of cardiac function after transplantation depend on the efficient differentiation and integration of CPC-CMs in host myocardium. Structural and functional integration of CPCs with host myocardium, including cellular adhesion, synchronous contraction, effective electromechanical coupling, and consistent signal transduction, is a crucial aspect of myocardial repair. However, due to limitations in transplantation techniques, the actual integration of CPCs with the failing host myocardium remains unclear.

Distinct from differentiated ESC-derived cardiomyocytes, the more immature CPCs are capable of directed migration and eventual specific homing prior to tissue integration [25]. It may be essential for stem cell therapy that supportive cells will be targeted to pathological locations of necrosis, fibrosis, or inflammation of the diseased heart. Homing to injured areas, such as inflammation and fibrosis, is a complex process that may depend on the coordination and interaction of chemokines and intercellular signal transduction-related factors in host

myocardial tissue. This directed migration of CPCs towards inflammation and fibrosis contributes to the functional recovery of injured myocardium, resulting in prevention of heart failure progression [25, 43]. Moreover, the regenerative potential of CPCs depends not only on their intrinsic properties, but also on the functional influence of the pathological microenvironment within host myocardium, including mechanical loading, extracellular matrix stiffness and topography, electrical stimulation, both direct and indirect cellular communication with host myocardium [44, 45]. Tissue integration of CPCs as exogenous xenobiotic is considered to be a prerequisite that coordinate their activity in relation to myocardial homeostasis and injury repair in heart disease, as previously demonstrated [46]. Integrin-involved adhesion between donor stem cells and host extracellular matrix facilitates the provision of mechanical stability [47], whereas the formation of gap junctions (connexin-43) between them is particularly critical for electromechanical coupling and functional coordination, which were observed in animal transplantations [48, 49]. Therefore, the establishment of cellular adhesion and subsequent integration is a critical determinant of the successful incorporation of donor CPCs into the host failing myocardium, signifying effective structural and functional connectivity.

Apart from direct cell-to-cell contacts between CPCs and host myocardium, crosstalk and communication are regarded to facilitate the establishment of symbiotic relationship, which is mainly mediated by EVs through remote paracrine signaling [50, 51]. CPCs are isolated and are introduced to the communication network in the pathophysiological microenvironment of failing myocardium. This bilateral impact involves CPCs differentiation and myocardial repair. Despite multiple interventions were proven to promote stem cell differentiation and maturation, such as long-term culture, electrical stimulation, mechanical stimulation, chemical induction, coculture, 3D culture, and cell-substrate interactions [52], CPCs maturation in authentic human failing myocardium has not yet been fully elucidated. In addition, the characteristic EVs secreted by CPCs during differentiation and maturation may also have the potential to reverse the remodeling of failing myocardium. Whether the therapeutic potential of CPCs against heart failure is predominantly related to replacement and contractile support of diseased cardiomyocytes, or to a recovery of the native myocardium under the influence of secreted factors, still needs to be clarified.

1.5 Objective

Due to the species differences between animals and human, and the challenging reproducibility of heart failure, clinical trials involving stem cell therapy for heart failure often fail to replicate the significant successes achieved in animal models of heart failure [53, 54]. Animal hearts may not accurately simulate the pathophysiology of failing hearts in patients, due to differences in intrinsic heart rates, epigenome and transcriptome, as well as distinct intramyocardial cell communication in native niche environment. Moreover, human heart failure is caused by a complex cascade reaction due to progressive tissue ischemia and hypoxia, as well as inflammatory myocardial fibrosis, which is difficult to simulate in animal models. We recently reported that long-term cultivated human failing myocardium under well-developed biomimetic condition preserves most structural and functional characteristics of myocardium ex vivo [55]. Such ex-vivo models provide the feasibility of transplanting CPCs into human failing myocardium. Biomimetic culture of myocardial slices enables survival for months, even a year, and maintains the entire morphology and gene expression of human myocardium.

Herein, we inoculated CPCs onto host human failing myocardial slices, and cocultured them for several weeks. Long-term coculture of CPCs and host myocardial slices facilitates the observation of CPCs migration, integration, survival, and maintenance in myocardial tissue. Compared to in-vivo animal models and in-vitro cell line models, more comprehensive cardiac functions can be assessed in our 3D ex-vivo cultured myocardial tissue slices, such as real-time contractility, force-frequency relationships, refractory period, post-pause potentiation, calcium handling.

The present study aims to explore the following issues regarding CPCs-based cardiac regeneration therapy in heart failure:

(1) To validate that CPCs migrate, differentiate, mature, and integrate with host human failing myocardium.

(2) To demonstrate that CPCs achieve functional coupling and synchronization with host myocardium.

(3) To reveal potential mechanisms permitting structural and functional integration of CPCs and host myocardium.

2. Material and Methods

2.1 Materials

2.1.1 Biological materials

Samples of human left-ventricular failing myocardium were obtained as about 3 cm x 3 cm large transmural specimen taken from the explanted hearts of heart transplant recipients on the occasion of heart transplantation. Tissues were acquired at the Clinic of Cardiac Surgery at the University Hospital of the Ludwig-Maximilians-University Munich, Germany, and at the Clinic of Thoracic and Cardiovascular Surgery of the Heart and Diabetes Center of Nordrhein-Westfalen, Bad Oeynhausen, Germany. The patients gave informed consent to the collection and scientific use of their heart tissue. Patients' characteristics are detailed in Table 1. The study has been approved by the ethics commission of the Medical Faculty of the Ludwig-Maximilians-University Munich and the ethics review committee of the Ruhr-University Bochum in accordance with the ethical standards outlined in the Declaration of Helsinki and the Data Protection Act. Upon excision, myocardial specimen was immediately transferred to cold cardioplegic slicing buffer (composition shown in Table 2), and were kept and eventually transported in this buffer at 4 °C for no more than 36 hours.

Cardiac progenitor cells (CPCs), derived from the human embryonic stem cell line SA121-eGFP, were provided by AstraZeneca Inc., Gothenburg, Sweden. The use of ESCs complies with Swedish laws and regulations. CPCs are not subjected to the German Law for the "Use and Import of Human Embryonal Stem Cells" since they have lost their pluripotent properties.

2.1.2 Culture medium and supplements

- M199 medium (ThermoFisher, Cat# 31150-022)
- ITS (Insulin-Transferrin-Selenium, ThermoFisher, Cat# 41400045)
- Pen/Strep (Penicillin &Streptomycin solution, Sigma-Aldrich, Cat# P0781)
- β-ME (β-mercaptoethanol, Applichem, Cat# A1108-0100)
- Hydrocortisone (Sigma-Aldrich, Cat# H0888)
- B-27 (+ insulin, ThermoFisher, Cat# 17504044)
- Vitamin B12 (Sigma-Aldrich, Cat# V6629)

Table 1. Patient characteristics

Age	Sex	BMI	LVEDD	Diabetes	LVAD	Diagnosis	EF
42	M	27.5	65 mm	No	No	DCM	30%
65	M	21.3	72 mm	No	No	DCM	25%
52	M	22.6	51 mm	No	No	ICM	20%
46	M	32.4	94 mm	No	Yes	DCM	10%
68	M	24.6	NDR	No	No	ICM	15%
55	F	25.7	69 mm	No	No	DCM	24%
35	M	23.1	50 mm	No	No	RCM	45%
48	F	20.6	NDR	No	No	DCM	35%
64	M	23.7	81 mm	Yes	No	ICM	20%
23	F	25..9	44 mm	No	No	HCM	60%
65	M	28.4	86 mm	No	No	ICM	21%
51	M	24.7	NDR	No	Yes	DCM	10%
19	M	20.1	76 mm	No	No	DCM	18%
64	M	26.8	60 mm	No	No	DCM	NDR
58	M	24.9	66 mm	No	No	ICM	21%
42	M	28.4	79 mm	No	No	DCM	15%
22	M	19.7	74 mm	No	No	DCM	20%
58	M	24.5	58 mm	No	No	ICM	20%
64	M	29.7	61 mm	No	Yes	ICM	25%
39	F	23.9	NDR	No	No	ICM	15%

See next page for footnotes of Table 1.

Footnotes of Table 1: M = male, F = female, BMI = body mass index, LVEDD = left ventricular end-diastolic diameter, NDR = no documentation in records, LVAD = left ventricular assist device, DCM = dilated cardiomyopathy, RCM = restrictive cardiomyopathy, ICM = ischemic cardiomyopathy, HCM = hypertrophic cardiomyopathy (non-obstructive), EF = ejection fraction.

Table 2. Formulation of cardioplegic slicing buffer

Substances	Amount (g/L)	Final concentration (mM)
NaCl	8	136
KCl	0.4	5.4
$MgCl_2 \bullet H_2O$	0.2	1
$NaH_2PO_4 \bullet H_2O$	0.046	0.33
Glucose • H_2O	2	10
$CaCl_2 \bullet 2H_2O$	0.13	0.9
BDM	3	30
HEPES	1.2	5
Add the substances listed above and dissolve them in ultrapure water. Adjust HEPES with 1M NaOH to pH 7.4, then filter and store at 4°C.		

BDM = 2,3-Butanedione, HEPES = 4-(2-hydroxyethyl)-1-piperazineethanesulfonic acid.

Table 3. Formulations of custom-made culture media

Name of culture medium	Supplements	Concentration
Culture medium for myocardial slices	M199 medium	50 mL
	ITS	1%
	Pen/Strep	1%
	β-ME	50 µM
	Hydrocortisone	20 nM
Coculture medium for myocardial slices and CPCs	M199 medium	50 mL
	B-27	2%
	Pen/Strep	1%
	Vitamin B12	3.7 nM

ITS = Insulin-Transferrin-Selenium, Pen/Strep = Penicillin-Streptomycin, β-ME = Beta-Mercaptoethanol.

Table 4. Formulations of cell nuclei isolation buffers

Name of buffer	Supplements	Concentration
Homogenization buffer in RNase-free water	Sucrose	250 mM
	KCl	25 mM
	$MgCl_2$	5 mM
	Tris-HCl	10 mM
	DTT	1 µM
	Protease inhibitor	1× dilution
	RNaseIn	0.4 U/µL
	SUPERaseIn	0.2 U/µL
	Triton X-100	0.1%
Storage buffer	PBS	1× dilution
	BSA	4%
	Protector RNaseIn	0.2 U/µL

DTT = Dithiothreitol, PBS = Phosphate-Buffered Saline, BSA = Bovine Serum Albumin.

2.1.3 Chemical reagents and antibodies

Chemical reagents

- HBSS (Hank's balanced salt solution, Ludwig-Maximilians-University Munich)
- PFA (paraformaldehyde, Sigma-Aldrich, Cat# 16005)
- OCT Compound (Sakura, Cat# 4583)
- Triton X-100 (AppliChem, Cat# A4975)
- BSA (bovine serum albumin, Sigma, Cat# A2153)
- DAPI (4',6-Diamidino-2-Phenylindole, Thermo Fisher, Cat# 62248)
- WGA (wheat Germ agglutinin, Biotium, Cat# 29024-1)
- Histoacryl (B/Braun, Cat# 9381104)
- Mounting medium (ibidi, Cat# 50001)
- Type F Immersion liquid (Leica, Cat# 11513859)
- Nail polish (Amazon, not applicable)
- Low-melt agarose (4%, ROTH, Cat# 6351.2)
- NucBlue Live Ready Probes reagent (Hoechst 33342, ThermoFisher, Cat# R37605)
- Chromium Single Cell Kits (v3, 10X Genomics, Cat# 1000075)
- Bioanalyzer High Sensitivity DNA Analysis reagents (Agilent, Cat# 5067-4626)
- Fluo-8L AM (AAT Bioquest, Cat# 21096)
- BDM (2,3-Butanedione, Sigma-Aldrich, Cat# B0753)
- ISO (isoprenaline, Sigma-Aldrich, Cat# I5627)
- RevitaCell (ThermoFisher, Cat# A26445-01)
- Geltrex (ThermoFisher, Cat# A14132-02)
- DMEM/F12 medium (ThermoFisher, Cat# 11320-033)

Primary antibodies

- GFP (chicken polyclonal, Abcam, Cat# ab1390)
- α-actinin (mouse monoclonal, Sigma, Cat# A7811)
- α-actinin (rabbit monoclonal, Thermo Fisher, Cat# 701914)
- MLC2v (myosin light chain 2v, ventricular marker, rabbit polyclonal, Proteintech, Cat# 10906-1-AP)
- MLC2a (myosin light chain 2a, atrial marker, mouse monoclonal, Synaptic Systems, Cat# 311011)
- N-cadherin (mouse monoclonal, BD Bioscience, Cat# BD-PH 610921)

- Connexin-43 (rabbit polyclonal, Sigma-Aldrich, Cat# C6219)

Secondary antibodies

- Donkey anti chicken Alexa Fluor 488 (Jackson Immune Research, Cat# 703-545-155)
- Goat anti chicken Alexa Fluor 488 (Invitrogen, Cat# A32931)
- Goat anti-mouse IgG Alexa 546 (Invitrogen, Cat# A11030)
- Goat anti-rabbit IgG Alexa 546 (Invitrogen, Cat# A11010)
- Goat anti-mouse IgG Alexa 633 (Invitrogen, Cat# A21052)
- Goat anti-rabbit IgG Alexa 633 (Invitrogen, Cat# A21070)

2.1.4 Equipment and software

Equipment

- Vibratome (VT1200S, Leica Biosystems, Germany)
- 15-L circulating water bath (Thermomix BU coupled to Frigomix U, B. Braun Biotech International, Germany)
- Razor blade (Gillette Silver Blue, Manufacturer reference: 7900086515371, Gillette)
- Small plastic triangles cut from 0.125 mm-thick polyethylene-tetraphalate (InVitroSys GmbH, Germany)
- Biomimetic cultivation chambers (BMCCs, InVitroSys GmbH, Germany)
- MyoDish biomimetic cultivation system (MD-01-01, InVitroSys GmbH, Germany)
- Tweezer (ZACRO, Cat# WSD-10, customized lateral bend of 45 degrees for slice clamping)
- Scalpel (Feather, Cat# 02.001.30.020)
- Customized four-needles fixation mold (custom-made)
- Cryomold (Sakura, Cat# 4557)
- 2 mL safe-lock tube (Eppendorf, Cat# 0030120094)
- Aluminum block and stick (custom-made)
- Parafilm (American Can Company, Cat# CT. 06830)
- Microscope slides (Epredia, Cat# 32550T)
- Round cover slides (⌀ 13 mm, Marienfeld, Cat# 0111530; ⌀ 15 mm, Marienfeld, Cat# 0111550)
- Multi-Shaker (PSU-20, SIA Biosan)

- Cryotome (NX70, Fisher Scientific GmbH)
- Microscope system with one/confocal and two-photon excitation (SP8 WLL DIVE Falcon, Leica, Germany)
- Confocal microscope (SP5, Leica, Germany)
- 7 ml glass Dounce tissue grinder kit (D8938, Merck, Germany)
- Cell strainer, 40 µm mesh (Falcon, 352340, Corning, USA)
- FACS (fluorescence-activated cell sorting, Influx, XDP, FACSAria, BD Biosciences, USA)
- Countess II Automated Cell Counter (AMQAX1000, Life Technologies, USA)
- Chromium Controller (GCG-SR-1, 10X Genomics, USA)
- Bioanalyzer (G2939BA, Agilent, USA)
- HiSeq 4000 Sequencing System (Illumina, USA)
- Inverted microscope (Axiovert 35, 20x objective, excitation 488 nm, Zeiss, Germany)
- High-speed camera (VLXT-06M.I, Baumer, Germany)
- Wavelength-selective image splitter (Optosplit II, Cairn Research, UK) equipped with emission filter (525/30 nm, AHF GmbH, Germany)
- Dichroic mirror (568 nm, AHF GmbH, Germany)

Software

- GraphPad Prism (v9.5, GraphPad Software, USA)
- OriginPro (v2021, OriginLab Corporation, USA)
- MyoDish Registration (v1.2, InVitroSys GmbH, Germany)
- Imaging-specific MyoDish (v2.0.7969.26226, InVitroSys GmbH, Germany)
- MyoDish Data File Converter (v1.1, InVitroSys GmbH, Germany)
- WinEDR (v3.9.7, University of Strathclyde, Scotland)
- LabChart Reader (v8.1, AD Instruments, Australia)
- Matlab (vR2021a, MathWorks, USA)
- Matlab-based MyoDish analysis scripts (v1.0, InVitroSys GmbH, Germany)
- ImageJ (v1.48, Java v1.6.0.31, National Institutes of Health, USA)
- Leica Application Suite X (LAS X, v3.5.7.23225, Leica Microsystems CMS GmbH, Germany)
- Baumer Camera Explorer (v3.3.0, Baumer, Switzerland)
- Cell Ranger (v6.1, 10x Genomics Inc., USA)
- bcl2fastq (v2.20, Illumina, USA)

- R (v4.3.3, R Core Team, USA)
- Rstudio (v2023.12.1+402, Rstudio, PBC, USA)
- Python (v3.10.12, Python Software Foundation, USA)
- Anaconda (v2023.03, Anaconda, USA)
- Jupyter Notebook (v6.5.5, NumFOCUS, USA)

2.2 Methods

2.2.1 Acquisition and cultivation of human failing myocardial slices

Specimen of failing myocardium were freshly obtained after transplantation, and were stored at 4 °C in slicing buffer for 1-36 hours. After transport to the laboratory, the tissue was placed in a petri dish containing slicing buffer at 4 °C. Subsequently, myocardial trabeculae, endocardium, epicardium, and adipose tissue were removed. The myocardium was immobilized by a custom-made mold (8 mm × 8 mm in length and width) with four needles, and was cut along the edges of the mold with a scalpel. The resulting tissue block was transferred to a 35 mm culture dish, and was embedded in 4% low-melt agarose applied at 37 °C. After solidification of the agarose at 4 °C, the embedded tissue was glued to the metal base of the vibratome with 50 µL of Histoacryl glue, and was then transferred to the cooling tray of the vibratome which has been filled with slicing buffer at 4 °C. Vibratome parameters were set for precise slicing (vibration amplitude 1.5 mm, feed rate 0.07 mm/s, slice thickness 300 µm). Upon completion of slicing, agarose around myocardial slices was detached, and myocardial slices were trimmed to a width of 7 mm. Two plastic triangles, each dipped in 1.2 µL of Histoacryl glue, were attached to the two ends of each tissue slice, so that a linear orientation of myocardial fibers was obtained between the triangles. Triangle-attached slices were gripped with customized tweezers, and were mounted in BMCCs which have been prefilled with 37 °C culture medium (composition detailed in Table 3). The BMCCs provided stimulation electrodes, magnetic force sensor, and mechanical linear drive for preload adjustment. They were transferred to a thermostatic incubator (37 °C, 5% CO_2, 20% O_2, 80% humidity), and the mechanical preload of slices was adjusted to 1000 µN. Cultivation parameters were set in the MyoDish software: electrical stimulation with bipolar impulses of 3 ms duration and 50 mA current at 0.5 Hz frequency; adequate oxygenation of

the medium was maintained by shaking the culture platform at 60 rpm with a tilt angle of 15°. Contraction force was monitored in real time, and recording files were automatically saved for subsequent analyses. The developed force of myocardial slices is linearly correlated to the mechanical stress based on the uniform cross-section (width 7 mm × thickness 300 µm) of myocardial slices (1 µN corresponds to 0.48 µN/mm^2).

To avoid the potential impact of hypercontracture, preload was re-adjusted 2 h after assembling myocardial slices into BMCCs, as well as the next 3 occasions of medium exchange. Two thirds of culture medium were exchanged every other day. After 2-3 weeks of stabilization, myocardial slices were used for coculture with CPCs (Figure 1 & Figure 2).

2.2.2 CPCs seeding and coculture with human myocardial slices

To ensure efficient transplantation, differentiation, and long-term coculture of CPCs with slices of native myocardium, an optimized protocol was developed. CPCs are usually generated and maintained in RPMI + B27 (+ insulin) medium, whereas myocardial slices are generally cultured in customized M199 medium. Based on the above media, coculture medium was reconstituted to ensure the viability of CPCs and myocardial slices. We compared the ingredients and concentrations of the above two media, and customized an optimized coculture medium that contains sufficient components for CPCs and myocardial slices (see Table 3 for composition).

For the pre-adaptation of myocardial slices, their culture medium was replaced with coculture medium a week before CPCs seeding. For optimized seeding, myocardial slices were transferred to a custom seeding module. CPCs suspension (500,000 cells/mL) was applied in a total volume of 500 µL coculture medium, supplemented with RevitaCell (1:100). After 4-6 h incubation in the seeding module, CPCs-seeded slices were returned to BMCCs, and were incubated with electrical stimulation and RevitaCell, but without preload, for 18-20 h. Subsequently, preload was re-adjusted to 1000 µN and RevitaCell was removed from the coculture medium. Culture of CPCs-attached myocardial slices was continued for 5 weeks (Figure 3).

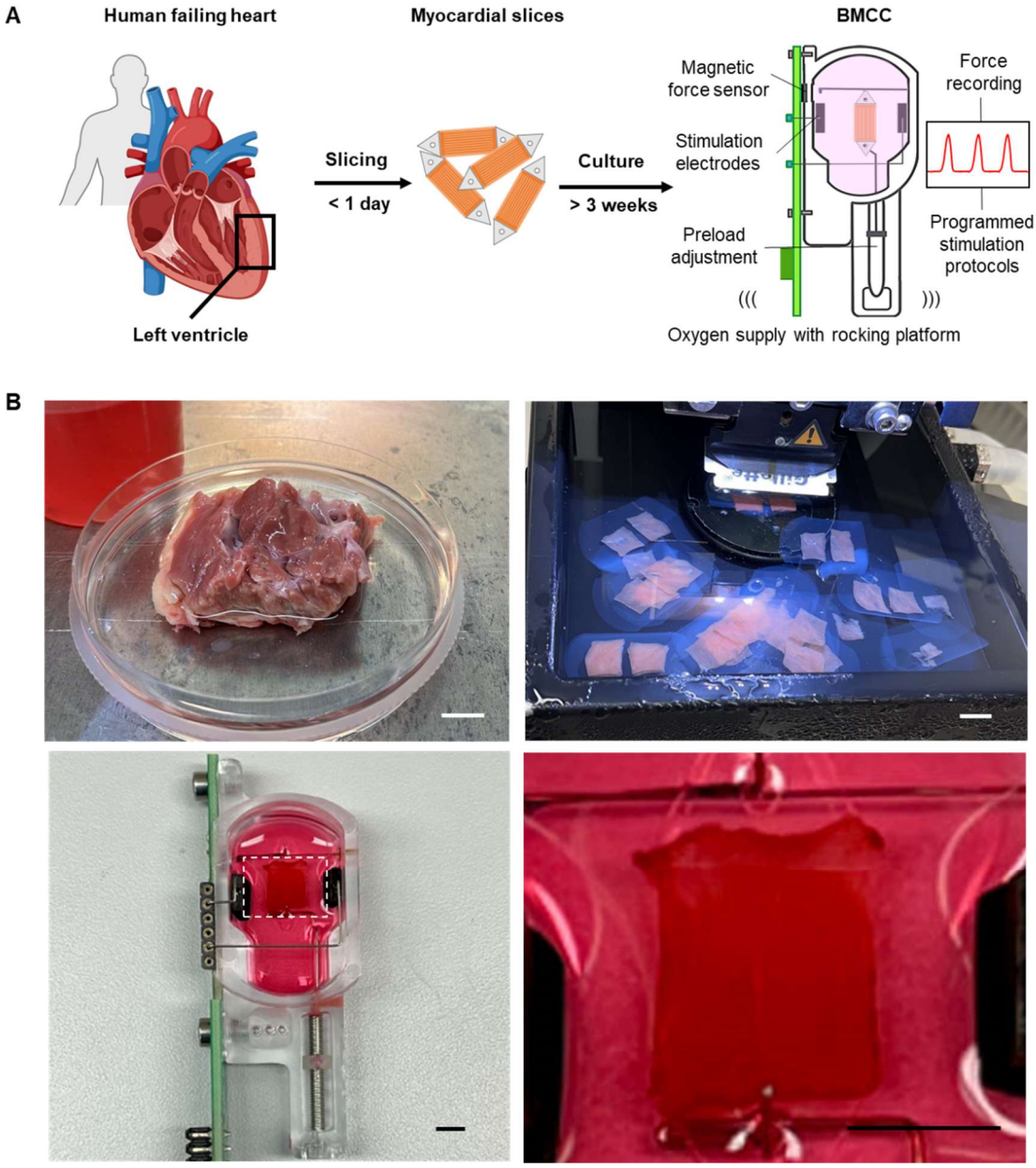

Figure 1. Preparation of human myocardial slices mounted in biomimetic culture chambers (BMCCs).

(A) Schematic of preparation and long-term culture of myocardial slices from failing left ventricular myocardium of patients. (B) Real-life images of human failing myocardium specimen (left ventricle), myocardium slicing in vibratome, myocardial slice mounting in BMCC and slice image at higher magnification. White scale bar 10 mm, black scale bar 5 mm.

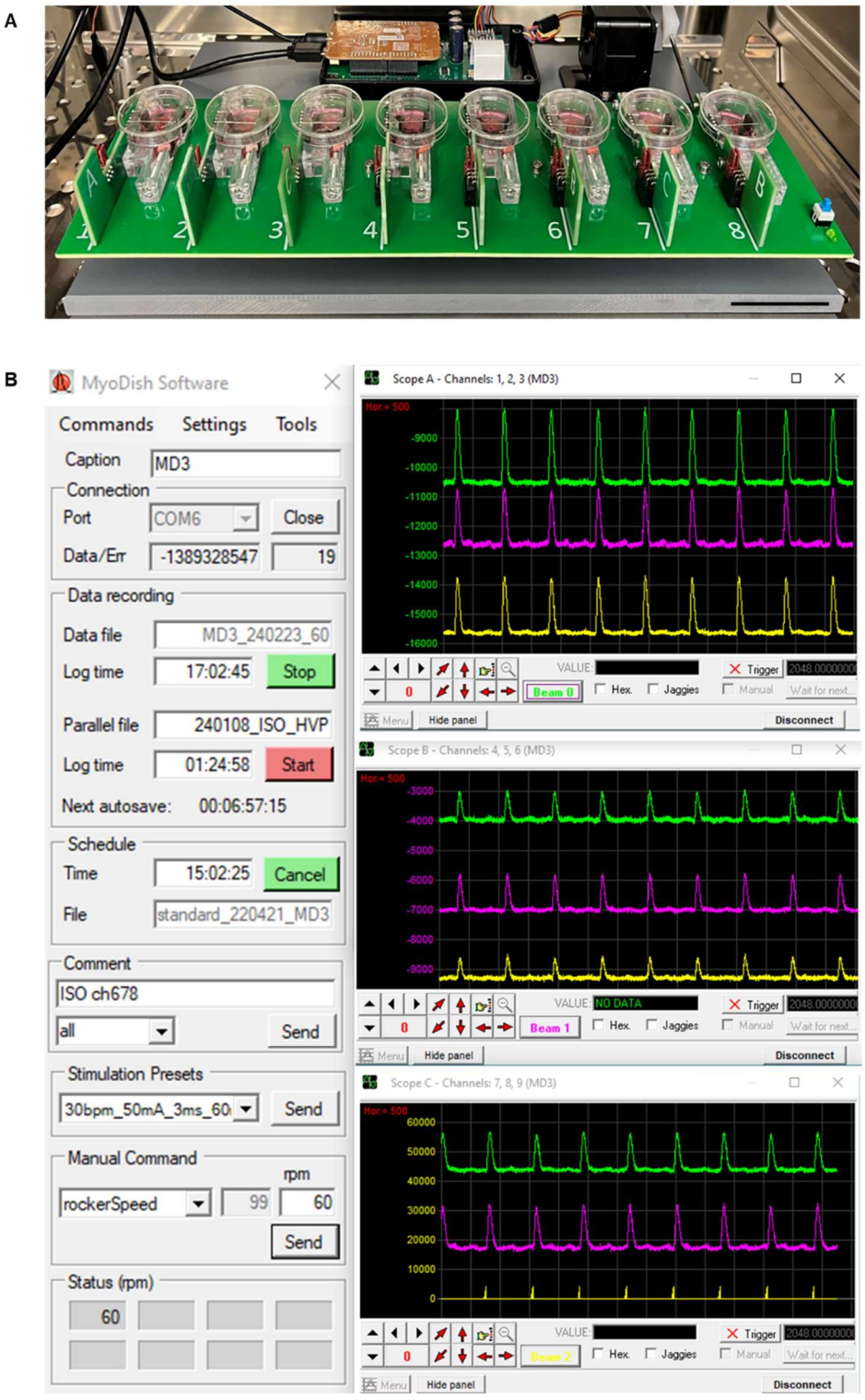

Figure 2. Long-term culture of human myocardial slices in a biomimetic culture system providing continuous stimulation and contractility recording.

(A) Biomimetic culture system with 8 biomimetic culture chambers, scale bar 50 mm. (B) MyoDish software for force monitoring and stimulation control. Recordings are shown at 0.5 Hz stimulation frequency (2 seconds per beat), and with a sensitivity of 1 µN per unit.

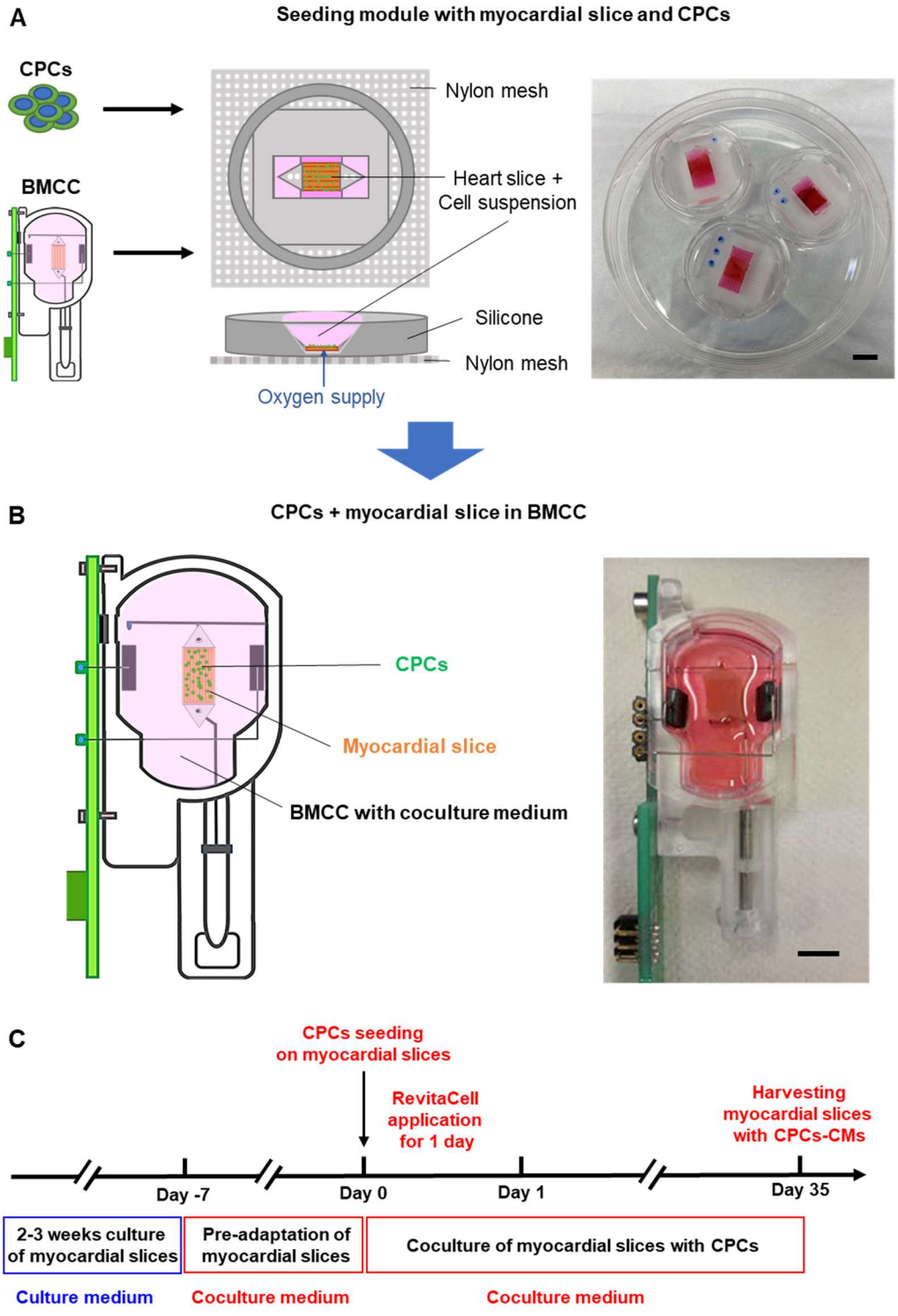

Figure 3. Procedure of CPCs seeding and coculture with myocardial slices.

(A) Engraftment of CPCs on cultured human failing myocardial slices in customized seeding module. BMCC = biomimetic culture chamber. Scale bar 10 mm. (B) Long-term coculture of myocardial slices with CPCs in BMCC. Scale bar 10 mm. (C) Timeline of coculture process for myocardial slices with CPCs.

2.2.3 Differentiation of CPCs to cardiomyocytes in 2D culture

CPCs were cultured on Geltrex-coated surfaces. These were prepared in 24-well tissue culture plates, or on 15 mm-diameter glass coverslips by incubation with 0,5 mL Geltrex solution (2% Geltrex stock solution diluted in DMEM/F12 medium at 4 °C). After incubation at 37°C for 1-2 h, the plates were wrapped with parafilm and were kept at 4°C until use. The Geltrex-coated plates were pre-warmed at room temperature on a laminar flow bench for 1-2 h before cell seeding, and then the DMEM/F12 medium was aspirated from the plates. After thawing and centrifugation (1100 rpm, 4 min), CPCs were resuspended with coculture medium and were added to the plates (500,000 cells/well). The medium was exchanged every other day, and the CPCs were harvested on day 35.

2.2.4 Assessment of myocardial contractile functions

Real-time contractility monitoring was automatically performed in MyoDish software. The twitch and diastolic forces were determined in plain myocardial slices and CPCs-grafted slices for 5 weeks. Raw data of twitch force were converted to the Axon Binary File Format using the MyoDish Data File Converter. Amplitude and time course of contractions were visualized by LabChart Reader software. All parameters of force temporal kinetics (time of stimulation to peak (STP); constant of exponential decay (Tau); duration of more than half-maximum contraction force (CD_{50}); time from peak contraction to 50 % decay (T_{50off})) were analyzed by Matlab-based MyoDish analysis scripts. Tau was calculated using an exponential decay model.

More detailed parameters of cardiac function were daily assessed by stimulation protocols automatically executed by the MyoDish software. Functional parameters included refractory period, post-pause potentiation (PPP), force-frequency relation (FFR), and maximum capture rate (MCR). Refractory period was defined as the longest stimulation interval that failed to induce two distinct contractions. Pairs of sequential stimuli were applied to detect refractory period, whereby the interval between the paired stimulations was stepwise decreased from 640 to 80 ms [55].

A stimulation protocol with stepwise increases in pacing frequencies (0.2-4 Hz) was implemented in myocardial slices for the assessment of FFR [56]. MCR is the maximum pacing rate at which each electrical stimulation induced a reliable

and consistent contraction in myocardium [57]. Time to 50% relaxation (T_{50off}) was defined as the crucial parameter in assessing frequency-dependent acceleration of relaxation (FDAR) [58].

PPP was defined as the first peak after ultra-high pacing rate (240 bpm = 4 Hz) and 5-second rest period. In this case, calcium storage in sarcoplasmic reticulum is considered to be depleted after tachycardia, and to be optimally refilled during the quiescent period. The first stimulated peak of contraction after the pause can be regarded to reflect the maximum of intracellular calcium release [59]. The ratio of post-pause contractility to normal contractility at 0.5 Hz reflects the calcium capacity of sarcoplasmic reticulum in the cardiomyocytes.

2.2.5 Calcium imaging of plain and cocultured myocardial slices

Calcium imaging was based on a self-developed method [60], that had been adapted to the requirements of CPCs-cocultured myocardial slices. Prior to dye-loading, GFP-expressing CPC-CMs were localized by fluorescence (488 nm excitation, 525 nm emission). The position of the area of interest was recorded by the motorized stage of the fluorescence microscope. The cocultured myocardial slice with CPCs were loaded with Fluo-8L AM at the final concentration 10 µM for 1 h. 30 mM BDM was applied for excitation-contraction uncoupling during the calcium imaging. Synchronization of stimulation and calcium imaging was processed by imaging-specific MyoDish software, which produced electrical impulses for excitation of myocardial tissue slices and synchronized rapid impulse sequences for camera triggering. The time points of a dedicated stimulation sequence and the corresponding calcium signals were recorded simultaneously for 60 s. Fluorescence intensity of each region of interest was extracted from image stacks by ImageJ, and the dye photobleaching was corrected by OriginPro software. The alignment of stimulation and calcium transients was performed by modified MyoDish software. The data format was translated by WinEDR, so that the kinetics of contractions and calcium transients (STP, CD_{50}, Tau) could be analyzed by OriginPro software.

2.2.6 Morphological and histological analyses

For the localization of CPC-CMs in host myocardial slices, combined bright field (DIC, differential interference contrast) and fluorescence imaging was performed with a confocal microscope (Leica SP5). The distinction between graft and host tissues was based on GFP fluorescence in CPC-CMs (Ex = 488 nm, Em = 525 nm) and autofluorescence in host myocardial slices (Ex = 546 nm, Em = 550-650 nm). The image stacks were captured and merged to optimal visualization by maximum intensity projection along the Z-axis.

For detection of CPCs migration into myocardial slices, label-free microscopic imaging was performed by two-photon microscopy. Living CPCs-cocultured myocardial slices were placed in PBS at room temperature. The combination of second harmonic generation (SHG, excitation at 490 nm) and native eGFP fluorescence of CPCs (excitation at 980 nm) using two-photon excitation with a Leica SP8 WLL DIVE Falcon microscope, enabled deep live imaging of cocultured myocardial slices without damage or staining. This technique visualizes the spatial location of CPC-derived cells and their myofiber alignments in myocardial slices, so that migration directions and invasion depths of CPCs can be determined [61].

For immunohistology, whole myocardial slices with and without CPCs were fixed with 4% PFA for 1 h. The slices were embedded into OCT and were cut to 50 µm-thickness myocardial cryosections by a cryotome, and were then collected and preserved at -80 °C in pre-cooled 2 mL tubes, individually. Free-floating myocardial cryosections were permeabilized with 1% Triton X-100 for 30 min, and were blocked with 1% BSA in HBSS for 20 min and 3 times in 2 mL tubes. These cryosections were then sequentially incubated with primary antibodies (GFP, α-actinin, connexin-43, N-cadherin, MLC2v, MLC2a, 1:200, 1% BSA in HBSS) overnight at 4 °C, and secondary antibodies (donkey anti chicken, goat anti chicken, goat anti-mouse, goat anti-rabbit Alexa Fluor at 488, 546, and 633 nm, 1:200, 1% BSA in HBSS) for 2h at room temperature in the dark. DAPI was added with secondary antibodies in parallel for DNA staining. HBSS solution (except 1% BSA in HBSS for washing between primary and secondary antibodies incubation) was used for washing steps (performed 3 times for 15 min each on a shaker) in between all incubations. For mounting and covering, the cryosections were resuspended in a droplet of HBSS on a horizontally extended parafilm, and were spread evenly by slow removal of the HBSS. Meanwhile, an appropriate area of

a microscope slide (2 cm × 2 cm) was coated with 1 µL Histoacryl glue, and was brought in contact with the myocardial cryosection. The mounted cryosections were embedded in mounting medium, covered with a coverslip which were sealed with nail polish to the microscope slides. Confocal imaging was performed with an upright Leica SP8 WLL DIVE Falcon system using single-photon excitation with a 63X oil immersion objective. Excitation wavelengths were set at 405 nm for DAPI, at 488 nm for GFP, at 546 and 633 nm for α-actinin, connexin-43, N-cadherin, MLC2v, and MLC2a. Different layers of myocardial slices (depths at 0-50 µm, 50-100 µm, 100-150 µm, 150-200 µm, 200-250 µm, 250-300 µm) were imaged using constant laser power of the confocal microscope.

2.2.7 Cell nuclei isolation and library preparation and snRNA-seq

Plain cultured myocardial slices and CPCs-cocultured myocardial slices were flash-frozen with dry ice, and were subsequently stored at -80 °C. Frozen myocardial slices with and without CPCs were resuspended in ice-cold homogenization buffer, and were transferred to a cold Dounce tissue grinder. Mechanical homogenization was performed to lyse cell membranes while keeping nuclei intact. The homogenate was filtered through a 40 µm cell strainer, and was centrifuged (500 g) for 5 min at 4 °C. The nuclear pellet was resuspended and was stored in storage buffer (buffer compositions, including homogenization and storage buffers, are shown in Table 4).

Cell nuclei were labeled with NucBlue Live ReadyProbes reagent, and were purified by fluorescence-activated cell sorting (FACS). Nuclei counting and quality check were performed at least twice using DAPI with Countess II automated cell counter. Single-nuclei suspension and gel beads-in-emulsion (GEMs) were mixed and uploaded into Chromium Controller (the range of recovery rate was 5,000-10,000 nuclei per reaction). Reverse transcription was carried out within the GEMs to synthesize cDNA. The GEMs were broken to release the cDNA, which was then cleaned and amplified. The amplified cDNA fragments were then processed, and sequencing adapters and barcodes were added. After amplification by PCR, the final sequencing library was obtained. The library fragment size distribution was checked using a Bioanalyzer, and the library concentration was quantified using Qubit, following the sequencer manufacturer's guidelines. The

prepared library was sequenced on a HiSeq 4000 platform with a minimum depth of 20,000–30,000 read pairs per nucleus.

2.2.8 Preprocessing of raw snRNA-seq data

After snRNA-seq, raw data was converted from BCL format to FastQ format using bcl2fastq. Initial data processing was performed using Cell Ranger. (1) Read assignment: Reads were assigned to the corresponding cell and transcript. (2) Quality control filtering: Low-quality reads and low-read-count cells were filtered and removed. (3) Reference genome alignment: High-quality reads were aligned to human reference genome GRCh38 using alignment algorithm with default parameters. (4) Gene expression quantification: Unique Molecular Identifiers (UMIs) were used for unique mRNA counting, and gene expression matrix was then generated. Raw read counts were normalized to adjust for variations in sequencing depth and capture efficiency.

2.2.9 Quality control and batch correction and clustering

Initial preprocessing of feature-barcode matrix was performed using Python package Scanpy v1.10.2. Cell Ranger pipeline v 8.0.1 was used to remove ambient RNA contamination. Subsequently, cell nuclei were filtered to exclude low-quality genes based on the following criteria: counts (500 ≤ nCount_RNA ≤ 20,000), genes (500 ≤ nFeature_RNA ≤ 6,000), mitochondrial genes (percent_mito_mt ≤ 0.5%), and ribosomal genes (percent_ribo ≤ 0.5%, percent_ribo_RPS ≤ 0.5%, percent_ribo_RPL ≤ 0.5%). SOLO algorithm was used to remove doublets.

For data integration and batch effect correction, scVI algorithm from Python package scVI-tools v 1.1.5 was utilized, with raw counts as input data. The data was normalized and standardized (target_sum=1e4, max_value=10). The scVI model was trained on top 2000 highly variable genes identified using ‘pp.highly_variable_genes’ function with parameters set to (lavor="seurat_v3") and (batch_key="batch") in Scanpy. All other parameters for the scVI algorithm were set to default.

For dimensionality reduction, principal component analysis (PCA) was used to reduce noise and to capture main variance. ElbowPlot was generated for principal components selection. Cell-cell neighborhood relationship was established

by scVI latent space (n_neighbors=10, n_pcs=40). Clustering was performed by unsupervised Leiden clustering in Scanpy, and visualized by UMAP (resolution = 0.5). For subsequent analyses, Python package Sceasy v0.2.2 was used to convert AnnData objects from Scanpy into Seurat objects in R. The function FindAllMarkers of R package Seurat was used for the identification of differentially expressed genes (DEGs) and the annotation of cell clusters. Cell type annotation of clustered cells was achieved by comparing highly variable genes against known cell type markers sourced from established databases CellMarker (http://xteam.xbio.top/CellMarker/) and PanglaoDB (https://panglaodb.se/). CPC-CMs was identified by distinguished clustering and cardiac differentiation-related genes. The expression of annotated clusters was visualized using dot plot to confirm the accuracy of cell type assignments. The proportion of cell clusters was calculated and visualized using R packages Seurat and ggplot. To quantify the proportion of functionalized CPC-CMs, the cell numbers of co-expressing multiple genes was counted using the R packages Seurat and dplyr. The expression threshold of genes was set at 0.5, based on their frequency distribution.

2.2.10 Differential gene expression and enrichment analyses

Differentially expressed genes (DEGs) between native cardiomyocyte populations in control and coculture were identified by function FindMarker in Seurat, with Wilcoxon rank sum test as default. Genes were referred to as DEGs with false discovery rate (FDR, adjusted p-value) < 0.05 and absolute average Log_2Fold change ($|log_2FC|$) > 0.25. R package EnhancedVolcano v1.20 was used for visualization of differential gene expression. Subsequently, DEGs of native cardiomyocytes in control and coculture were included in enrichment analysis. Gene Ontology (GO) enrichment analysis for biological processes (BP) was performed using 'clusterProfiler' package v4.10.1 in R. The gene symbols were annotated against the human reference database 'org.Hs.eg.db'. P-values were adjusted using the Benjamini-Hochberg (BH) method, with significance thresholds set at p-value < 0.05 and q-value < 0.05.

Gene set enrichment analysis (GSEA) and its visualization were performed using R package clusterProfiler v4.10.1. Upregulated and downregulated genes were enriched to GO terms separately. The enrichment was visualized by func-

tion ‘gseaplot2’ in clusterProfiler. Dot plots of DEGs with high expression proportion (> 50% in coculture) in the top enrichment sets were generated using the Seurat function ‘DotPlot’, with scaling disabled (scale = FALSE) to display the actual gene expression levels in control and cocultured native cardiomyocytes.

2.2.11 Trajectory analysis

Subclusters of CPC-CMs were identified and extracted based on clustering analysis in Seurat object. Trajectory and pseudotime analyses were conducted using R package Monocle v2.30.1. The Seurat object was converted to Monocle object CellDataSet. The latter was initialized with the expression data, phenotype data, and feature data. Data was preprocessed by estimating size factors and dispersions, and highly variable genes were then selected by filtering for genes with a mean expression of at least 0.1 and an empirical dispersion greater than or equal to 1.5. After dimensionality reduction using DDRTree method, cell nuclei were ordered to construct pseudotime trajectory [62]. The position and state transitions of cell nuclei were visualized by functions ‘plot_cell_trajectory’ (‘Cluster’ and ‘Pseudotime’). Gene expression trend was visualized using function ‘plot_genes_in_pseudotime’ in Monocle.

2.2.12 Cell-cell communication and interaction analysis

Cell-cell communication and interaction between cell populations of CPC-CMs and hfCMs in coculture, were analyzed by R package CellChat (v1.6.1, CellChat human database (secreted signaling, cell-cell contact, extracellular matrix-receptor), http://www.cellchat.org/cellchatdb/) [63]. Intercellular communication probabilities were inferred through the identification of highly expressed genes and corresponding ligand-receptor pairs. Circle plot and bubble plot of communication probability were generated using visualization functions (‘netVisual_circle’ and ‘netVisual_bubble’) with default settings in CellChat.

2.2.13 Gene regulatory network analysis

Expression matrix was extracted from the Seurat object, and was converted to loom format. The analyses were conducted by Python package pySCENIC v 0.12.1. Target genes-related gene regulatory network (GRN) was established based on SCENIC (Single-cell regulatory network inference and clustering) [64].

Human databases, including a transcription factor list (hs_hgnc_tfs.txt), a motif ranking file (hg38_10kbp_up_10kbp_down_full_tx_v10_clust.genes_vs_motifs.rankings.feather), and a motif annotation file (motifs-v9-nr.hgnc-m0.001-o0.0.tbl), were used in the SCENIC workflow. Running 3 steps of SCENIC: (1) Construction of co-expression networks was performed using method GRNBoost; (2) Regulatory network was inferred through identification of transcription factors (TFs) and TFs-binding motif enrichment; (3) Regulatory module activity was scored using AUCell. Sub-regulons are merged if they are regulated by the same transcription factor and bind to multiple DNA motifs. Subsequently, target genes were enriched in BP of GO terms by R package 'clusterProfiler' v4.10.1. GRN was visualized using software Cytoscape v3.7.0.

2.2.14 Statistics and reproducibility

Statistical analysis was performed using GraphPad Prism for morphological and functional measurements. Statistical differences were calculated with paired Student’s t-test, and one-way and two-way ANOVA with Fisher’s LSD test. For gene expression in snRNA-seq, Kruskal-Wallis test was performed to determine statistically significant differences among multi-groups in R. If significant, Dunn's test was proceeded for pairwise comparisons. All the experiments were performed independently with at least 3 biological replicates. Data are presented as mean ± SEM or median with interquartile range (IQR). *$p < 0.05$, **$p < 0.01$, ***$p < 0.001$, and ****$p < 0.0001$ were applied as significance cut-offs at all instances.

3. Results

3.1 Effects of CPCs on excitation, contractility and force kinetics of cocultured myocardium

3.1.1 Enhanced myocardial contractility in cocultured myocardium

The contractility of cocultured myocardium was gradually enhanced with the continuation of coculture (Figure 4). There was no difference of contractility between control and coculture on day 7. From day 14 onwards, the contractility of cocultured myocardium increased significantly compared to control (+ 49 ± 18.2% on day 14, + 64.1 ± 24.1% on day 21, + 83.1 ± 31.8% on day 28). At the fifth week, the contractility of cocultured myocardium showed an increase of 101.9 ± 42.3%.

3.1.2 Synchronized contraction and delayed force kinetics of CPCs and cocultured myocardium

The equivalent shapes of contraction kinetics of control and cocultured slices demonstrate the synchrony and consistency of excitation between CPCs and host myocardium. The absence of aberrant peaks indicates fully synchronous contractions (Figure 5A). Temporal kinetics of force transients, reflecting the velocity of contraction and relaxation, were delayed in cocultured myocardium compared to control (stimulation to peak, STP, +12.2 ± 4.9%; transient duration at half-peak, CD_{50}, +13.6 ± 2.7%; Tau (decay constant), +19.3 ± 7.6%) (Figure 5B).

3.1.3 Catecholamine responses in control and cocultured myocardium

Positive inotropic response to isoproterenol (ISO) is an important criterion for assessing myocardial performance, because it induces the maximum biological efficacy of myocardial excitation-contraction coupling. Our results indicate an absolute increase (+3496.2 ± 1465.4 µN) and a relative decrease (-14.9 ± 3.5%) of contractility amplitude in the positive inotropic response of cocultured myocardium compared to control (Figure 6).

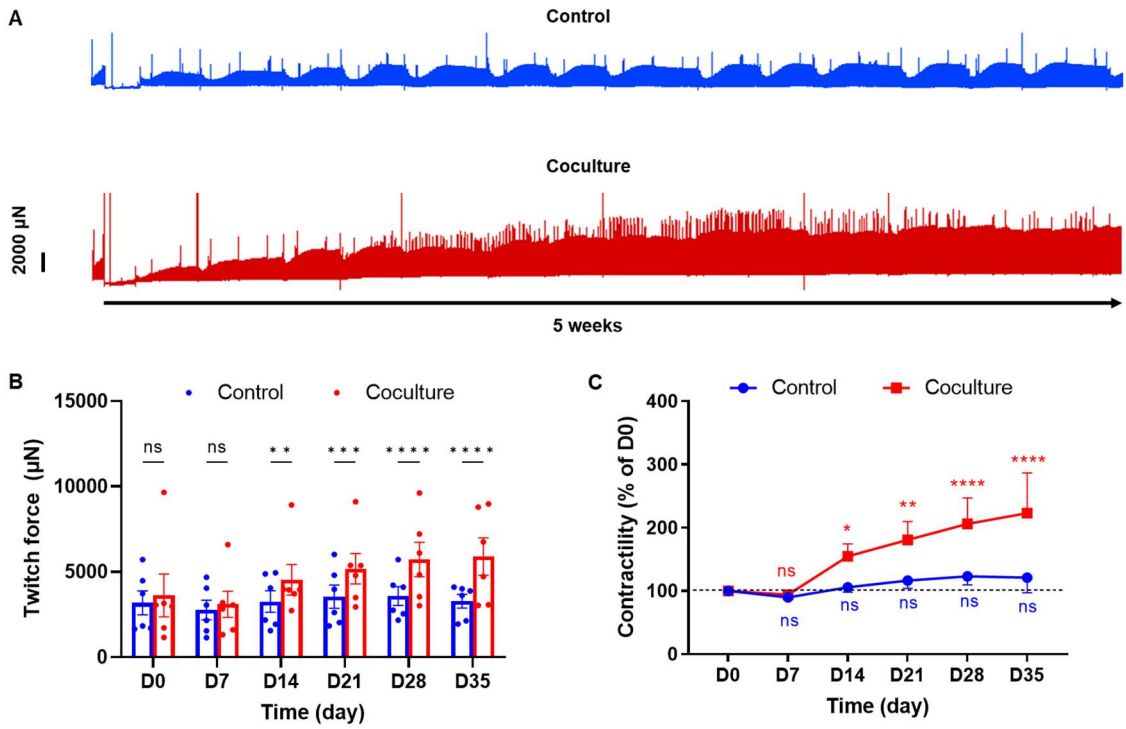

Figure 4. Enhancement of contractility in CPCs-cocultured myocardium.

(A) Representative contractility registrations of long-term culture with or without CPCs for 5 weeks. (B) and (C) Weekly absolute and normalized contractility of myocardial slices in control and coculture. n = 6 pairs of myocardial slices from 6 patients. Two-way ANOVA with Fisher's LSD test (control versus coculture for D0-D35 on the left, D7-D35 versus D0 for control and coculture on the right). Data are presented as mean ± SEM. *p < 0.05, **p < 0.01, ***p < 0.001, and ****p < 0.0001 were applied as significance cut-offs at all instances, and ns indicates non-significant difference.

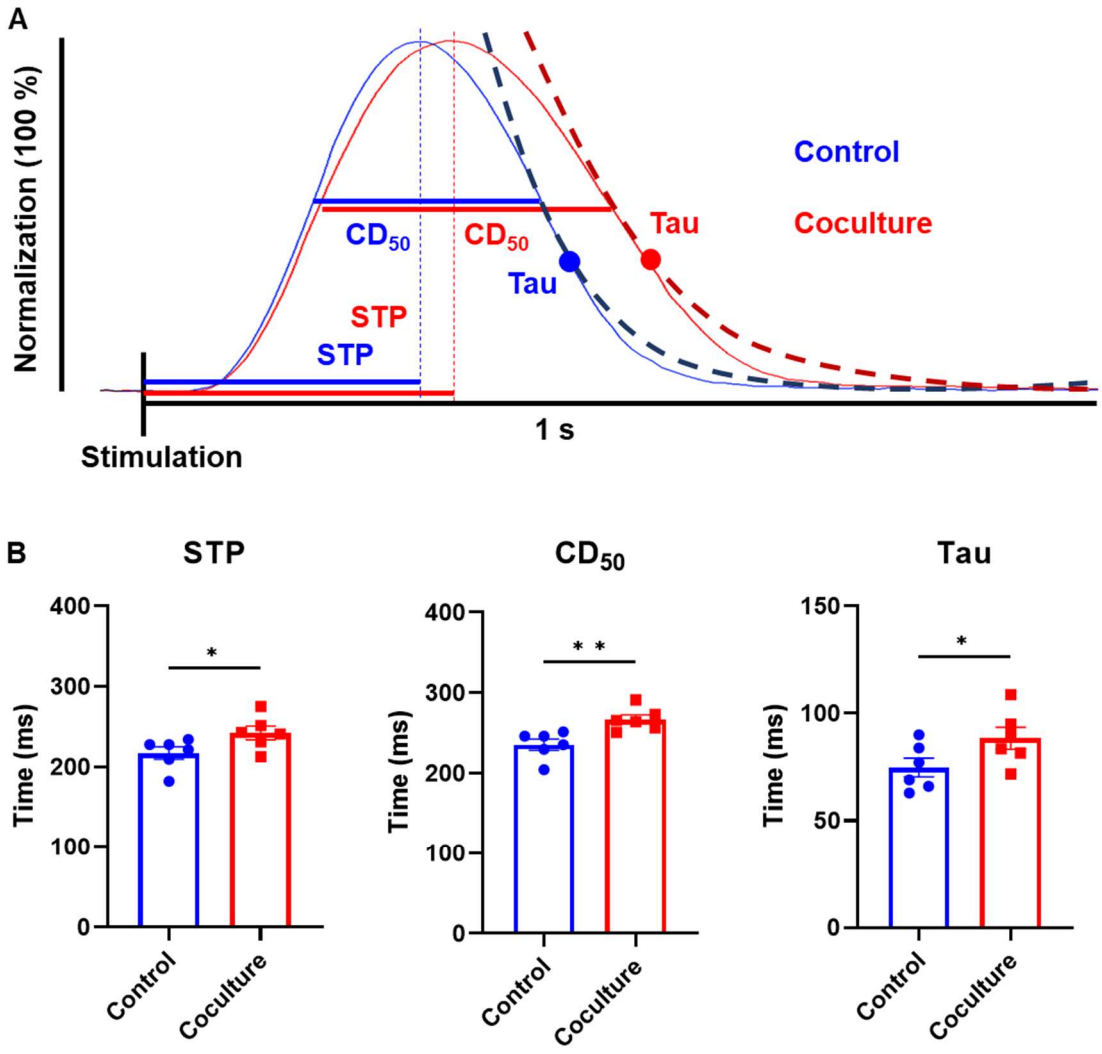

Figure 5. Synchronization and modified kinetics of contractions in CPCs-cocultured myocardium.

(A) Schematic representation of contraction and relaxation kinetics in control and cocultured slices. STP = stimulation to peak, CD_{50} = full width of contraction exceeding half maximum, Tau = time constant of force decay based on an exponential decay model. Dash lines indicate exponential curves for Tau. (B) Temporal parameters (STP, CD_{50}, and Tau) of force transients in control and coculture at 0.5 Hz pacing rate, n = 6 pairs of myocardial slices from 6 patients, mean ± SEM, paired t-test, *p < 0.05, **p < 0.01 were applied as significance cut-offs at all instances.

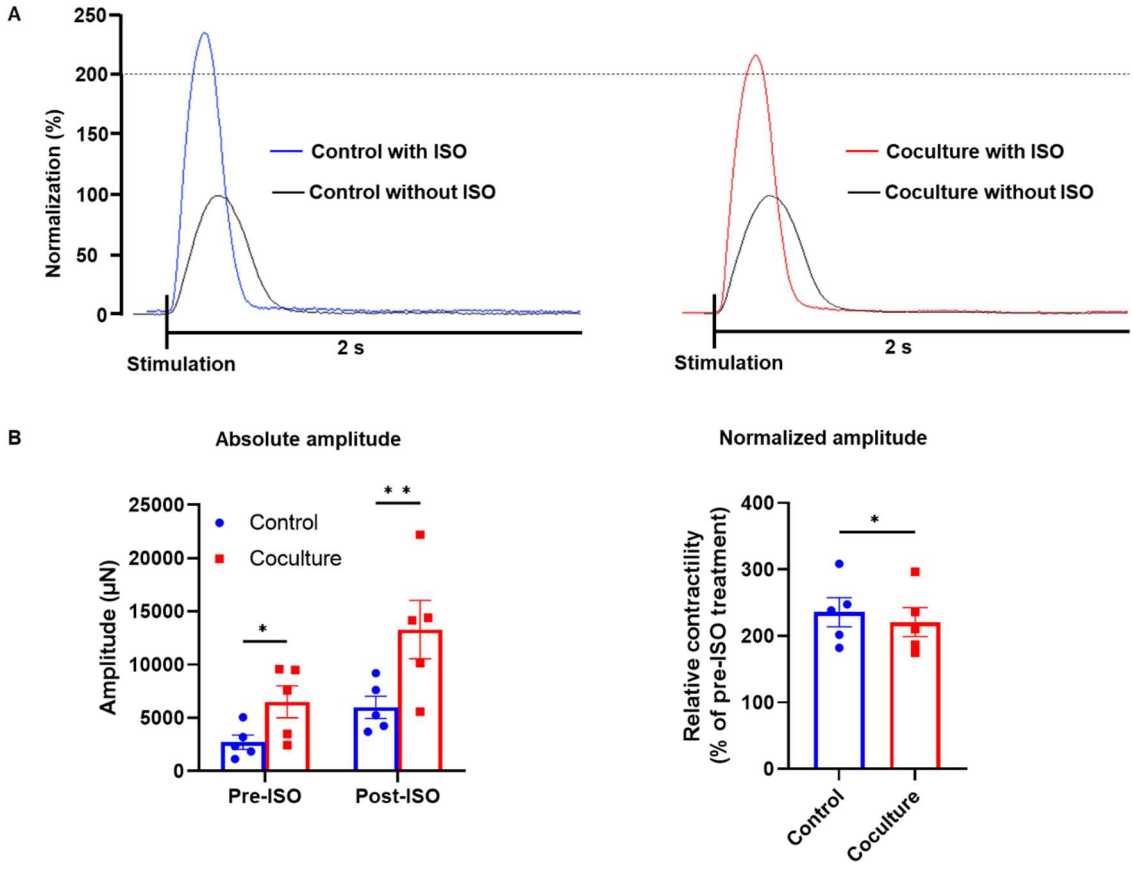

Figure 6. Inotropic response of myocardial slices with and without CPCs.

(A) Representative example of isoprenaline (ISO)-induced inotropic effects in control and coculture. (B) Absolute and relative changes of contraction amplitude at 0.5 Hz for control and coculture in absence and presence of ISO. n = 5 pairs of myocardial slices from 5 patients, mean ± SEM, paired t-test, *p < 0.05, **p < 0.01 were applied as significance cut-offs at all instances.

3.2 Effects of CPCs on frequency-dependent properties of cocultured myocardium

3.2.1 Modification of force-frequency relation

CPCs greatly increased total contractility over the full range of pacing rates (30-210 bpm), but attenuated the increase of contraction force at optimum frequency, and further blunted the force-frequency relationship (FFR) in failing myocardium. The FFR of coculture was downregulated at 120-180 bpm compared to control, and the pacing rate corresponding maximum contractility was shifted from 120 bpm in control to 100 bpm in coculture (Figure 7).

3.2.2 Prolongation of maximum capture rate of stimulation frequency

Maximum capture rate (MCR) is the highest frequency at which myocardium can effectively respond to and follow an external stimulation. MCR of cocultured myocardium increased substantially (223.3 ± 5.3 bpm) compared to control (190 ± 11.2 bpm), which facilitates myocardial adaptation to high-pacing rate (Figure 8).

3.2.3 Reduction of frequency-dependent acceleration of relaxation

Frequency-dependent acceleration of relaxation (FDAR) is critical for maintaining cardiac function at high pacing rates and reflects the efficiency of calcium handling of cardiomyocytes, which can be quantified by T_{50off}-frequency relation. T_{50off} in coculture was prolonged than that in control, but this difference of T_{50off} decreased with pacing increasing and eliminated at 180 bpm and 210 bpm. T_{50off}-frequency relation was accelerated in cocultured myocardium, compared to control (Figure 9).

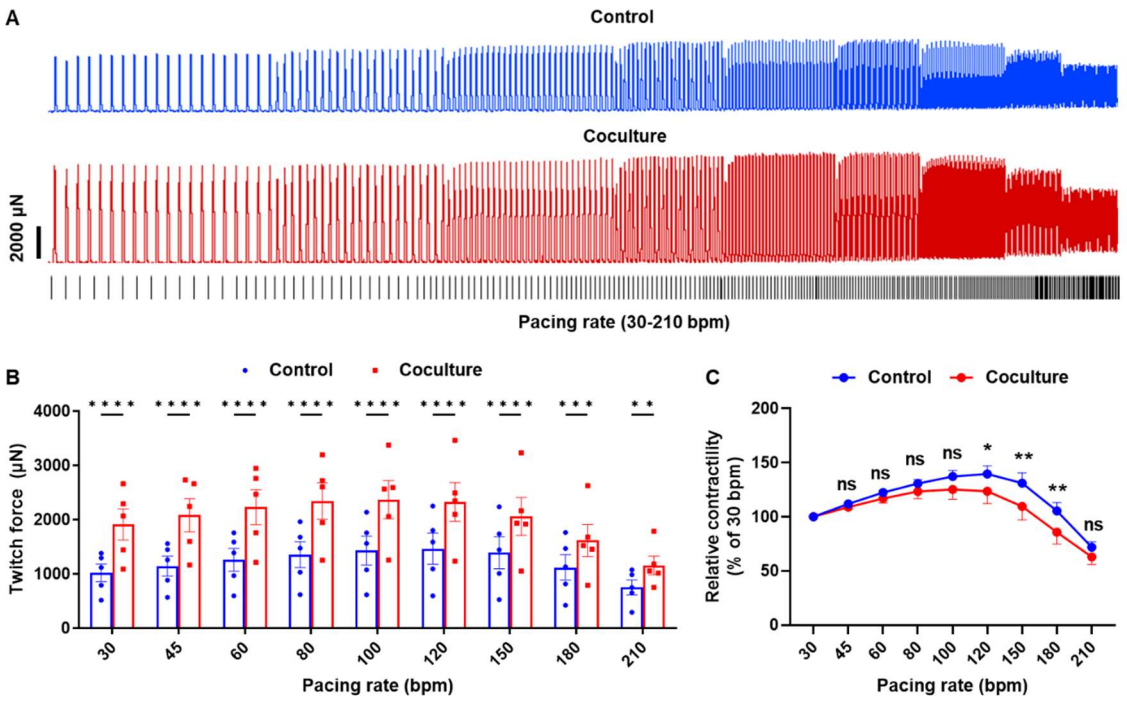

Figure 7. Attenuation of positive force-frequency relation (FFR) in CPCs-cocultured myocardium at 30-120 bpm.

(A) Representative recordings of FFR in control and coculture at the range of pacing rates (30-210 bpm). bpm = beat per minute. (B) Twitch force of control and cocultured slices at different pacing rates. (C) Twitch forces normalized to the contractility at 30 bmp of the individual slices. n = 5 pairs of myocardial slices from 5 patients, two-way ANOVA with Fisher's LSD test of coculture versus control. Data are presented as mean ± SEM. *p < 0.05, **p < 0.01, ***p < 0.001, and ****p < 0.0001 were applied as significance cut-offs at all instances, and ns indicates non-significant difference.

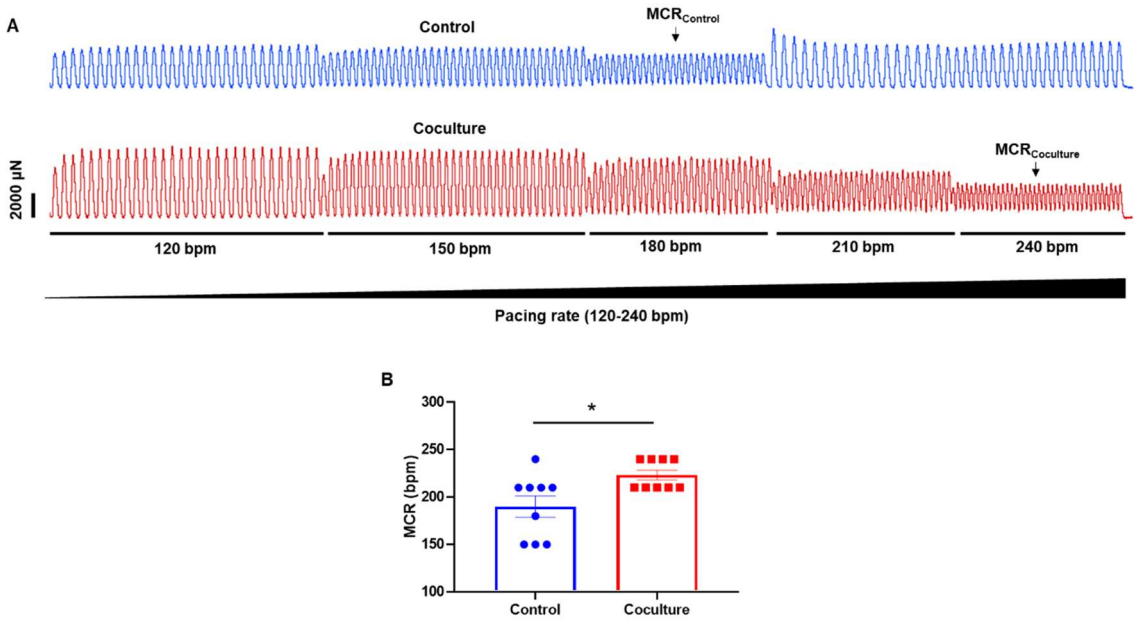

Figure 8. Increased maximum capture rate (MCR) of stimulation frequency in CPCs-cocultured myocardium.

(A) Representative example of MCR assessment with a series of increasing pacing rates (120-240 bpm). Only stimuli resulting in regular contractions with constant forces were considered to be captured. Bpm = beats per minute. $MCR_{Control}$ and $MCR_{Cocolture}$ = Maximum capture rate of stimulation frequency in control and coculture. (B) Absolute MCR in control and cocultured slices after 35 days of culture. Data are presented as mean ± SEM. n = 9 pairs of myocardial slices from 9 patients. Paired t-test, *p < 0.05 was applied as significance cut-off.

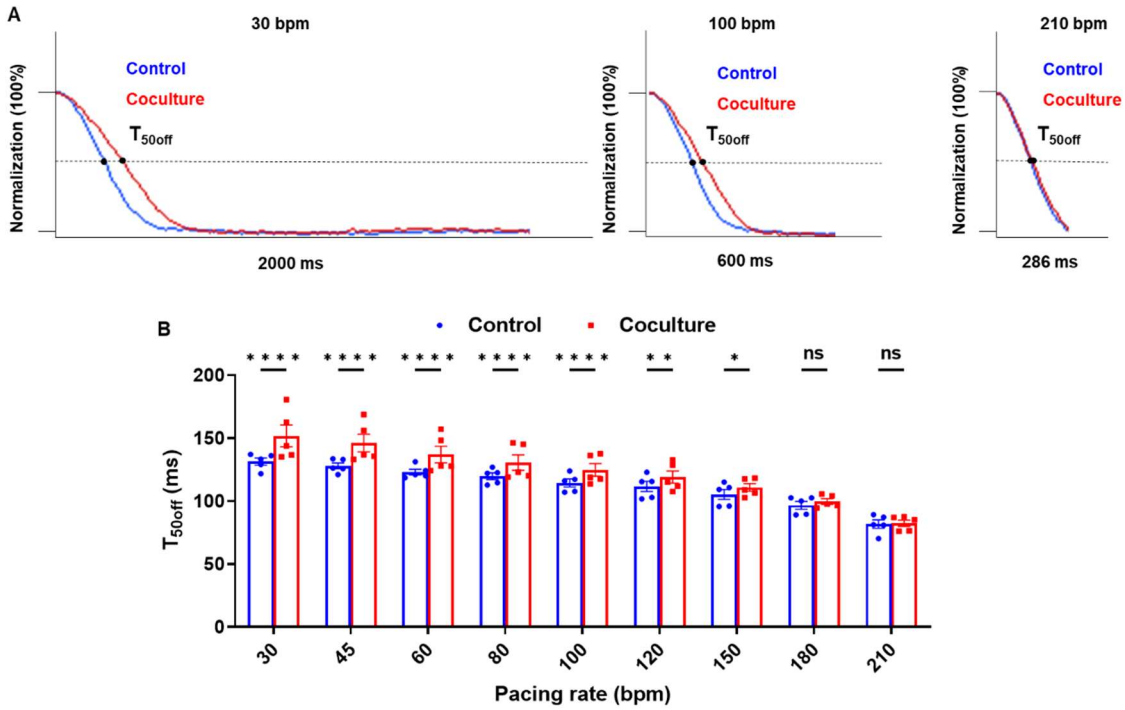

Figure 9. Frequency-dependent acceleration of relaxation (FDAR) in control and cocultured slices.

(A) Representative relaxation phases of contractile force at different pacing rates (30 bpm, 100 bpm, and 210 bpm) in control and coculture. Bpm = beats per minute. T_{50off} = Time to 50% relaxation. (B) T_{50off} of myocardial slices in control and coculture groups at various pacing rates (30-210 bpm). n = 5 pairs of myocardial slices from 5 patients, two-way ANOVA with Fisher's LSD test versus control. Data are presented as mean ± SEM. *p < 0.05, **p < 0.01, and ****p < 0.0001 were applied as significance cut-offs at all instances, and ns indicates non-significant differences.

3.3 Dynamics of intracellular calcium in cocultured CPC-CMs and native myocardium

3.3.1 Temporal kinetics of intracellular calcium

Consistent with the kinetic properties of contractility at 0.5 Hz, the kinetics of calcium transients in cocultured CPCs and host myocardium were also delayed and slowed down compared to control myocardium. This effect was reflected in all assessed kinetic parameters (STP, CD_{50}, Tau). Surprisingly, calcium transients of CPCs and host myocardium in coculture were very similar. Only the STP of CPCs was further prolonged relative to that of cocultured native cardiomyocytes, whereas no difference was present in CD_{50} and Tau of CPCs and host myocardium (Figure 10).

3.3.2 Post-pause potentiation in CPCs-cocultured myocardium

The intense contraction in post-pause potentiation (PPP) induced by rest following ultra-high frequency stimulation reflects the calcium capacity of sarcoplasmic reticulum in cardiomyocytes. The PPP of cocultured myocardium was attenuated compared to that of control (contractility ratio of PPP to normal, 2.1 ± 0.2 in control, 1.6 ± 0.1 in coculture) (Figure 11).

3.3.3 T-tubule-like development in CPC-CMs

We visualized the presence and location of CPC-CMs and host failing cardiomyocytes according to the expression of GFP, α-actinin, and DNA. The transverse tubular system (t-system) was labeled by WGA (Wheat Germ Agglutinin) which is known for specific binding to glycoproteins and glycolipid-rich structures on the t-tubular membrane. Spotted t-tubule-like structures were observed in CPC-CMs, whereas sheet-like structures of the t-system were more prevalent in chronic failing cardiomyocytes (Figure 12A). Quantitative morphological parameters of t-tubules in CPC-CMs and host failing cardiomyocytes (hfCMs) were extracted and calculated from image stacks of WGA fluorescence. T-tubules of CPC-CMs (1.2 ± 0.2 μm) were found to be shallower than those of hfCMs (2.1 ± 0.1 μm). Regarding the shape of t-tubules, their ratio of length to width was less in CPC-CMs than hfCMs (1.2 ± 0.1, and 1.7 ± 0.1, respectively). As such, the

characteristics of tubular structures were better developed in CPC-CMs than in hfCMs which feature a sheet-like tubular system (Figure 12B).

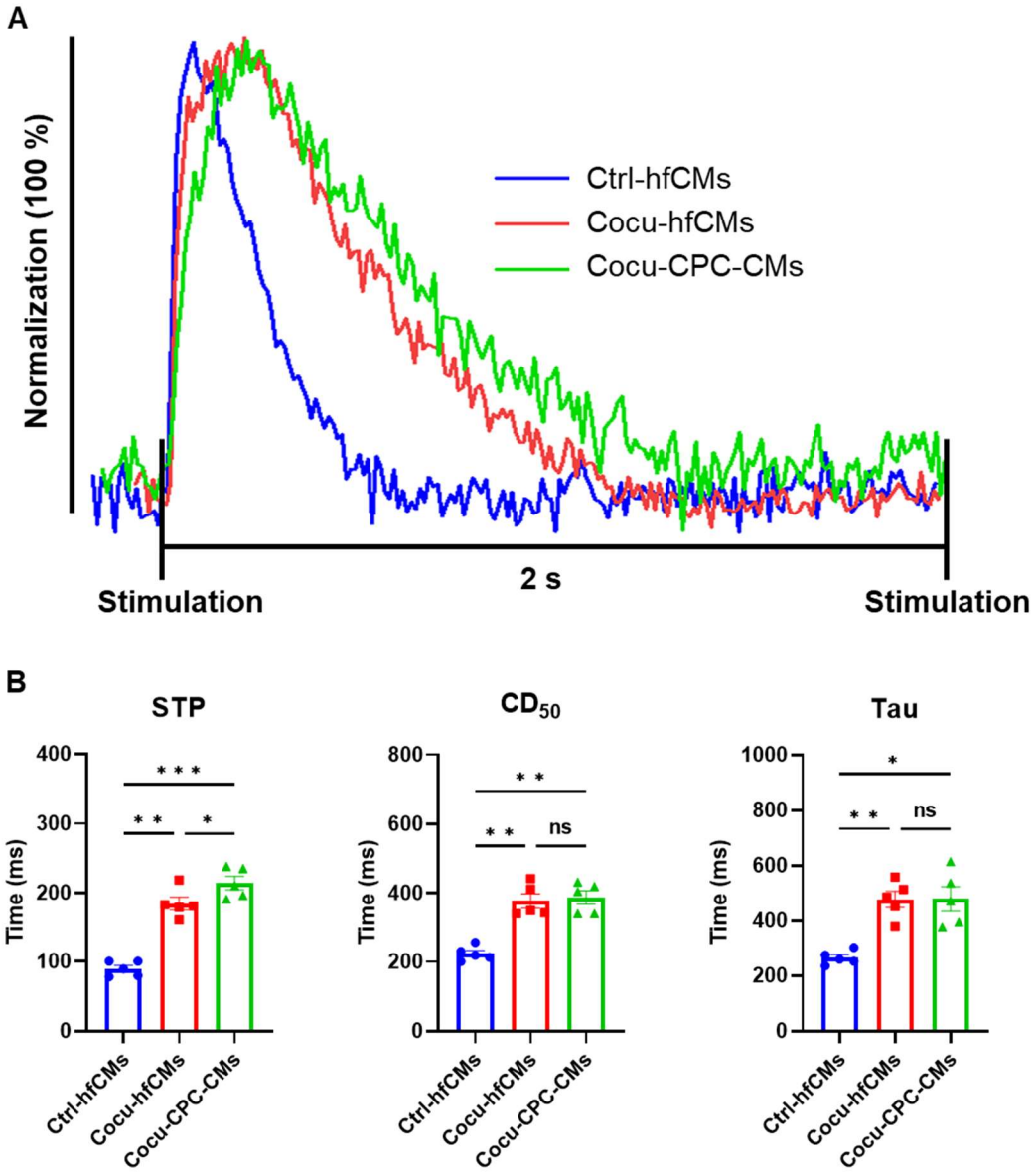

Figure 10. Calcium handling in control and cocultured myocardium.

(A) Representative normalized calcium transients of myocardial slice in control and CPCs-cocultured myocardial slices. Ctrl-hfCMs = failing cardiomyocytes in control, Cocu-hfCMs = host failing cardiomyocytes in coculture, Cocu-CPC-CMs = CPC-derived cardiomyocytes in coculture. (B) Temporal kinetics of calcium transients (STP, CD_{50}, and Tau). STP = stimulation to peak, CD_{50} = full width of calcium exceeding half maximum, Tau = time constant of calcium decay. n = 5 control and 5 CPCs-cocultured myocardial slices from 5 patients, one-way ANOVA with Fisher's LSD test. Data are presented as mean ± SEM. *p < 0.05,

**p < 0.01, and ***p < 0.001 were applied as significance cut-offs at all instances, and ns indicates non-significant difference.

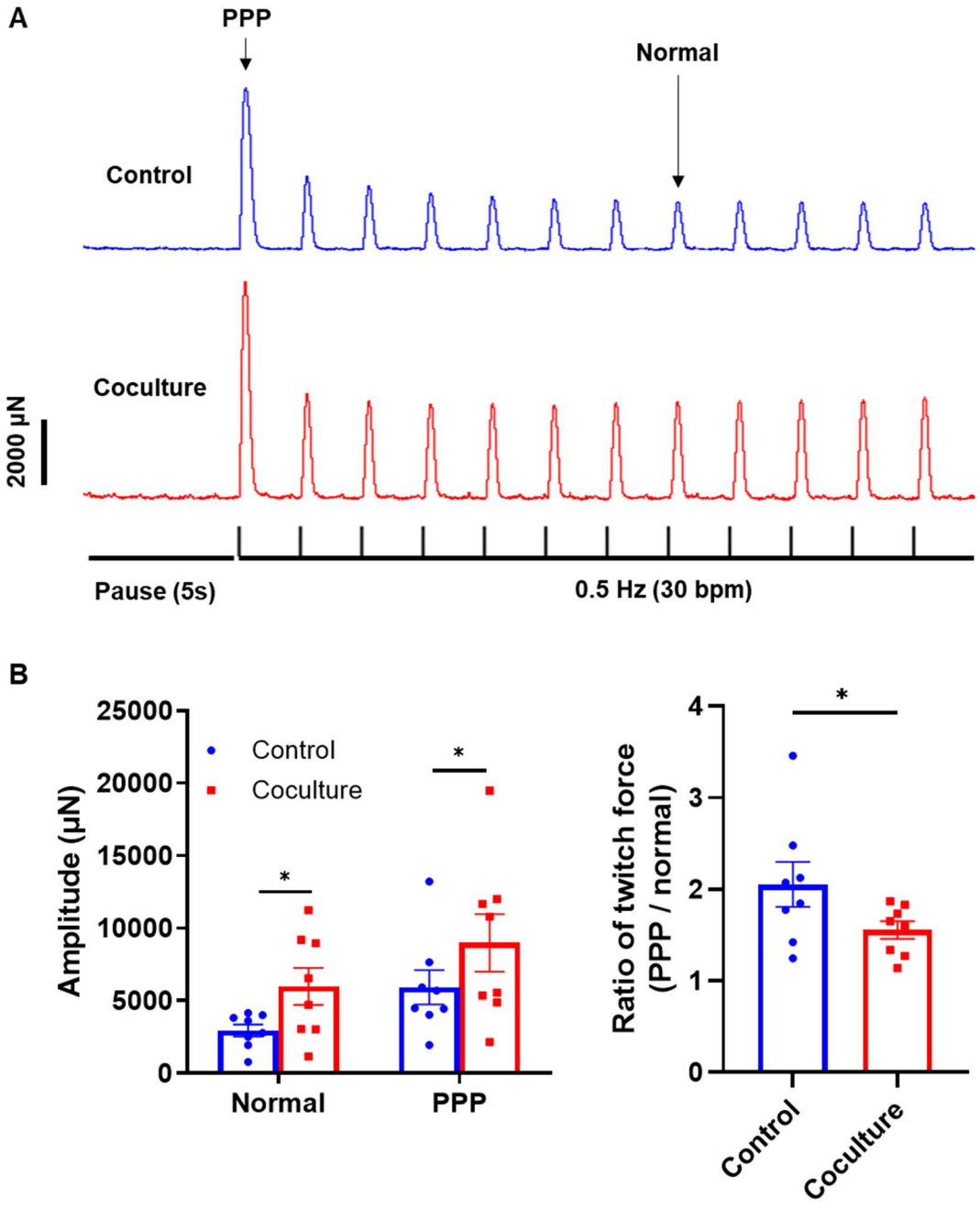

Figure 11. Post-pause potentiation in control and cocultured myocardium. (A) Representative recordings of PPP after ultra-high stimulation frequency (4 Hz) followed by a 5-second pause. PPP = post-pause potentiation, Normal = contractions at normal stimulation frequency (0.5 Hz). (B) Absolute and relative changes of contractility to PPP in control and coculture. n = 8 pairs of myocardial slices from 8 patients. Paired t-test versus control, data are presented as mean ± SEM. *p < 0.05 was applied as a significance cut-off.

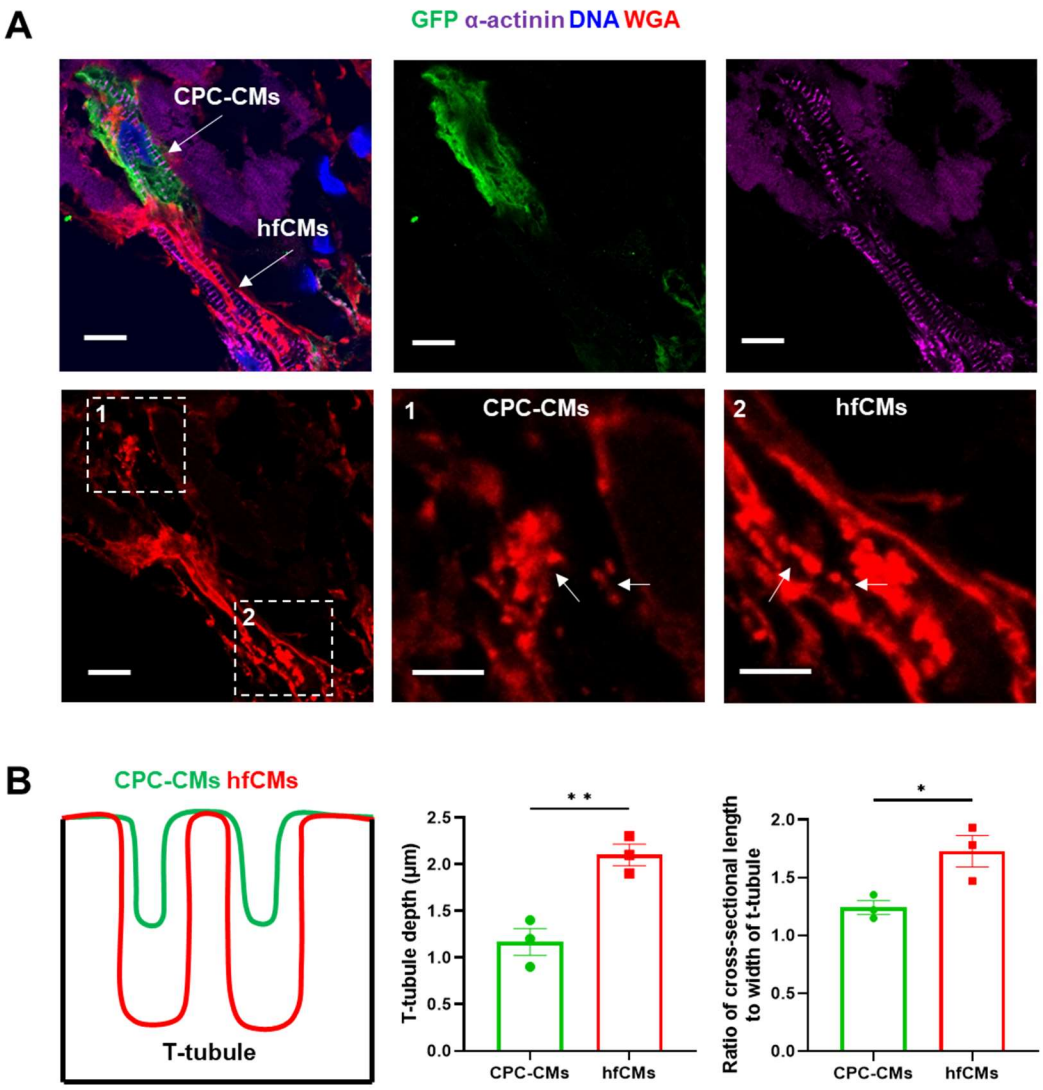

Figure 12. T-tubule-like structures in CPC-derived cardiomyocytes (CPC-CMs) and sheet-like t-system in host failing cardiomyocytes (hfCMs).

(A) Fluorescence images of t-tubules in CPC-CMs and hfCMs. GFP = green fluorescent protein selectively expressed in CPC-CMs, and stained with a GFP-specific primary antibody. White dashed areas 1 and 2 represent regions of interest, with their magnifications of t-tubules in CPC-CMs and hfCMs, respectively. White arrows indicate t-tubules. Scale bar, 10 µm, 5 µm (inset 1 and 2). (B) Schematic example and dimensional parameters (depth, ratio of cross-sectional length to width) of t-tubules in CPC-CMs and hfCMs. Data are presented as mean ± SEM. n = 3 pairs of CPC-CMs and hfCMs in 3 cocultured myocardial slices from 3 patients. Paired t-test, *$p < 0.05$ and **$p < 0.01$ were applied as significance cut-offs.

3.4 Synchronized excitation of CPCs and failing myocardium

3.4.1 Unchanged refractory period in cocultured myocardium

The refractory period of cultured tissues was assessed by application of paired stimulation impulses, the interval between them being programmatically stepped down from 640 ms to 80 ms. The first pair of stimuli which did not result in a noticeable contraction response to the second impulse was considered to delimit the refractory period of the tissue (Figure 13A). We found that the refractory period remained at 312.4 ± 5.3 ms in coculture and at 312.9 ± 6.3 ms in control, with no significant difference between them (Figure 13B).

3.4.2 Interference of spontaneous activity of CPCs to continuous electrical stimulation in cocultured myocardium

Whether transplantation of CPCs may provoke arrhythmias has been of high concern in clinical applications. In slices cocultured with CPCs, spontaneous contractions were observed when external electrical pacing was ceased, or reduced to frequencies less than 30 bpm (Figure 14A). In the presence of low-rate electrical stimulation, double peaks of contraction occurred in CPCs-cocultured myocardial slices, with the precedent contractions triggered by CPC-derived pacemaker cells, and the subsequent contraction by electrical stimulation (Figure 14B). Pacing rates that exceeded an individual threshold frequency (> 12 bpm) fully suppressed the spontaneous activities, indicating that any pacemaker activity has been reset by the external stimulation events. Consequently, the spontaneous pacing was overridden by the electrical stimulation at routine pacing rate and above (30-240 bpm). On the other hand, 43 % of CPC-cocultured slices did not interfere with electrical pacing of any stimulation frequency (Figure 14C). These might indicate that CPC-derived pacemaker cells adaptively regulate their spontaneous pacing to the frequency of routine stimulation (30 bpm).

In coculture, CPCs completed their initial differentiation and started to induce single spontaneous contractions on day 8 ± 0.3, but triggered regular spontaneous beating from day 12 ± 0.7 onwards (Figure 15A). The spontaneous pacing rate decreased during the long-term coculture (0.54 ± 0.05 Hz on day 14, 0.43 ± 0.04 Hz on day 35, Figure 15B). Upon cessation of the continuous field stimulation, the spontaneous pacing from CPC-derived pacemaker cells took over the

regular stimulation of cocultured myocardial slices. Intermittent assessments of the spontaneous pacing rate revealed that this stayed close to the routine pacing rate (30 bpm) throughout the culture period (Figure 15B&C).

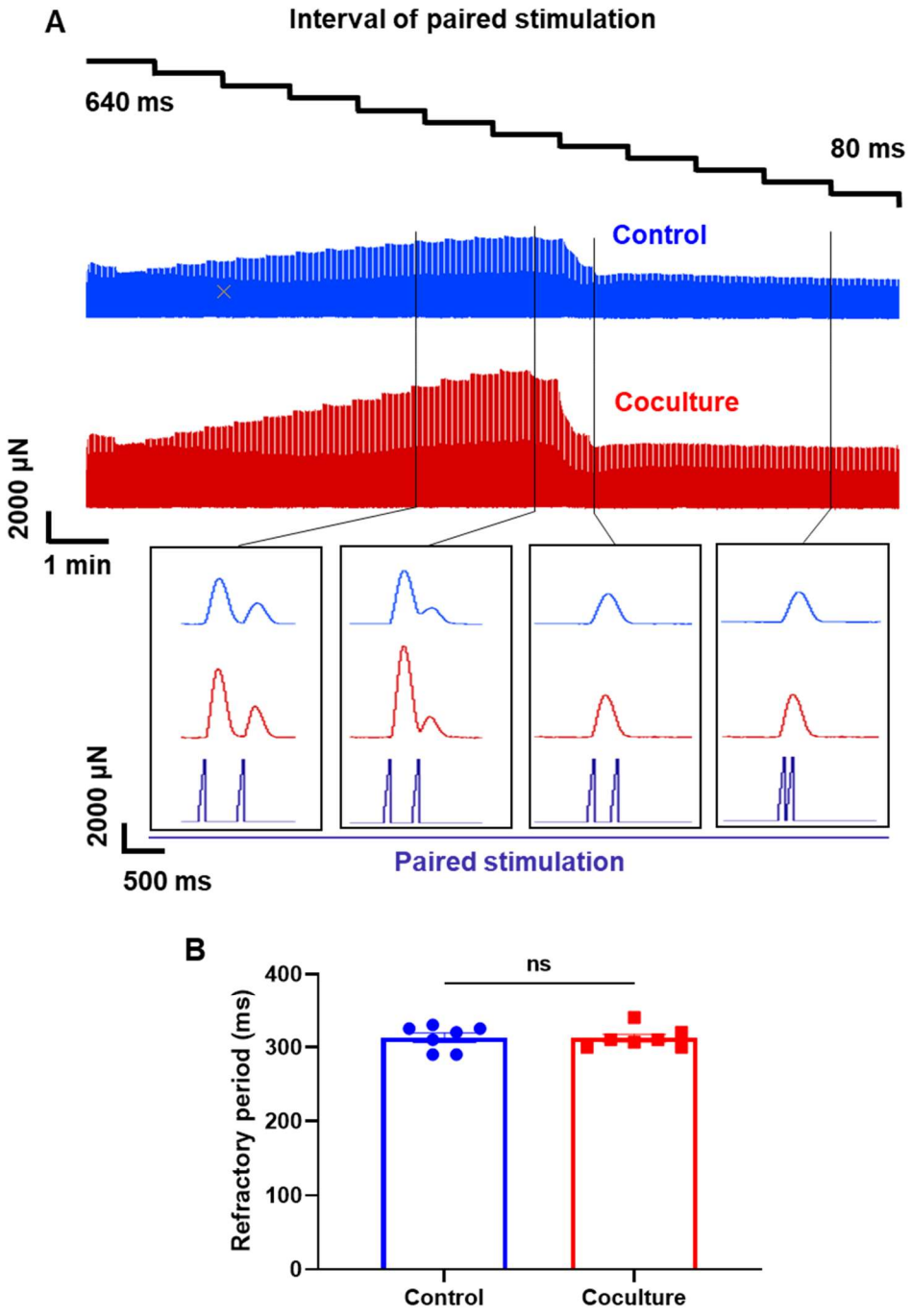

Figure 13. Refractory period in control and cocultured myocardium.

(A) Representative assessment of refractory period from 640 ms to 80 ms, and magnification of contractions at the critical timepoints. The time interval at which

the loss of subsequent contraction in paired stimulation impulses represents the duration of refractory period in stimulation protocol. (B) Refractory period in control and coculture. n = 7 pairs of myocardial slices from 7 patients. Paired t-test versus control. Data are presented as mean ± SEM. ns indicates non-significant difference.

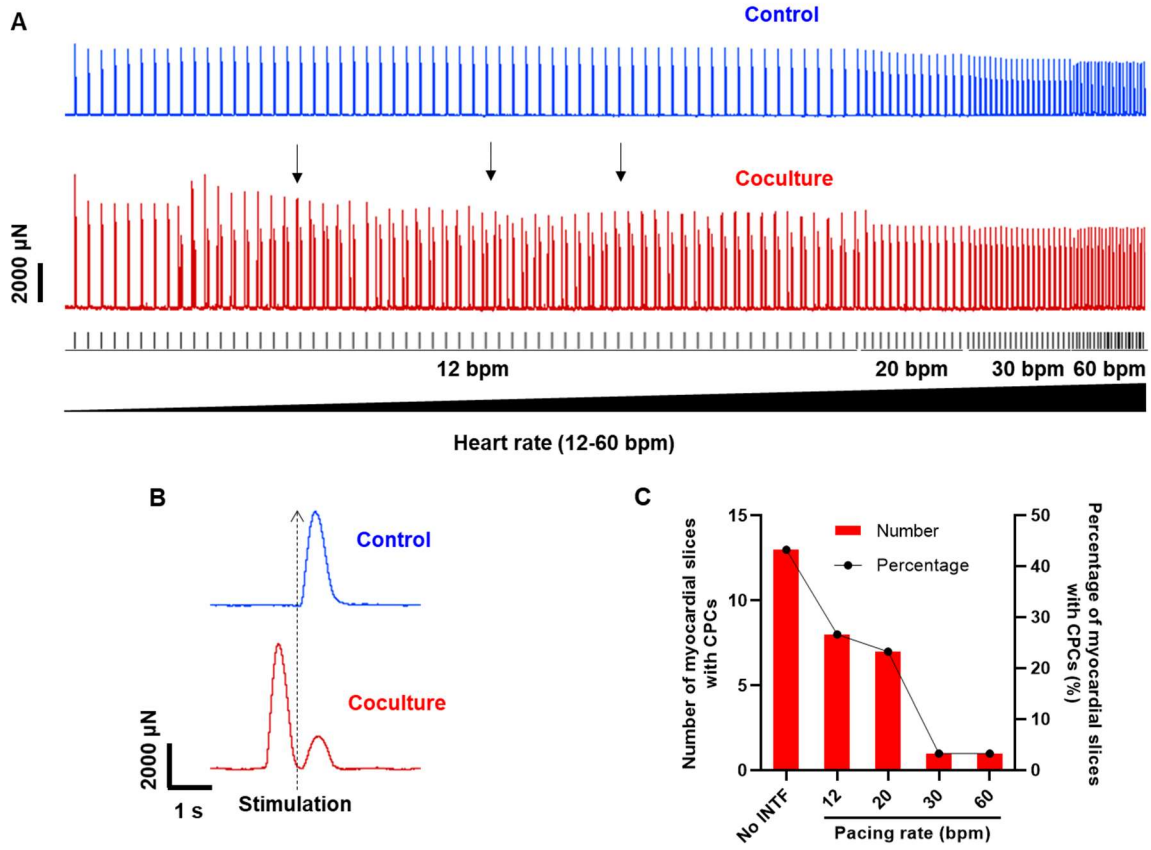

Figure 14. Interference from CPC-derived pacemaker cells with electrical stimulation at ultra-low pacing rates.

(A) Examples of interference of CPC-derived pacemaker cells with external electrical stimulation in cocultured myocardial slices. Black arrows indicate the interference (double peaks) of spontaneous pacing at 12 bpm. (B) Magnified view of interference of spontaneous pacing to external stimulation at a contraction rate of 12 bpm. (C) Incidence of autonomic contractions in CPCs-cocultured myocardial slices at different rates of external pacing. The standard electrical stimulation frequency (30 bpm) suppressed spontaneous contractions in 29 of 30 CPCs-cocultured myocardial slices. Pacing rate = electrical stimulation frequency. No INTF = no interference observed in the terminal stage of coculture.

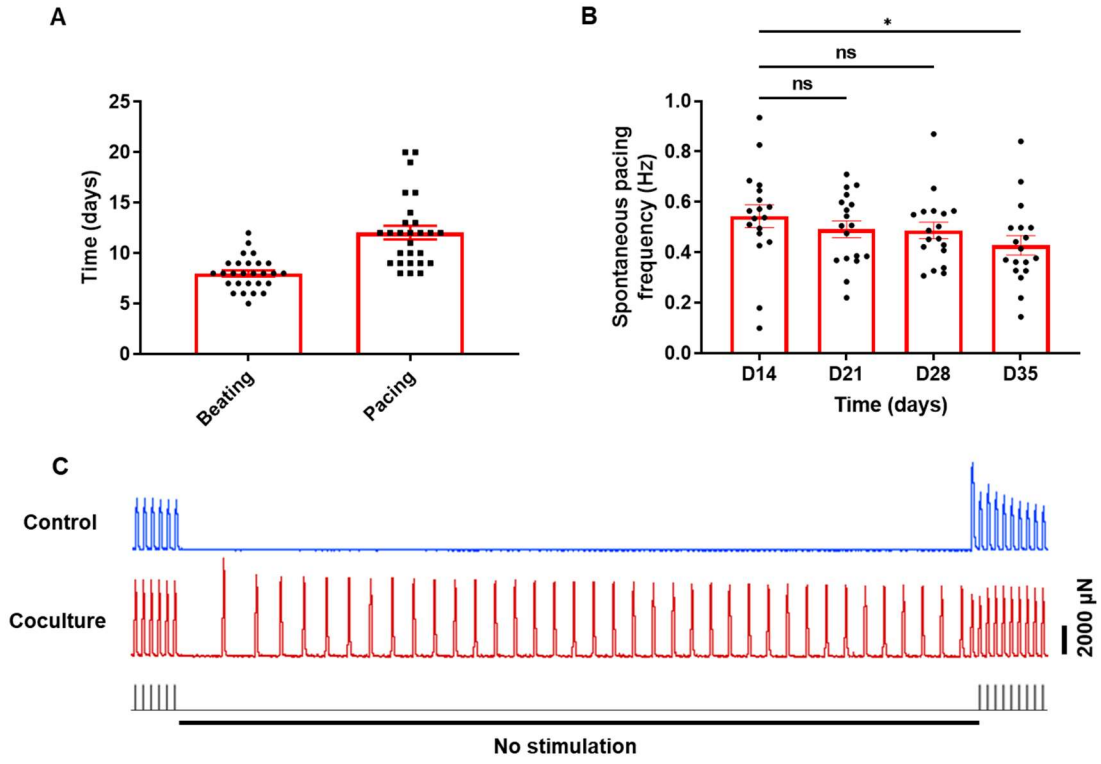

Figure 15. Regular pacing by CPC-derived pacemaker cells without exogenous electrical stimulation in cocultured myocardium.

(A) Average occurrence timepoints of single spontaneous beating and regular spontaneous pacing in coculture. n = 27 CPCs-cocultured myocardial slices from 13 patients. (B) Spontaneous pacing rate of CPC-derived pacemaker cells declined in the course of long-term coculture. n = 18 CPCs-cocultured myocardial slices from 10 patients. One-way ANOVA with Fisher's LSD test versus D14. Data are presented as mean ± SEM. *p < 0.05 applied as a significance cut-off, and ns indicates non-significant difference. (C) CPC-derived pacemaker cells stimulated the contraction of myocardial slices in the absence of external electrical stimulation.

3.5 Targeted tissue integration of CPC-CMs with host failing myocardium

3.5.1 Migration and tissue invasion of CPCs

As intrinsic characteristics of CPCs, remarkable autonomous migration was observed in 2D-cultured CPCs. Initially, CPCs were evenly distributed after seeding. In between days 7-14, CPCs converged to dense cluster (Figure 16A). Expression of specific markers of CPC-CMs (GFP and α-actinin) was detected on day 35 (Figure 16B). We further found that CPCs extensively migrated and invaded into the deep layers of 3D myocardial tissue, reaching from surface down to 80 μm depth, and achieved a widespread presence rather than localized clustering. Moreover, CPCs invasion did not disrupt the myofibers alignment of hfCMs, but led to well-aligned integration of CPCs with the existing structure of hfCMs, as shown in Figure 17.

3.5.2 Localization and distribution of CPC-CMs in cocultured myocardium

Slices of failing myocardium frequently displayed regions devoid of hfCMs and filled with dense extracellular matrix, which might reflect the incidence of fibrosis (Figure 18A). Interestingly, CPC-CMs exhibited a distinct positional orientation in the myocardial fibrotic regions, and prominently located to adjacent host native cardiomyocytes (Figure 18B). CPC-CMs preferentially attached and distributed around the myofibrils of host failing cardiomyocytes (Figure 19). Unlike clustered CPC-CMs in 2D culture, transplanted CPCs distributed homogeneously in the host myocardium, and time-dependently formed network structures throughout the myocardial regions (Figure 20A), and eventually differentiated to α-actinin-expressing cardiomyocytes (Figure 20B).

3.5.3 Morphology of electrical and mechanical coupling of CPC-CMs and cocultured myocardium

Immunofluorescence images demonstrated the formation of gap junctions (identified by connexin-43) and of adherens junctions (identified by N-cadherin, a calcium-dependent cell adhesion molecule) between CPC-CMs and host cardiomyocytes. Connexin-43 was primarily localized at the intercellular junctions, showing a punctate distribution, indicating the formation of typical gap junctions

for electrical and calcium coupling with hfCMs (Figure 21). N-cadherin was expressed at cell-cell contact areas, displaying a continuous band-like distribution, indicating the formation of firm intercellular adhesion junctions for established mechanical coupling with hfCMs (Figure 22).

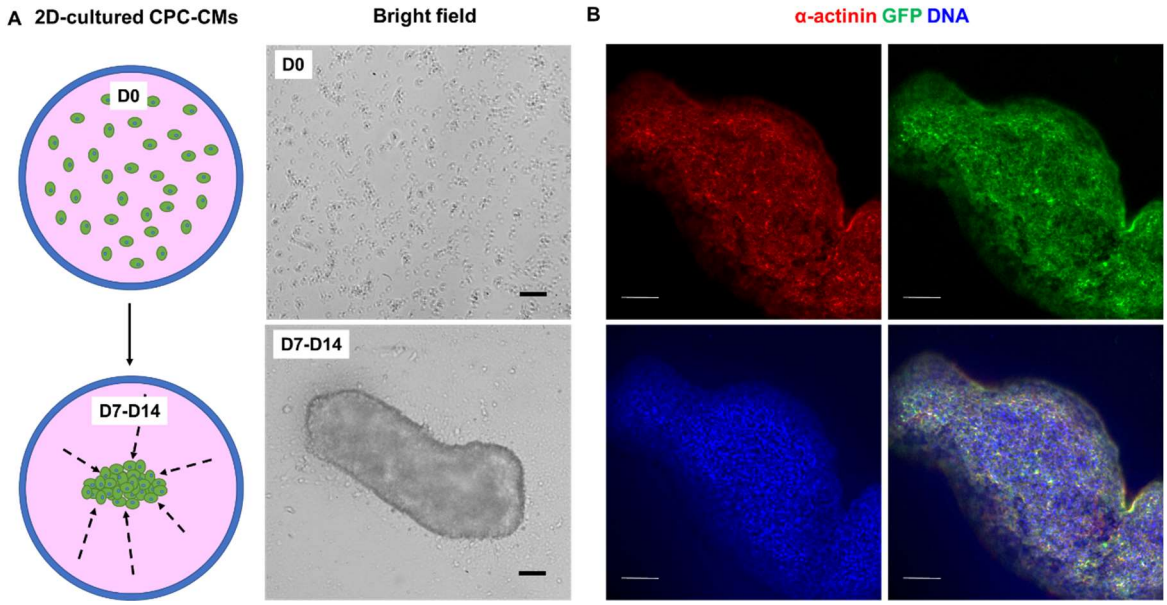

Figure 16. Autonomous migration and morphological structure of 2D-cultured CPC-CMs.

(A) Schematic and bright-field imaging of CPCs migration in 2D culture. D0 and D7-D14 = Day 0 and day7-day14. Dashed arrows indicate the migration direction of CPCs. Scale bar 100 μm. (B) Immunofluorescence imaging of tissue formed through CPCs migration. GFP = GFP antibody. Scale bar 100 μm.

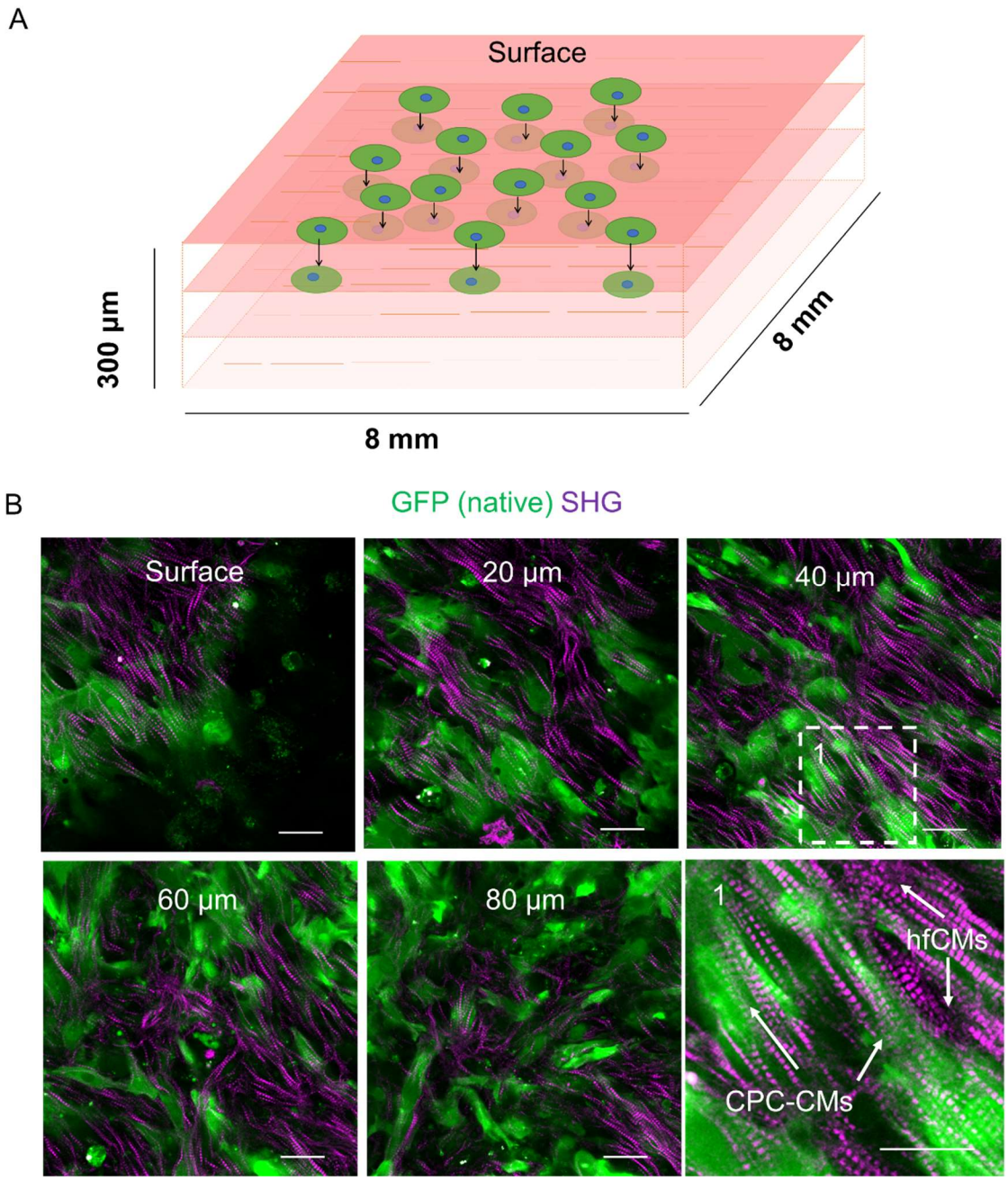

Figure 17. Migration and invasion of CPCs into deep myocardial layers.

(A) Schematic of CPCs-migration in the 3D volume of a cocultured myocardial slice. (B) Layer-by-layer two-photon imaging of a cocultured myocardial slice (surface, 20 µm, 40 µm, 60 µm, 80 µm) and magnified view at 40 µm depth. GFP (native) = eGFP expression in CPC-CMs, SHG = second-harmonic generation to label myofibers. Scale bar, 30 µm, 15 µm (inset 1).

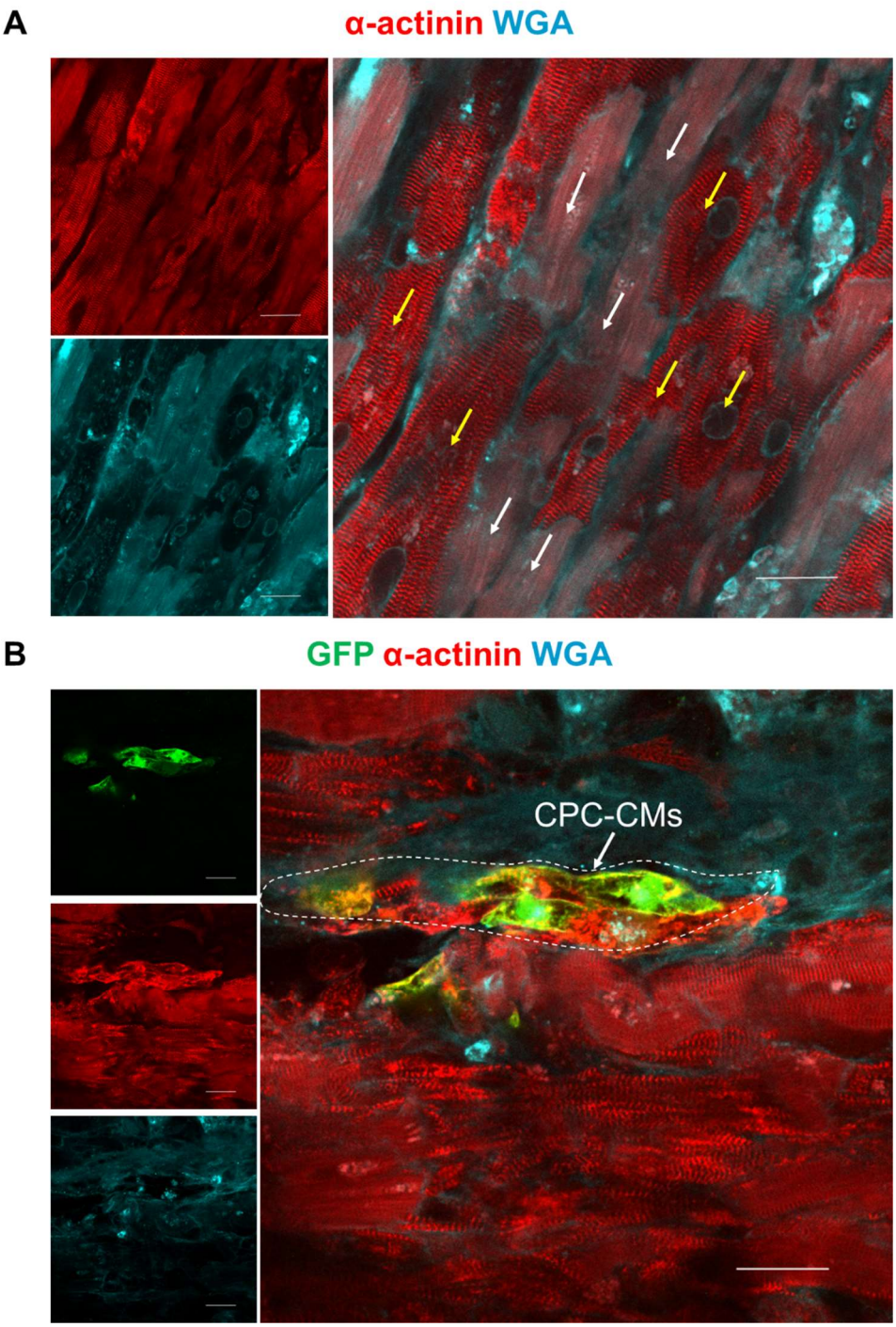

Figure 18. Typical localization of CPC-CMs at the interface of fibrosis and native cardiomyocytes.

(A) Spatial arrangement of cardiomyocytes and connective tissue in failing myocardium. Yellow arrows point to adult failing cardiomyocyte, white arrows indicate the extracellular matrix. Scale bar, 30 µm. (B) Clustering of CPC-CMs at the interface of connective tissue and hfCMs. GFP = GFP antibody. Dashed area represents CPC-CMs. Scale bar, 30 µm.

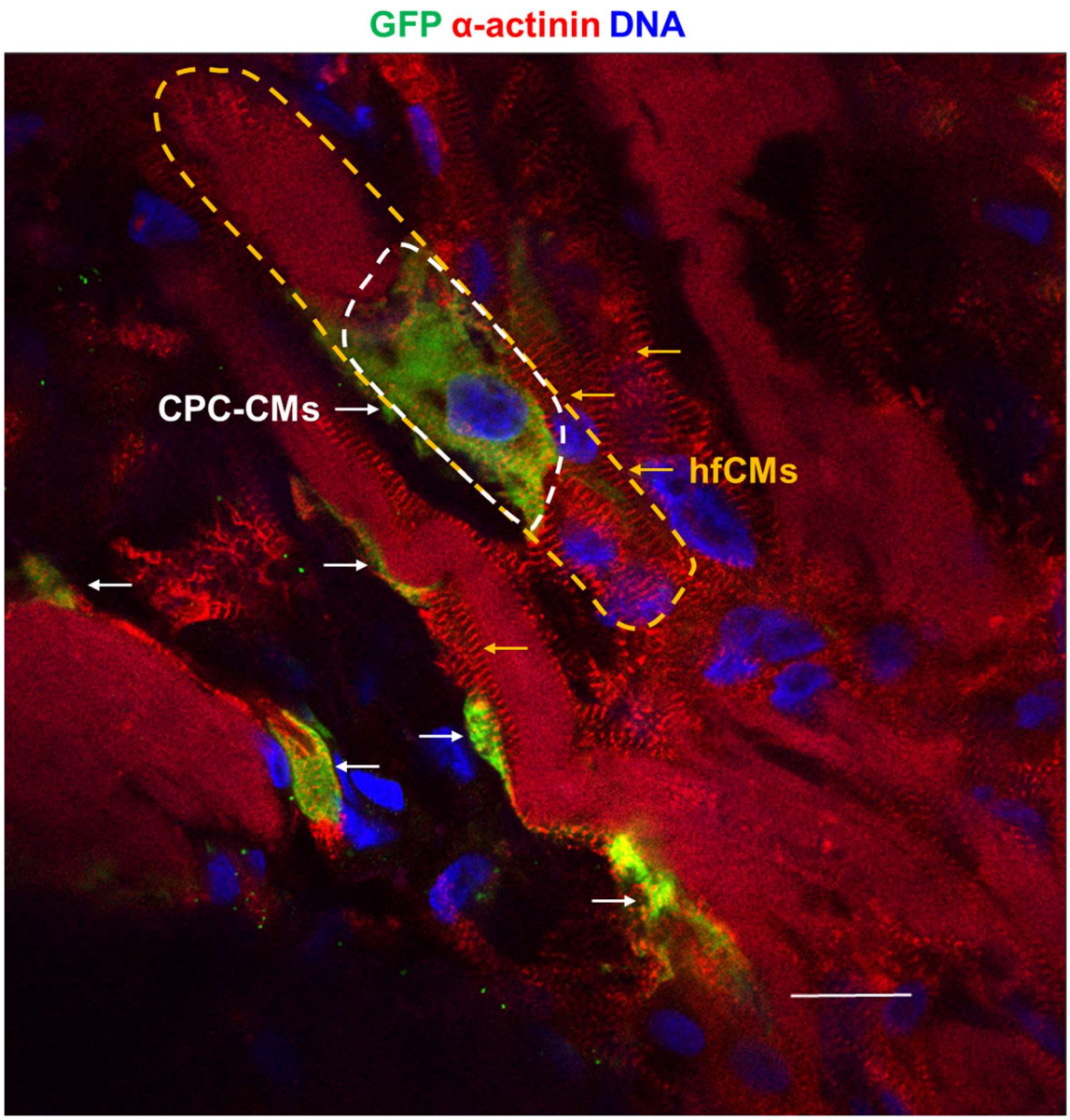

Figure 19. Preferential attachment of CPC-CMs in damaged areas of cocultured myocardium.

White dashed area and white arrows indicate CPC-CMs. Yellow dashed area and yellow arrows indicate hfCMs. GFP = GFP antibody. Scale bar, 20 µm.

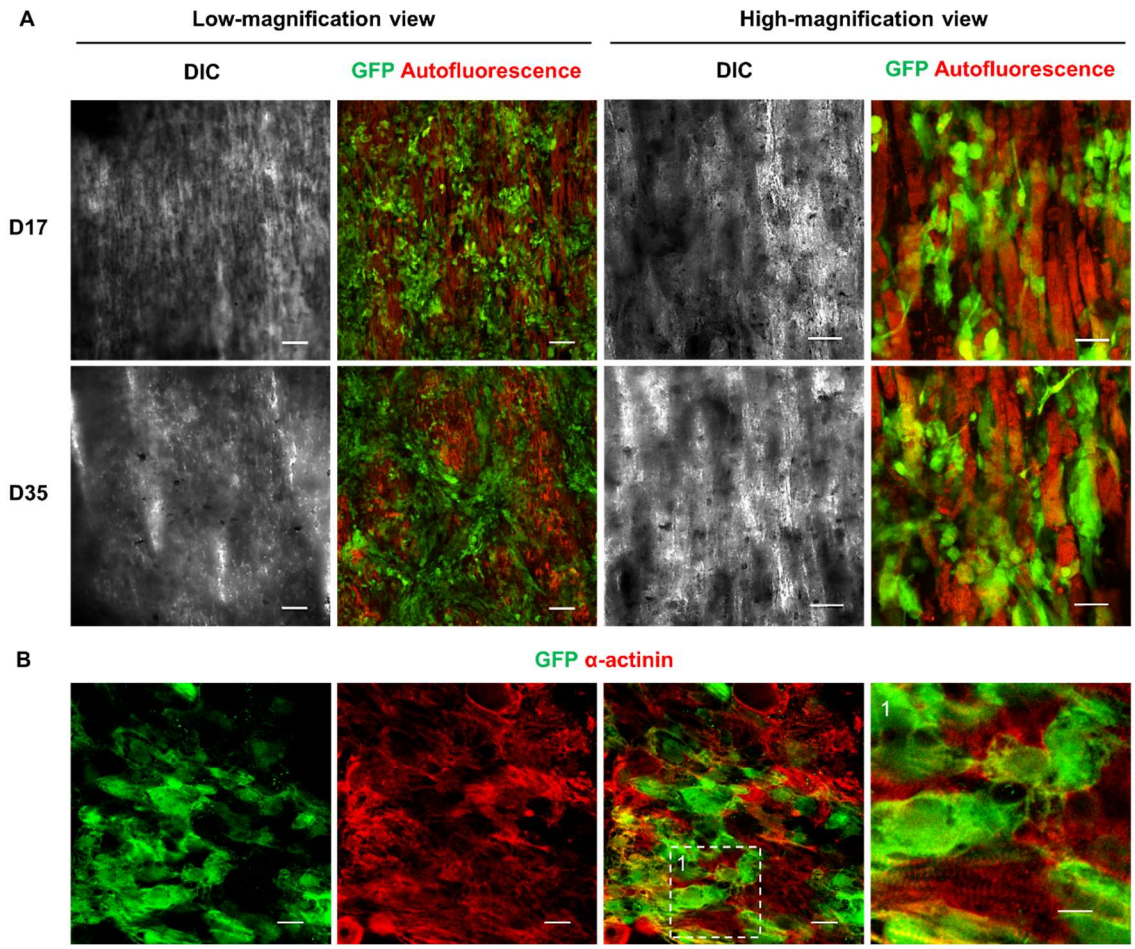

Figure 20. Distribution of CPC-CMs in host failing myocardial slices.

(A) Fluorescence images of CPC-CMs on the surface of host myocardium. DIC = differential interference contrast. D17/D35 = Day 17 and day 35, namely the mid-term and final stages of coculture. GFP (native) = eGFP expression in CPC-CMs at 488 nm excitation, autofluorescence = total autofluorescence at 546 nm excitation. Scale bar, 150 μm in low-magnification view, 50 μm in high-magnification view. (B) Immunofluorescence images of CPC-derived and native cardiomyocytes in 50 μm depth of myocardium. GFP = GFP antibody. Scale bar, 20 μm, 10 μm (inset 1).

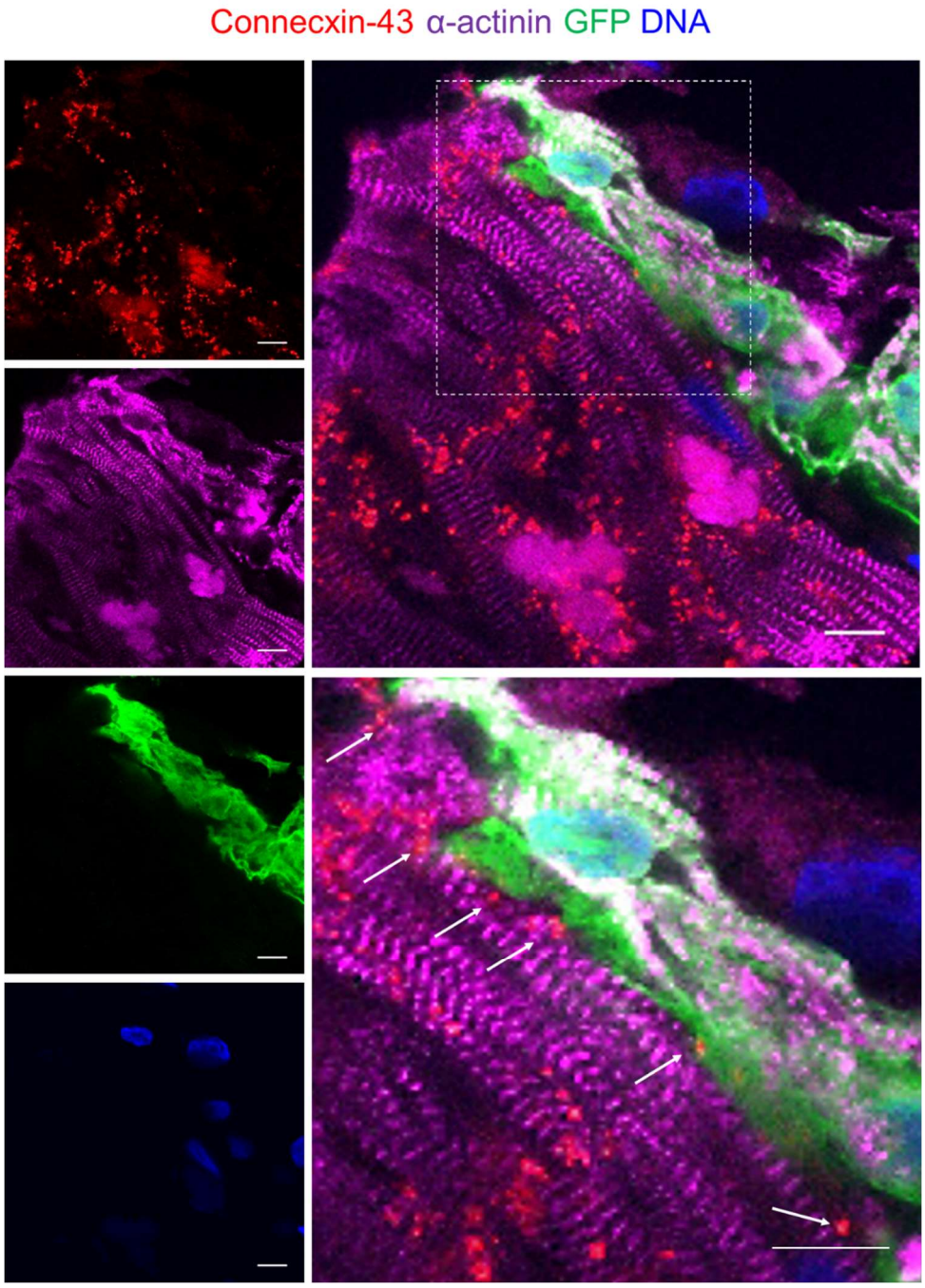

Figure 21. Gap junction formation (connexin-43) between CPC-CMs and hfCMs.

GFP = GFP antibody. Scale bar, 10 µm, 10 µm (inset). White arrows indicate connexin-43.

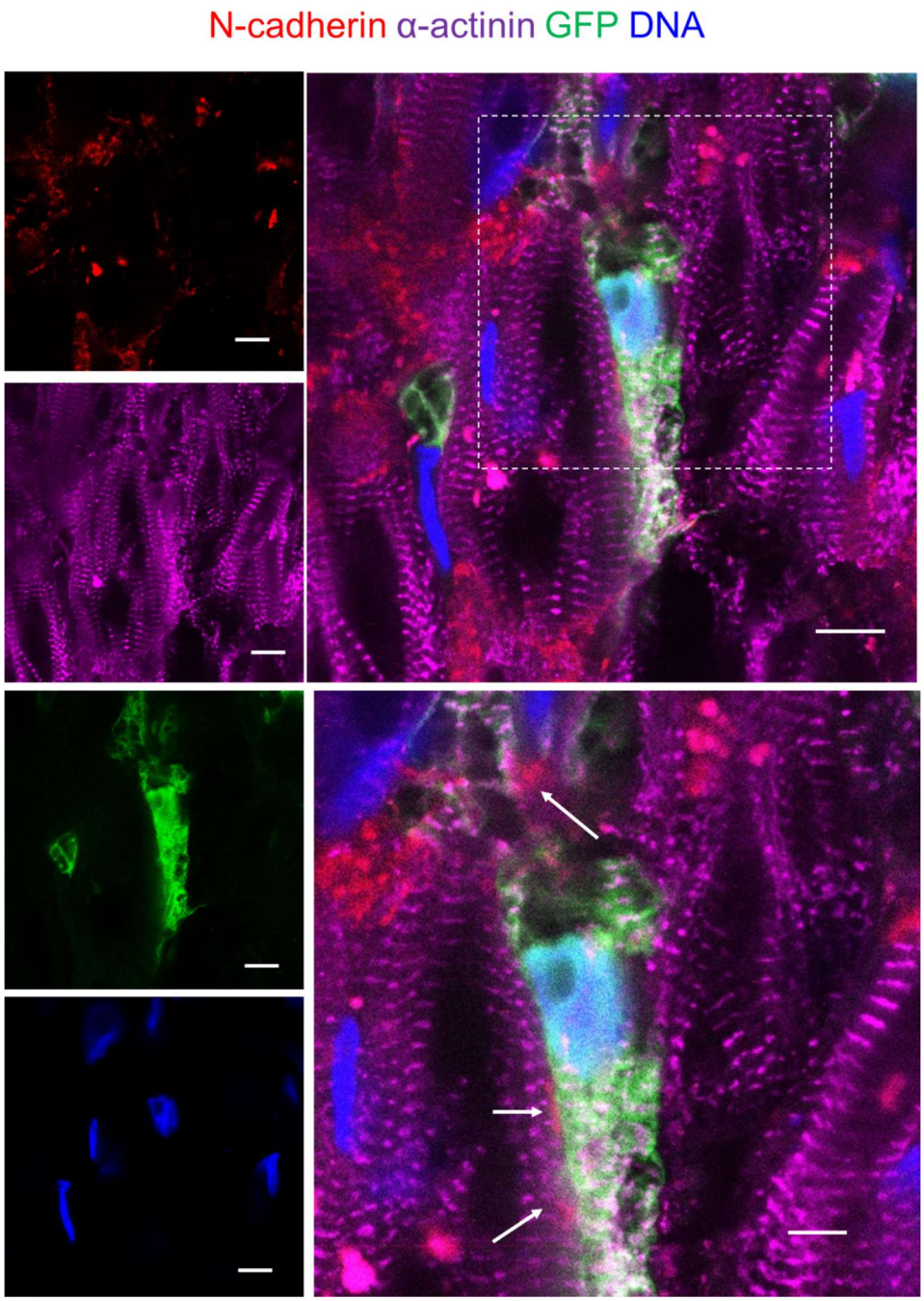

Figure 22. Intercellular adherens junction (N-cadherin) between CPC-CMs and hfCMs.

GFP = GFP antibody. Scale bar, 10 µm, 5 µm (inset). White arrows indicate N-cadherin.

3.6 Transcriptomic identification of cell populations in control and coculture

After 5 weeks of culture, the harvested control and cocultured myocardial slices were individually processed for single-nucleus RNA sequencing. The distinct cell populations in the slices were clustered and visualized by UMAP (main panel of Figure 23). Importantly, new cell clusters emerged adjacent to native cell clusters in the cocultured slices, distinct from those in the control, and are considered to be CPC-derived cell populations (complementary subpanel of Figure 23). Subsequently, these populations were characterized as typical myocardial tissues and CPC-CMs with consistent expression of well-established marker genes. Combined dot plots showed the expression of marker genes in the different cell types of global cell populations, encompassing control and coculture conditions. Both CPC-CMs and hfCMs expressed pan-cardiomyocyte-specific genes, whereas CPC-CMs were distinguished from hfCMs by highly expressed genes specific to myocardial development (BMP5, KIF26B, SLIT3) (Figure 24A). Additionally, the above two cell populations (CPC-CMs and hfCMs) were precisely discriminated by sex-specific genes based on their origins: hfCMs, derived from a female patient, were marked by XIST, while CPC-CMs, derived from a male donor, were marked by UTY, as the example shown in Figure 24B. The composition and proportion of cell populations in control and cocultured myocardium are as follows: CPC-CMs (0%, 54.2%), host failing cardiomyocytes (9.3%, 11.1%), fibroblasts (50.5%, 12.6%), pericytes (11.5%, 11.1%), macrophages (12.9%, 6.5%), dendritic cell (11.9%, 3%), endothelial cells (2.2%, 0.5%), neurons (1.6%, 1%), respectively (Figure 24C).

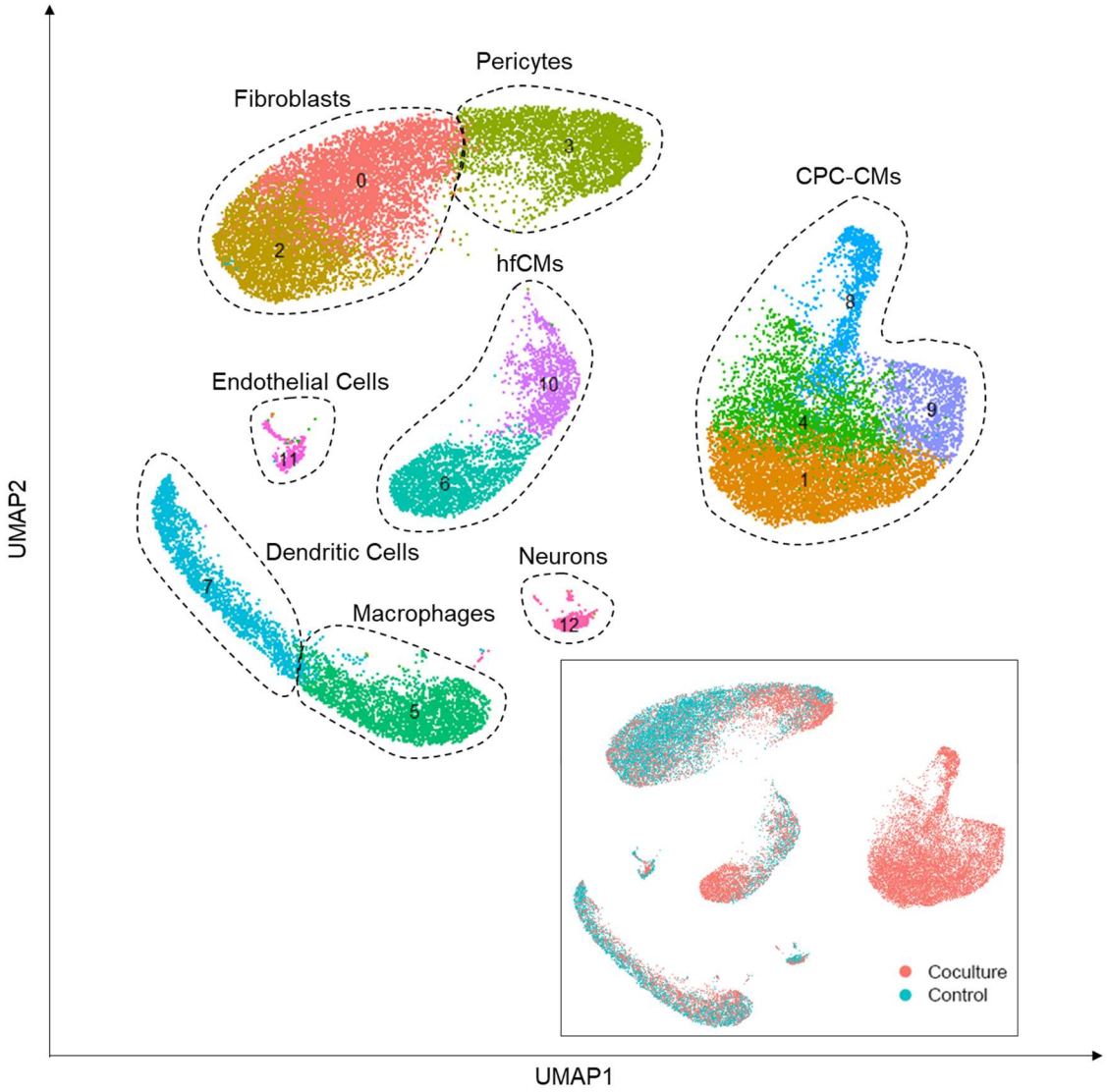

Figure 23. Uniform manifold approximation and projection (UMAP) of cell nuclei in failing myocardium with and without CPCs.

Cell clusters are colored by cell types and are grouped by dashed areas in UMAP. Complementary subpanel is shown in two groups: control myocardium in cyan (n = 3 myocardial slices from 3 patients), and CPCs-cocultured myocardium in coral (n = 3 myocardial slices from the same 3 patients, were each seeded with CPCs).

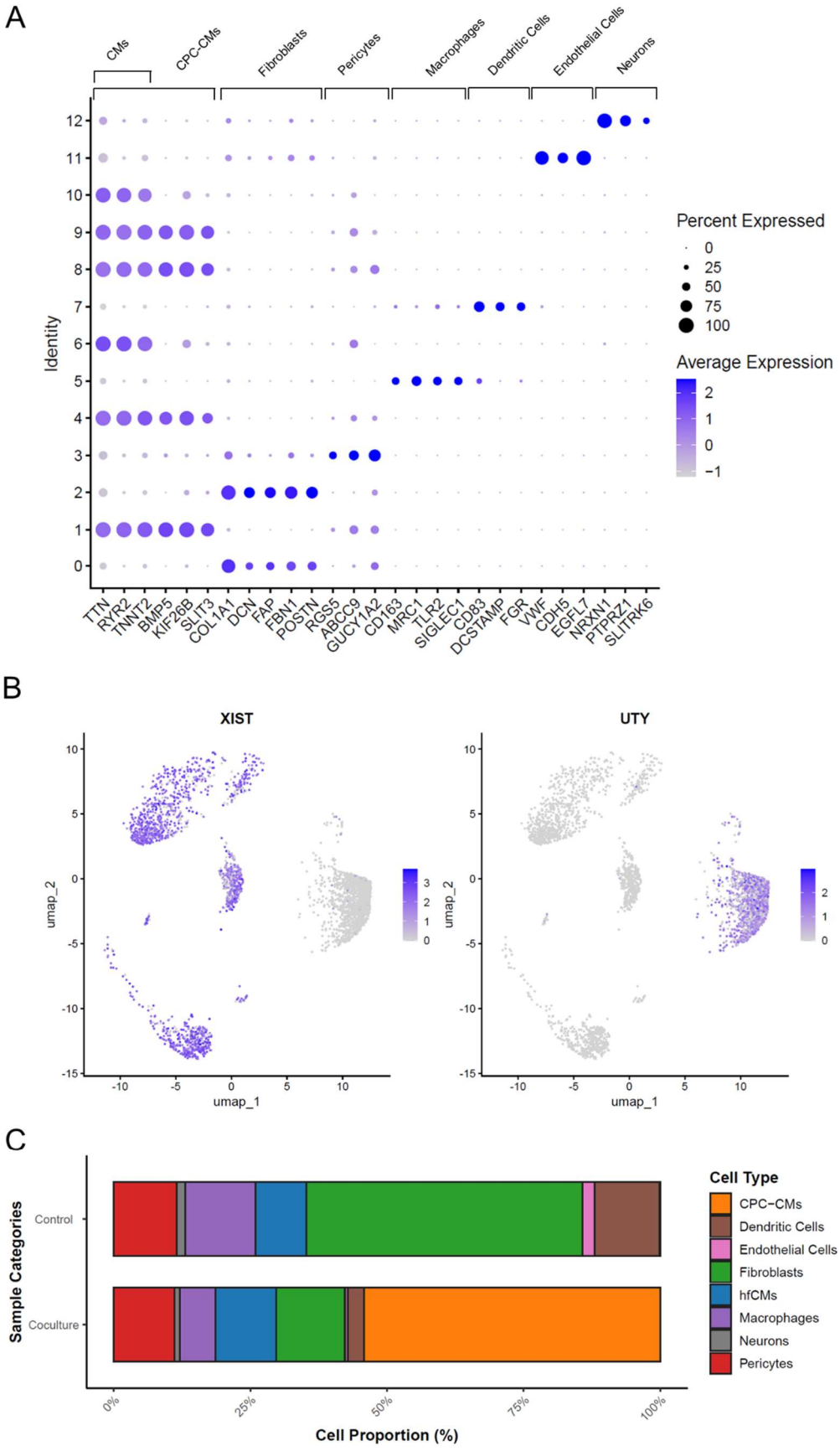

Figure 24. Identification and proportion of cell populations in failing myocardium with and without CPCs.

(A) Relative expression plots of marker genes for cell type annotation. CMs = cardiomyocytes. (B) Example feature plot of sex-specific genes (XIST for female in host myocardial slice, UTY for male in CPC-CMs). (C) Average proportions of cell types in control and CPCs-cocultured myocardium. n = 3 pairs of myocardial slices from 3 patients, with and without CPCs equally.

3.7 Differentiation and maturation of CPC-CMs

3.7.1 Morphological and genetic maturation of CPC-CMs

Structural quantification of cardiomyocytes in immunostaining revealed morphological changes in CPC-CMs, from an irregular pattern in 2D culture to a rod shape in coculture. CPC-CMs were more elongated in coculture (65.8 ± 4.9 µm) compared to 2D culture (15.9 ± 0.9 µm), but their length remained shorter than that of hfCMs (122 ± 5.2 µm). There was no significant difference between the width of cocultured (12.8 ± 1.1 µm) and 2D-cultured (11.1 ± 0.8 µm) CPC-CMs. Both of them were narrower than hfCMs (24.1 ± 2.4 µm). Distinct from 2D-cultured CPC-CMs, length to width ratio of cocultured CPC-CMs resembled to that of hfCMs (1.5 ± 0.1, 5.3 ± 0.7, 5.2 ± 0.5, respectively). Sarcomere length of cocultured CPC-CMs (1.91 ± 0.12 µm) and hfCMs (1.71 ± 0.04 µm) were similar, which was extended than that of 2D-cultured CPC-CMs (1.33 ± 0.06 µm) (Figure 25). To investigate the structural organization of CPC-CMs in relation to hfCMs, we observed that the majority of CPC-CMs (82.6 ± 3.6%) formed spindle-like structures, aligned along the orientation of hfCMs. Whereas a small proportion of CPC-CMs (17.4 ± 3.1%) aggregated into clusters, forming radial α-actinin distribution and node-like structures (Figure 26).

The coexistence of MLC2v and MLC2a, marker proteins of ventricular and atrial myocytes encoded by MYL2 and MYL7 respectively, was found in cocultured CPC-CMs, indicating the lineage diversity and maturity of CPC-CMs differentiation (Figure 27). Furthermore, we quantified the cell proportion of cardiomyocyte specialization in cocultured CPC-CMs based on co-expressed marker genes: co-expression of pan-cardiomyocyte-specific marker genes (RYR2 and TTN, 99.6 ± 0.1%), co-expression of ventricular myocyte-specific marker genes (MYH7 and MYL2, 85 ± 2.6%), co-expression of atrial myocyte-specific marker

genes (MYH6 and MYL7, 24.3 ± 3.7%), co-expression of ventricular and atrial myocyte-specific marker genes (MYH7, MYL2, MYH6 and MYL7, 20.5 ± 1.8%), co-expression of pacemaker cell-specific marker genes (HCN4 and CACNA1G, 1.6 ± 0.4%) as shown in Figure 28.

3.7.2 Developmental trajectory of CPCs differentiation to functional cardiomyocytes

To visualize the dynamic differentiation of CPCs into mature cardiomyocytes, we analyzed pseudotime trajectory of CPC-CMs, which captures continuous differentiation states and pseudotime progression within the cellular development pathway. This analysis revealed the advanced maturation of four CPC-CMs subclusters along the cardiac lineage, progressing toward adult ventricular myocytes in both control and coculture. Remarkably, a minority of cells in subclusters 4 and 9 are close to adult cardiomyocytes in terms of maturity (Figure 29A). The gradual increase in marker gene expression with pseudotime in subclusters indicates that the maturation of CPC-CMs aligns with the temporal variability in cardiomyocyte differentiation. Preferential differentiation into ventricular myocytes occurred in subclusters of CPC-CMs 4 and 9, which highly expressed ventricular specific-markers (MYL2 and PLN). In contrast, subcluster 1 moderately expressed MYL2, PLN, and MYL7, which indicates that these cells were undergoing transitional phase of ventricular differentiation. Additionally, the relatively low expression of pan-cardiomyocyte genes (ACTC1, TNNT2, TPM1) and cardiac lineage-specific genes (MYL2, PLN, MYL7) was present in subcluster 8, which implies that these CPC-CMs were relatively immature and possess a higher differentiation potential (Figure 29B).

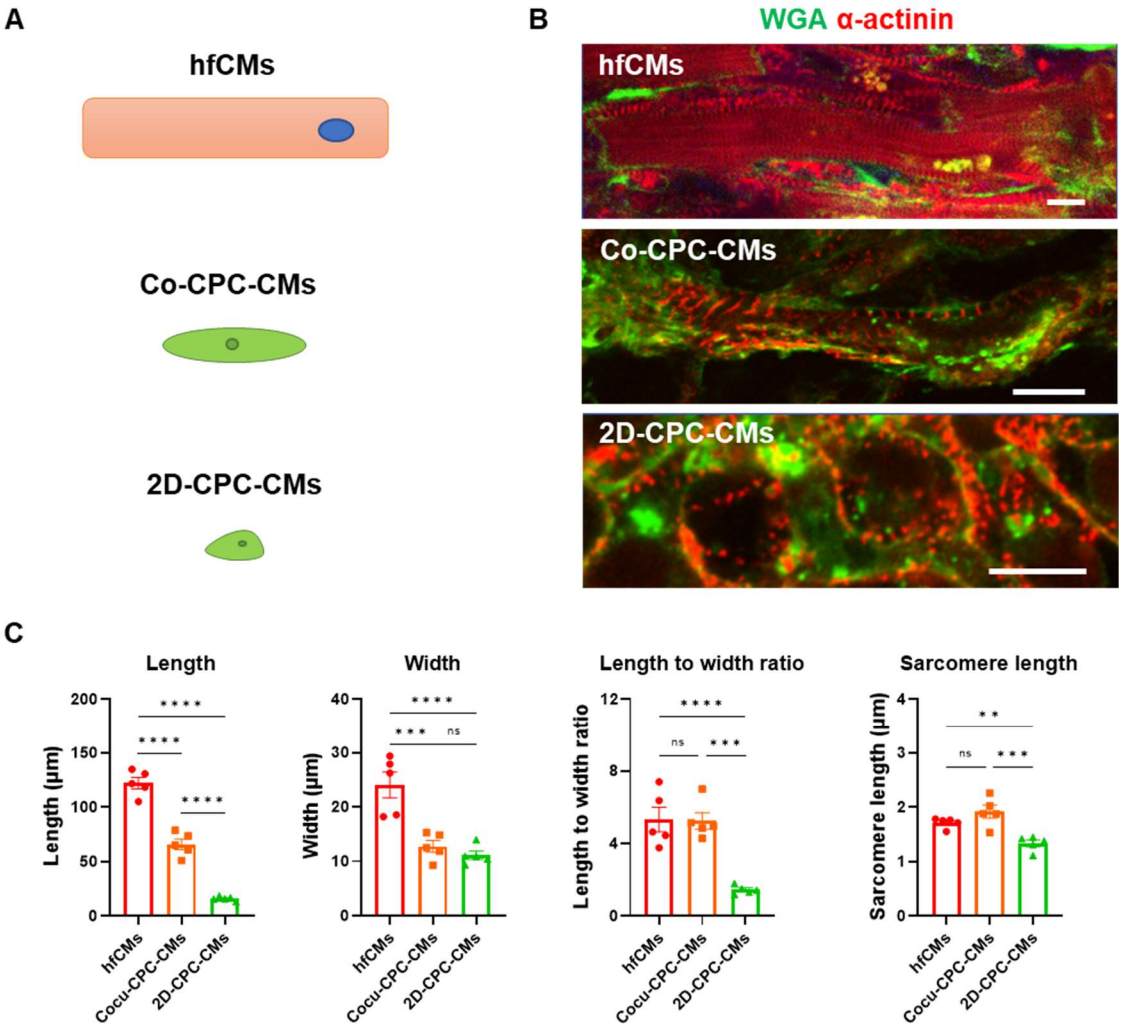

Figure 25. Morphological characteristics of hfCMs and cocultured and 2D-cultured CPC-CMs.

(A) Schematic of cellular morphology of hfCMs, Cocu-CPC-CMs, and 2D-CPC-CMs. hfCMs = host failing cardiomyocytes, Cocu-CPC-CMs = cocultured CPC-derived cardiomyocytes, 2D-CPC-CMs = two dimensional-cultured CPC-derived cardiomyocytes. (B) Immunofluorescence images of hfCMs, Cocu-CPC-CMs, and 2D-CPC-CMs. WGA stains cell membrane. Scale bar, 10 µm. (C) Length, width, length to width ratio, and sarcomere length of hfCMs, Cocu-CPC-CMs, and 2D-CPC-CMs. n = hfCMs and Cocu-CPC-CMs in 5 myocardial slices from 5 patients, 2D-CPC-CMs in 5 repeats. Data are presented as mean ± SEM, one-way ANOVA with Fisher's LSD test. **p < 0.01, ***p < 0.001, and ****p < 0.0001 were applied as significance cut-offs at all instances, and ns indicates non-significant difference.

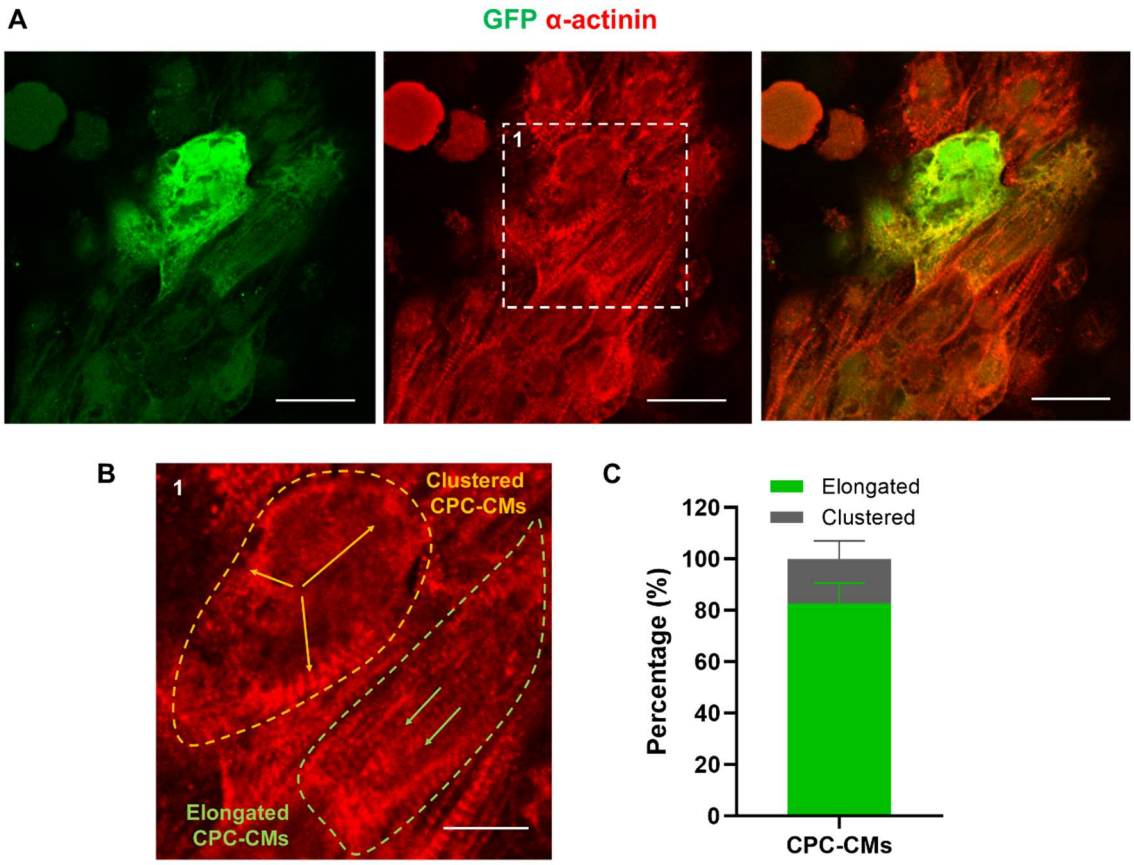

Figure 26. Elongated and clustered structure with arranged myofibers in cocultured CPC-CMs.

(A) Immunofluorescence images of cocultured myocardial slice with CPC-CMs in 50 µm tissue depth. GFP = GFP antibody. Scale bar, 30 µm. (B) Magnification of α-actinin with white dashed box 1 in subfigure (A). Yellow dashed area and arrows in the upper-left indicate clustered CPC-CMs. Green dashed area and arrows in the lower-right indicate elongated CPC-CMs. Scale bar, 15 µm. (C) Percentage of cell number of elongated and clustered CPC-CMs in cocultured myocardium. n = CPC-CMs in 5 cocultured myocardial slices from 5 patients.

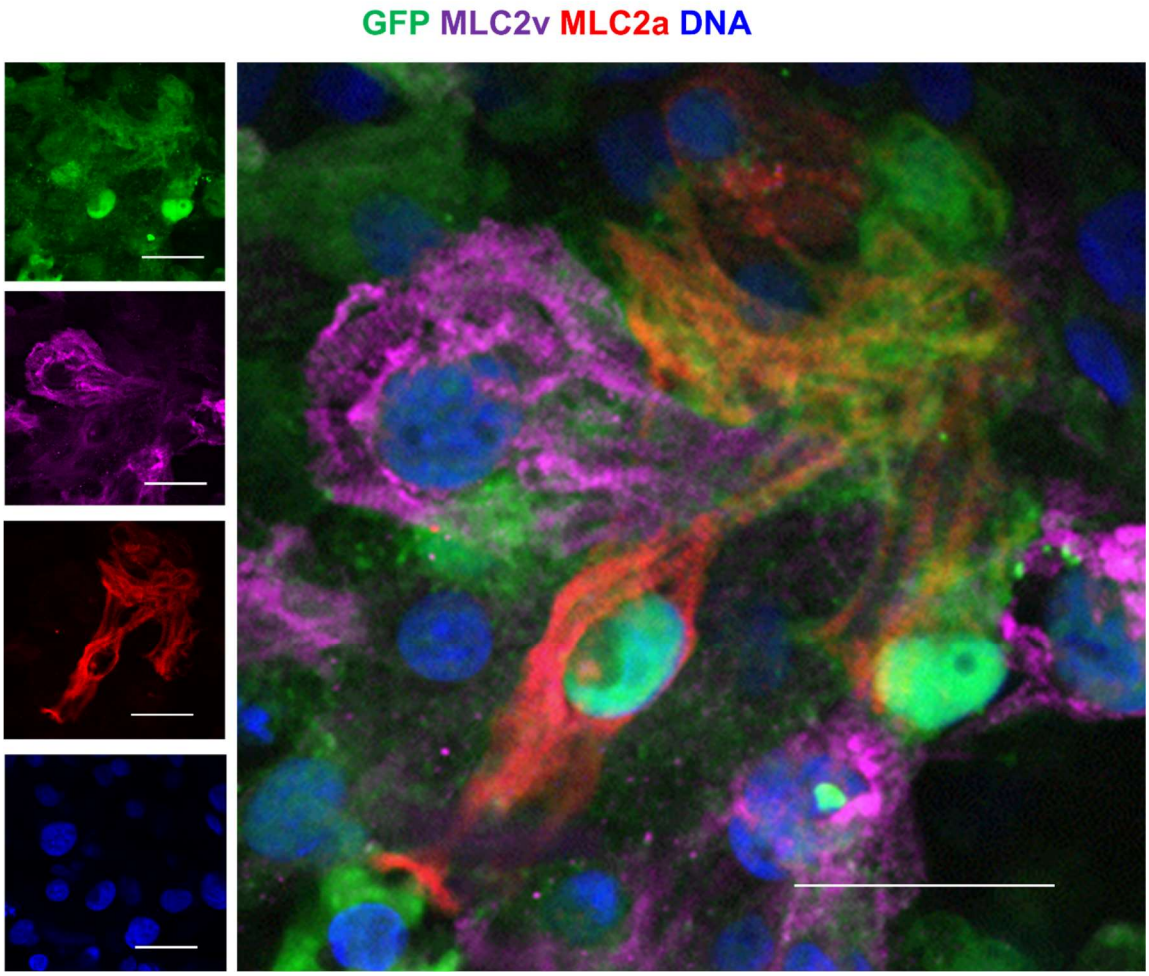

Figure 27. Coexistence of ventricular and atrial lineage-specific proteins (MLC2v and MLC2a) in cocultured CPC-CMs.

GFP = GFP antibody. Scale bar 30 µm.

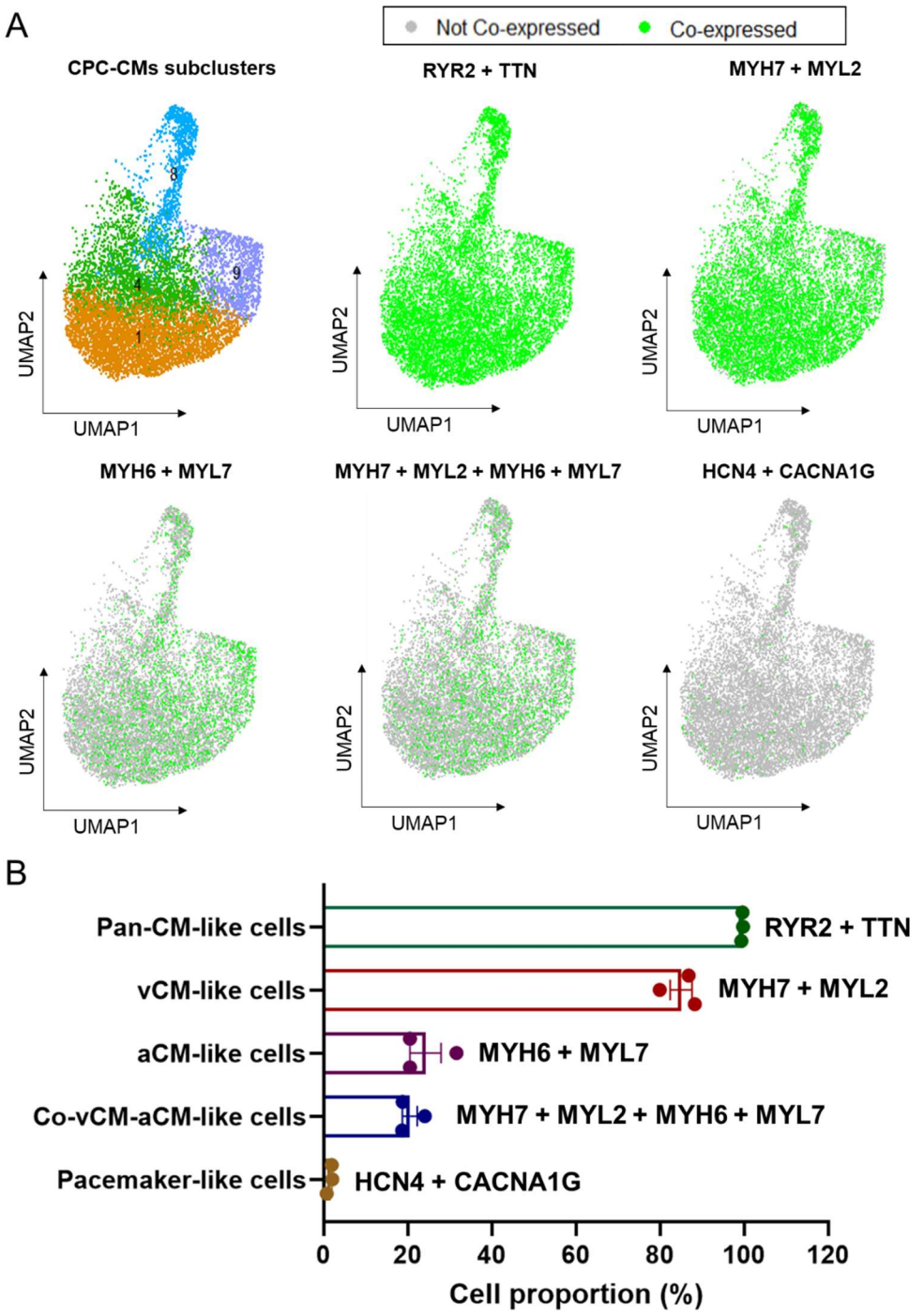

Figure 28. Distribution and proportion of CPC-derived cell types in coculture.

(A) Distribution of cell types of CPC-CMs subclusters in UMAP based on cardiac lineage-specific gene co-expression (RYR2 and TTN for pan-cardiomyocytes, MYH7 and MYL2 for ventricular cardiomyocytes, MYH6 and MYL7 for atrial cardiomyocytes, MYH7 and MYL2 and MYH6 and MYL7 for co-ventricular-atrial cardiomyocytes, HCN4 and CACNA1G for pacemaker cells). (B) Proportion of cardiac-like cell types in CPC-CMs. Pan-CM-like cells = pan-cardiomyocyte-like cells,

vCM-like cells = ventricular cardiomyocyte-like cells, aCM-like cells = atrial cardiomyocyte-like cells, Co-vCM-aCM-like cells = co-expressing ventricular and atrial cardiomyocyte-like cells. n = CPC-CMs in 3 cocultured myocardial slices from 3 patients.

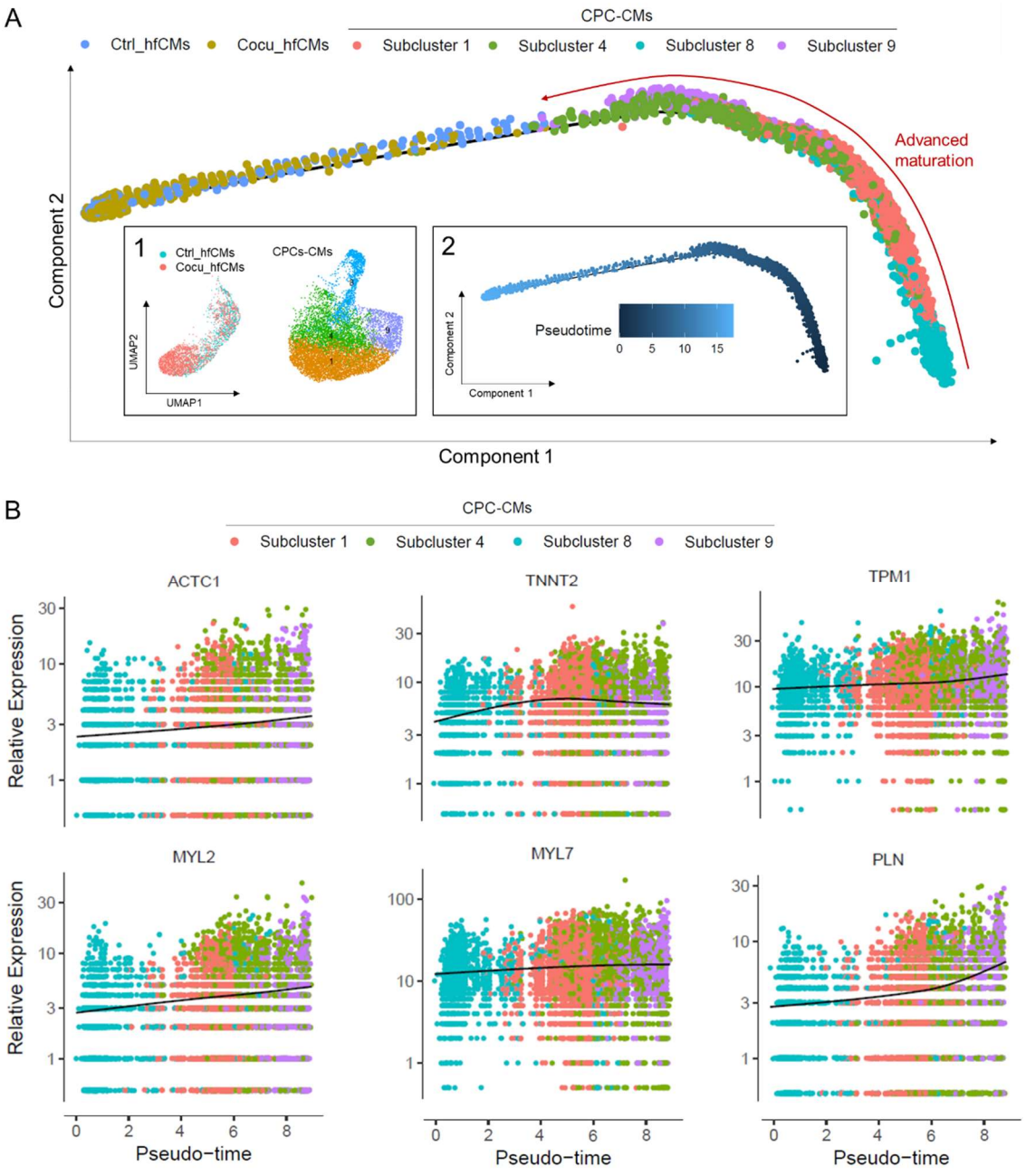

Figure 29. Advanced maturation of cocultured CPC-CMs in pseudotime trajectory.

(A) Trajectory plot of advanced maturation and specification of CPC-CMs compared to adult cardiomyocytes. Ctrl_hfCMs and Cocu_hfCMs = adult cardiomyocytes in control and in coculture, Subcluster 1, 4, 8, 9 = four subclusters of CPC-

CMs. Red-arrowed curve shows the direction of advanced maturation of CPC-CMs subclusters towards adult cardiomyocytes. Inset 1 indicates cell clusters of Ctrl_hfCMs, Cocu_hfCMs, and CPC-CMs in UMAP. Inset 2 depicts a pseudotime plot of adult cardiomyocytes and CPC-CMs. (B) Pseudotime gene expression plots with subclusters of CPC-CMs, including pan-cardiomyocyte-specific genes (ACTC1, TNNT2, TPM1) and cardiac lineage-specific genes (MYL2 and PLN for ventricle, MYL7 for atrium). Relative expression refers to log-normalized gene expression counts. n = CPC-CMs in 3 cocultured myocardial slices from 3 patients.

3.8 Alterations of gene expression and enrichment of native cardiomyocytes in control and coculture

In gene expression profiling of native cardiomyocytes, 1205 differentially expressed genes (DEGs) were downregulated and 364 DEGs were upregulated were in coculture compared to control. However, there were more significant DEGs in coculture than that in control, with higher $-\text{Log}_{10}$ adjusted p-values and Log_2 fold changes. Notably, the contraction-related genes MYL4 and TNNI1, which are specifically expressed during heart development, were significantly upregulated in cocultured native cardiomyocytes (Figure 30A). To understand the functional changes of coculture native cardiomyocytes, we performed the GO enrichment analysis of DEGs on biological processes. In coculture, the top 5 GO enrichments for upregulated DEGs were concentrated on heart contraction and cardiac muscle tissue development, whereas the top 5 GO enrichments for downregulated DEGs were associated with intrinsic apoptotic signaling pathway and response to endoplasmic reticulum stress (Figure 30B).

We conducted GSEA to capture the overall gene expression trends of GO enrichments across the entire gene set in control and cocultured native cardiomyocytes. Enrichment patterns were particularly pronounced for the GO terms 'Cardiac muscle tissue development' (GO:0048738) and 'Heart contraction' (GO:0060047), both of which showed significantly higher enrichment scores in coculture. Furthermore, the running enrichment score curves exhibited a pronounced positive shift towards coculture (Figure 31A). In the enriched gene sets above, genes related to cardiac development and heart contraction that have high expression proportions (defined as being expressed in over 50% of cells within

the coculture population) showed substantially increased expression in coculture compared to control. Among these genes involved in cardiac development, the expression of cardiac morphogenesis and functional adaptation-related genes TBX5 and TBX20 and FHL2 was prominently upregulated in cocultured hfCMs. Meanwhile, the expression of CORIN and ERBB4 and FGF12 was increased in regulatory signaling of cardiac development. Whereas cell-cycle-inhibiting gene G0S2, which maintains the non-proliferative state of cardiomyocytes, were also enhanced in coculture. Regarding heart contraction, intracellular calcium reuptake-associated gene ATP2A2 (SERCA2) exhibited a significantly increased expression in cocultured hfCMs. Concurrently, CACNA2D3 and CACNB2, encoding subunits of L-type voltage-dependent calcium channels for calcium influx, were significantly upregulated. More importantly, MYL4 and MYL7, genes encoding myosin light chains in developing cardiomyocytes, exhibited a pronounced and more widespread expression pattern in cocultured hfCMs. In addition, PDE4D and MYLK3, which are respectively involved in the modulation of cAMP signaling and myosin light chain phosphorylation, were highly expressed in coculture compared to control (Figure 31B).

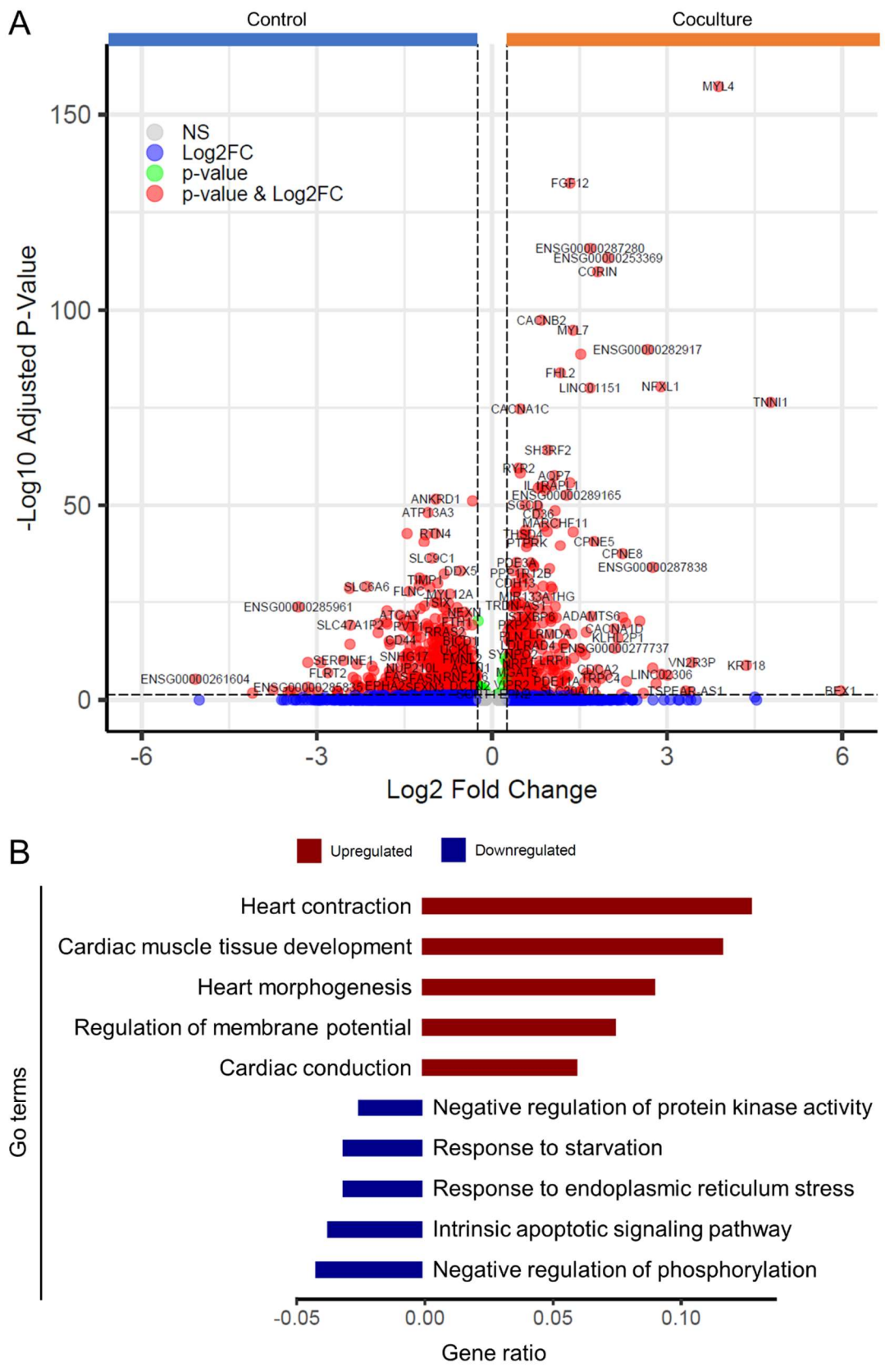

Figure 30. Differentially expressed genes (DEGs) analysis and GO enrichment of native cardiomyocytes in control and coculture.

(A) Volcano plot of DEGs of native cardiomyocytes in control and coculture. Cut-off criteria are p-value < 0.05, $|\log_2 FC| > 0.25$. Upregulated DEGs of native cardiomyocytes in control and coculture were presented on the left and right sides of plot, respectively. (B) Top-ranked GO enrichments for upregulated and down-regulated DEGs of native cardiomyocytes in coculture versus control. Dark red and dark blue bars represent GO terms associated with upregulated and down-regulated DEGs in the coculture compared to the control, respectively. Gene ratio refers to the proportion of DEGs associated with a given GO term relative to the total number of DEGs. n = 3 plain and 3 CPCs-cocultured myocardial slices from 3 patients.

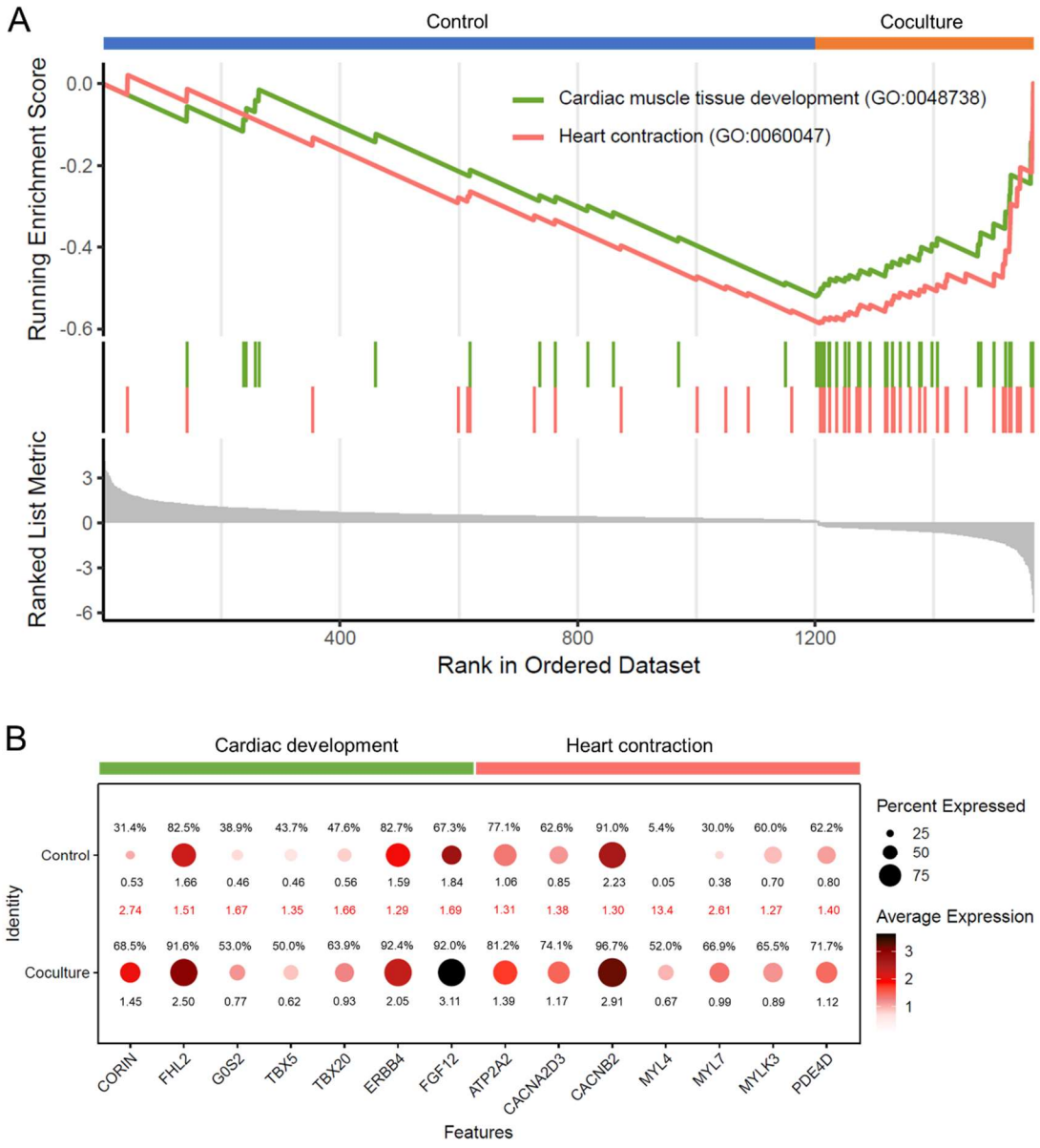

Figure 31. Gene set enrichment analysis (GSEA) of native cardiomyocytes in control and coculture.

(A) GSEA plot of top 2 enriched Go terms: cardiac muscle tissue development and heart contraction. Upregulated genes in control and coculture concentrate on the left and right side (blue and red bars), respectively. Colorful curves reflect the enrichment trend of gene sets, and colorful vertical lines indicate the positions of ranked genes within the enriched GO terms. Genes are ordered by Log_2Fold-Change (Log_2FC) in ranked list metric. (B) Expression plots of selectively enriched genes of native cardiomyocytes related to myocardial contraction and development in control and coculture. Gene selection criteria are as follow: expression proportion in coculture > 50%, average Log_2FC > 0.5, p value < 0.05. Black percentage and values denote the expression proportion and average expression level of genes in control and coculture. Red values show the fold change of gene expression in coculture relative to control. Dot size represents the proportion of cells expressing each gene, color intensity indicates the average expression level. n = 3 plain and 3 CPCs-cocultured myocardial slices from 3 patients.

3.9 Comparative analysis of excitation-contraction coupling-related gene expression in control and cocultured hfCMs with CPC-CMs

To investigate the alteration of excitation-contraction coupling (ECC) among hfCMs in control, hfCMs in coculture, and CPC-CMs in coculture, the key genes on calcium handling (RYR2, CACNA1C, ATP2A2, PLN, CAMK2D, SLC8A1) and on ventricular contractility (MYH7, MYL2, ACTC1, TNNT2, MYBPC3, TPM1) were detected by snRNA-seq. We found that the expression levels of genes involved in calcium-induced calcium release, including RYR2, CACNA1C, ATP2A2, and PLN, were elevated in cocultured hfCMs compared to control. On calcium homeostasis of heart failure, CAMK2D expression was reduced, while SLC8A1 expression was upregulated in coculture. Subsequently, the expression of both myosin-related genes (MYH7, MYL2, MYBPC3) and actin-related genes (ACTC1, TNNT2, TPM1) in hfCMs were upregulated in coculture compared to control. By contrast, the expression pattern of ECC-related genes during cardiac development was observed in cocultured CPC-CMs. In terms of calcium handling, the relatively low expression of RYR2, ATP2A2, PLN, and CAMK2D, combined with the higher expression of CACNA1C and SLC8A1, aligns with the characteristics

of developing cardiomyocytes that sarcoplasmic reticulum remains immature, resulting in calcium handling that mainly relies on sodium-calcium exchange. In terms of contractility, pan-cardiomyocyte-related genes (ACTC1, TNNT2, TPM1) were highly expressed, whereas ventricle-enriched genes (MYH7, MYL2, MYBPC3) were lowly expressed in cocultured CPC-CMs compared to hfCMs, indicating an incomplete development of ventricular contractile machinery relative to fully developed cardiomyocytes (Figure 32).

3.10 Cellular communication and cross-talk between CPC-CMs and hfCMs in coculture

Our results suggest the potential for ligand-receptor-mediated intercellular communication between hfCMs and CPC-CMs. Based on CellChat predictions, CPC-CMs-to-hfCMs communication was more intense than the reverse, while CPC-CMs-to-CPC-CMs communication was more frequent than hfCMs-to-hfCMs communication (Figure 33A). Contact-dependent communications were inferred between hfCMs and CPC-CMs through signaling pathways of homophilic cell adhesion (CDH2-CDH2, NCAM1-NCAM1, PTPRM-PTPRM), which maintained high frequency of communication strength. In addition, PTPRM-PTPRM communication was not predicted in CPC-CMs-to-CPC-CMs communication. The hfCMs communicate with CPC-CMs via SEMA3C-(NRP1 + PLXNA4) signaling pathway, while CPC-CMs interact with hfCMs through NRG3-ERBB4 and BMP5-(BMPR1A + BMPR2) signaling pathways. In particular, BMP5-(BMPR1A + BMPR2) signaling pathway exhibits moderate communication strength. Moreover, extracellular matrix-mediated communications, those involving laminin and collagen, were extensively identified between hfCMs and CPC-CMs, especially in communications where LAMA2 functions as a ligand (Figure 33B).

3.11 CPC-CMs-mediated gene regulatory network in cocultured hfCMs

Through gene co-expression-based SCENIC, we characterized the gene regulatory networks in cocultured hfCMs, and predicted a potential correlation between CPCs-mediated intercellular communications and functional alterations of cocultured hfCMs. Based on ligand-receptor pairs (CDH2-CDH2, PTPRM-

PTPRM, NCAM1-NCAM1, BMP5-BMPR1A, and NRG3-ERBB4) inferred in CPC-CMs-to-hfCMs communications, we found that these receptor genes were involved in the same gene regulatory network (GRN). Furthermore, we identified that three transcription factors NFIA, NFIB, and ZBTB20 co-regulated these above receptor genes, which respectively comprised three independent regulons in GRN. Interestingly, the target genes associated with cardiac development (TBX5, GATA6, MEF2A, MEF2C, FOXP1, SMAD2, SMAD5, FHL2, IGF1R, ZFPM2) and excitation-contraction coupling (RYR2, TPM1, CACNA2D1, CACNB2, CAMK2D, SCN5A) signaling pathways were modulated by the above three transcription factors. These findings suggest that CPC-mediated intercellular communications may regulate signaling pathways associated with cardiac development and contraction in hfCMs (Figure 34).

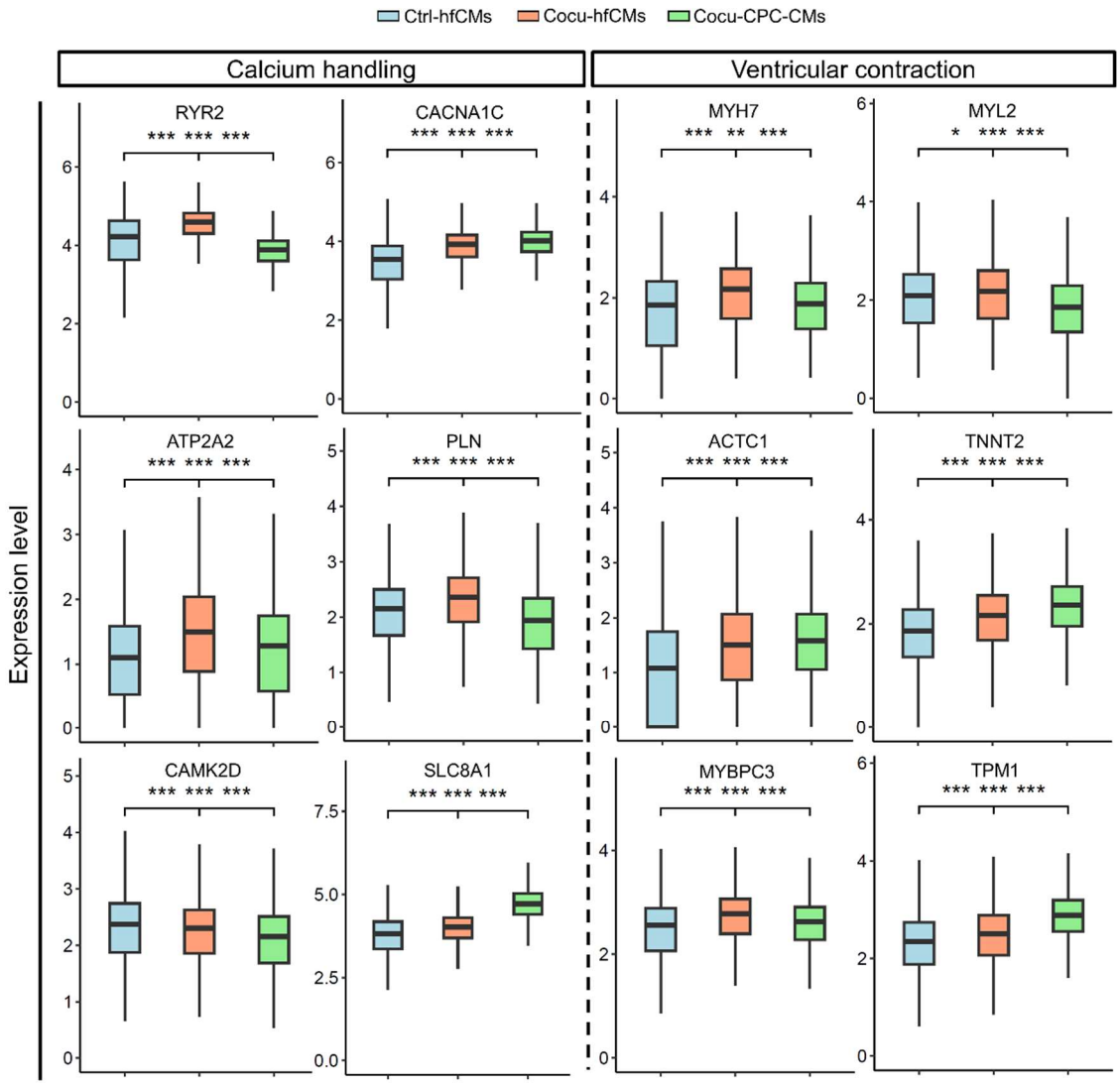

Figure 32. Comparison of calcium handling and ventricular contraction-related gene expression in control and cocultured failing cardiomyocytes with CPC-CMs.

Ctrl-hfCMs = failing cardiomyocytes in control, Cocu-hfCMs = host failing cardiomyocytes in coculture, Cocu-CPC-CMs = CPC-derived cardiomyocytes in coculture. Expression level represents log-normalized gene expression counts. n = 3 plain and 3 CPCs-cocultured myocardial slices from 3 patients. Kruskal-Wallis test with Dunn's test was performed for multi-comparisons. Data are presented as median with interquartile range (IQR). *p < 0.05, **p < 0.01 and ***p < 0.001 were applied as significance cut-offs at all instances.

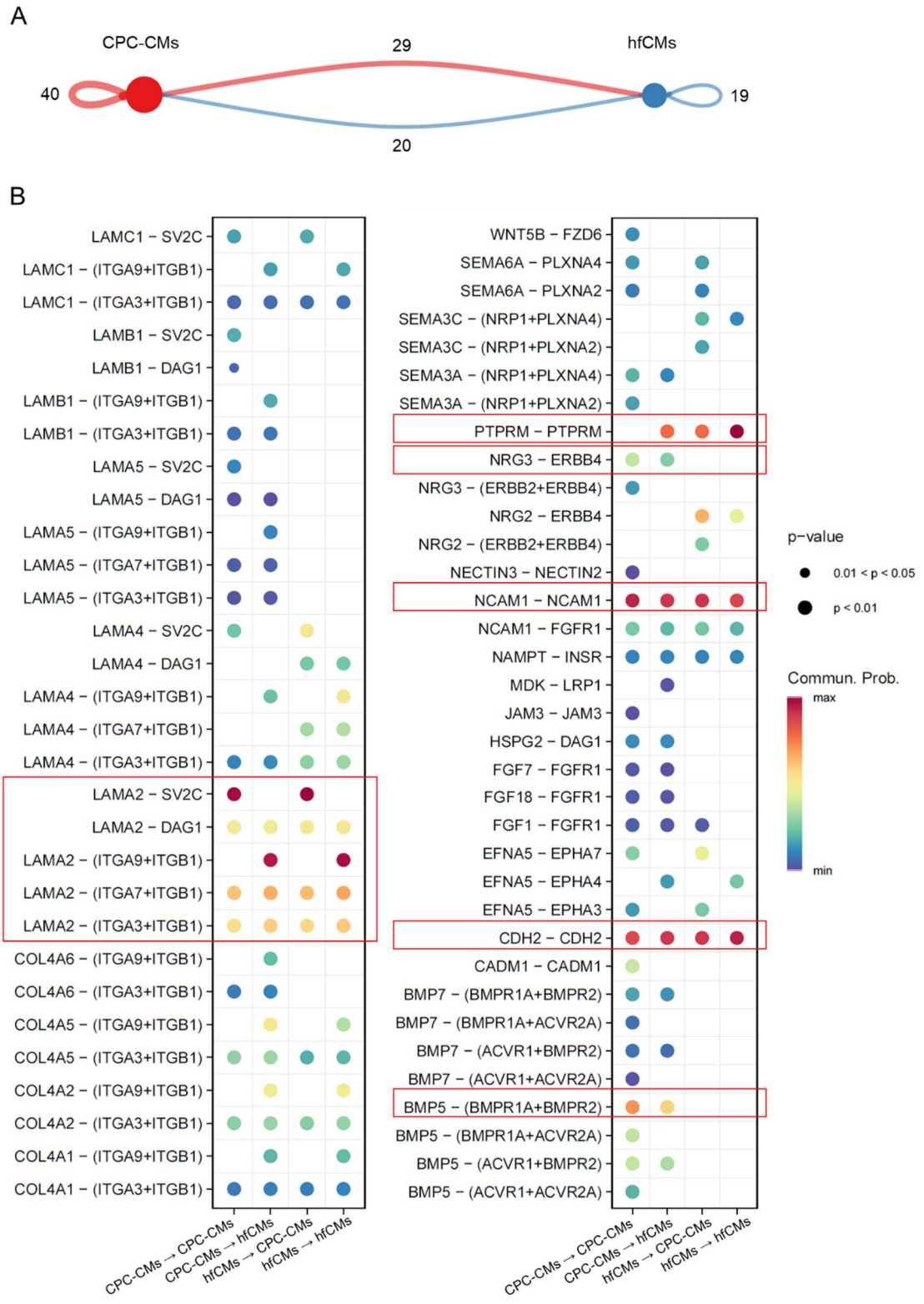

Figure 33. Cell-to-cell communications between hfCMs and CPC-CMs in co-culture.

(A) Overview of cell-to-cell communications between hfCMs and CPC-CMs in co-culture. Numerical values represent the total probability of communications, defined as communication strength. (B) Signaling pathways of mutual and internal

interactions between hfCMs and CPC-CMs in coculture. Commun. Prob. = communication probability. n = 3 myocardial slices from 3 patients, all cocultured with CPCs. Red rectangles indicate the significant and frequent signaling pathways.

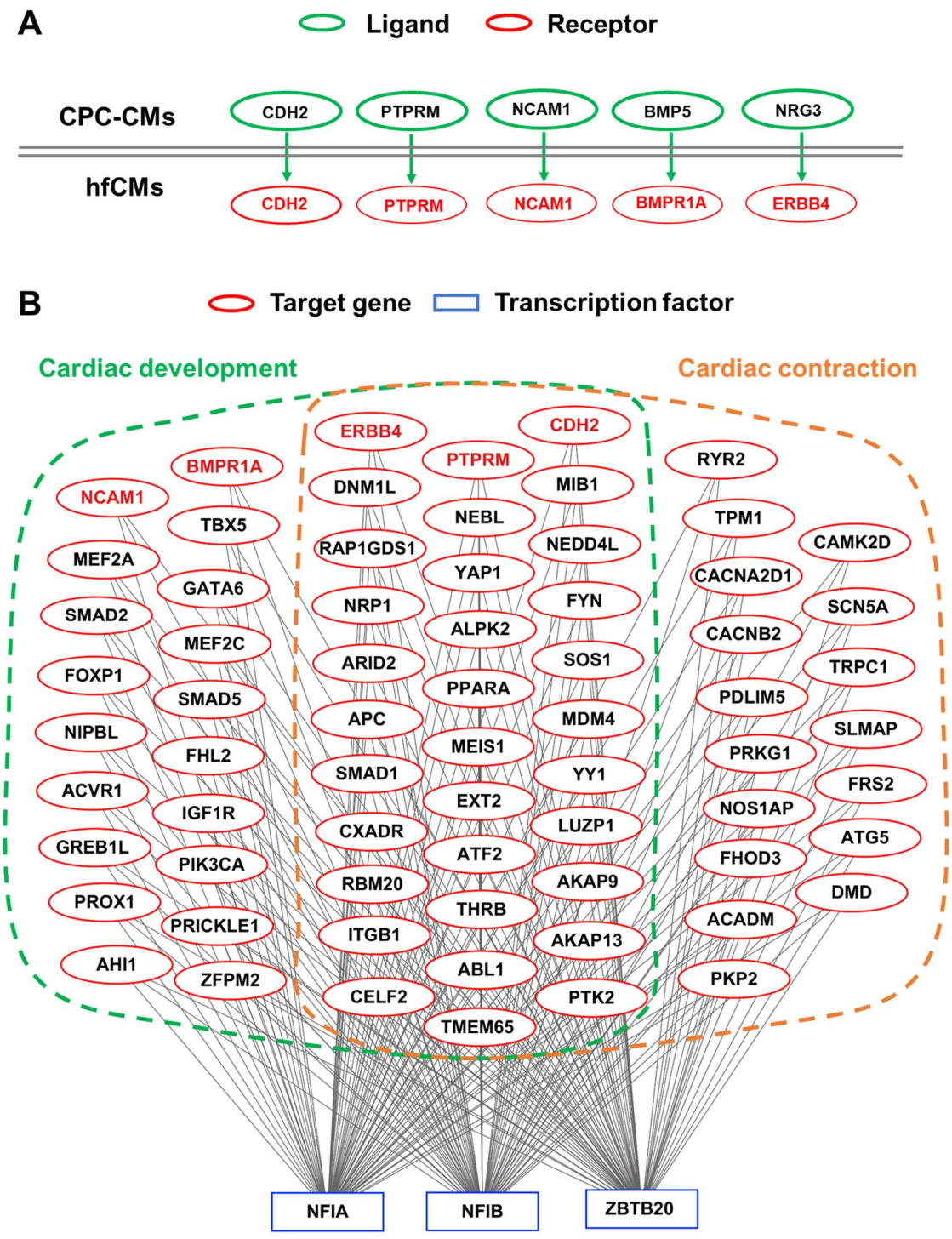

Figure 34. Gene regulatory networks in cocultured failing myocardium.

(A) Selected and frequent receptor-ligand communications from CPC-CMs to hfCMs in coculture, based on data from Figure 33. (B) Predicted downstream

regulatory networks of target genes, including receptor genes, in cocultured hfCMs. The target genes were co-regulated by three transcription factors (TFs: NFIA, NFIB, and ZBTB20), forming TFs-governed regulons. Dashed areas represent enriched target genes which are involved in cardiac development and cardiac contraction, including the intersection of both enrichments. Red-labeled target genes are receptor genes involved in CPC-CMs-to-hfCMs communications. n = 3 myocardial slices from 3 patients, all cocultured with CPCs.

4. Discussion

Distinguished from previous in-vivo animal and in-vitro cell line models of heart failure [65-67], the present study is based on our developed technique for long-term culture of myocardial tissues. We have been able to maintain the structural integrity and sustained functionality of excised human failing myocardial tissue slices for several months, while monitoring real-time force development and continuously recording functional changes. By inoculating CPCs onto these myocardial tissue slices and coculturing them, we demonstrated the beneficial effects of CPCs on the cardiac function of failing myocardium. This study represents the comprehensive evaluation of the tissue integration and functional synchronization between CPCs and host human failing myocardium from left ventricle of patients with heart failure ex vivo, revealing cellular interactions between graft and host. Our findings indicate that CPCs firmly attach to myocardial tissue in high abundance, and their proportion far exceeds that of native cardiomyocytes in coculture. This attachment facilitates tissue integration between them, forming the structural foundation for electromechanical coupling. Remarkably, the significant increase in contractility was accompanied by a delay in ECC in CPCs-cocultured myocardium, and there was minimal interference from the spontaneous activity of CPC-CMs to the routine pacing. Single-nucleus sequencing suggests that both direct and indirect communication between them may modulate the maturation of CPC-CMs and the dedifferentiation-redifferentiation of host failing cardiomyocytes, potentially influencing their functional synchronization.

4.1 Functional improvement and synchronization in CPCs-cocultured host failing myocardium

A substantial enhancement of contractility was detected in CPCs-grafted myocardial slices, which has not been elucidated previously due to the low survival rate of CPCs after intramyocardial injection in vivo [68]. In the early stage of our coculture, a modest increase of contractile force was observed, which parallels the improvement in myocardial function attributed to the application of CPC-derived EVs [31]. In contrast, a marked intensification of total contractile force was developed in the late stage, likely resulting from the contractile contributions and mechanical coupling of differentiated CPC-CMs with the host myocardium [69].

Our results demonstrate that CPC-CMs effectively coupled with hfCMs and enhanced integral coupling in cocultured myocardium, which manifests the mutual adaptation of CPC-CMs and host myocardium. Synchronized contraction of CPC-CMs and host failing myocardium across the full range of pacing frequencies indicates the achievement of electromechanical coupling between them. Moreover, the increase of MCR in cocultured myocardium demonstrates that electromechanical coupling was improved after CPCs transplantation. Likewise, the contractile characteristics of cocultured myocardium were altered due to the functional synchronization. Contractility enhancement co-occurred with the compensatory prolongation of contraction kinetics at low frequencies, which implies certain adaptive modifications in host myocardium. The more negative FFR at high pacing frequencies may be attributed to the immaturity of CPC-CMs and their heterogeneity relative to the host myocardium. Despite the majority of CPC-CMs co-expressing ventricular marker genes (MYL2 and MYH7), MYL7 was also widely and highly expressed as the marker gene of intermediate differentiation stage, which occurs throughout the specific functionalization of CPC-CMs [70]. Correspondingly, the expression of non-ventricle-specific myofibers-related genes (MYL4 and MYL7) and ventricle-specific myofibers-related genes (MYL2 and MYH7) concurrently upregulated in cocultured hfCMs. The introduction of multiple myosin subtypes in both CPC-CMs and hfCMs may partially account for the delayed contraction kinetics and the altered force-frequency properties.

Mutual adaptation similarly occurred in calcium handling of both CPC-CMs and hfCMs in cocultured myocardium. Simultaneous calcium transients in both CPC-CMs and the surrounding host myocardium, along with resemblance in the kinetics of these transients, provide compelling evidence for the establishment of a functional syncytium. Synchronized calcium handling and transduction in cocultured myocardium adaptively downregulated temporal kinetics of intracellular calcium transients. This synchronization of calcium signaling has been previously demonstrated in donor cardiomyocytes transplanted into host murine hearts [71]. Intracellular calcium cycling relies on the structural integrity of intracellular t-tubules and the calcium handling capacity of sarcoplasmic reticulum (calcium storage, release, and reuptake) during myocardial contraction and relaxation [72]. The increase of total contraction amplitude to positive inotropic stimulation and

post-pause potentiation demonstrates that the overall capacity of calcium handling was enhanced in coculture. However, the weakening of these responses in relationship to the preexistent contractility, reflects that the introduction of CPCs reduced the efficiency of calcium handling in cocultured myocardium. Most CPC-CMs achieved functionalization toward ventricular myocytes and developed t-tubule-like structure. However, compared to the sheet-like structure of t-tubules in hfCMs, there were still structural discrepancies [73]. In terms of gene expression, we observed the upregulation of RYR2, CACNA1C, and ATP2A2 in cocultured hfCMs compared to control hfCMs, but the concurrent increase in PLN expression, decrease in CaMK2D expression, and increase in SLC8A1 expression may finally inhibit the function of ATP2A2 and RYR2, as well as reduce the calcium storage of SR due to calcium efflux. In contrast, calcium handling-related gene expression in coculture CPC-CMs implies a greater reliance on sodium-calcium exchange than on the sarcoplasmic reticulum, as reflected by lower RYR2 and higher SLC8A1 expression levels. These alterations may cause a prolonged peak time and an extended relaxation of calcium transients in cocultured myocardium. Such transcriptional differences in the expression of calcium handling-related genes have been consistently reported between stem cell-derived cardiomyocytes and native cardiac tissue [74]. However, the above changes require further validation through analysis of protein phosphorylation. Additionally, the formation of circumferentially scattered and distributed gap and adherens junctions (connexin-43 and N-cadherin) between them may affect the efficiency of ECC, particularly in contrast to the polarized gap junctions that are typically found at the longitudinal termini of adult cardiomyocytes [75]. In spite of structural and functional heterogeneity, these above alterations may lead to the mutual adaptive adjustments to synchronized calcium handling, where the relatively weaker calcium handling of CPC-CMs is compensated by the improved capability in hfCMs.

The electrophysiological maturation and integration of partially differentiated cardiomyocytes directly impacts the efficiency of myocardial coupling in cardiac regeneration [76-79]. Compared to fully differentiated cardiomyocytes, partially differentiated CPCs that completing differentiation and integration within the host myocardium appear to be more advantageous in reducing the heterogeneity of electrical activity in the host myocardium. Refractory period of myocardium is highly correlated with action potential duration, which has been well established

[55, 80]. There was no alteration of refractory period in CPCs-cocultured myocardium, which demonstrates that non-prolonged action potential duration of CPC-CMs sufficiently maintains synchrony and consistency with host myocardium. It enhances electrical coupling efficiency and coordination of myocardial contraction. Moreover, it provides the possibility for anti-arrhythmic potential between CPC-CMs and host myocardium. On the other hand, a small proportion of ISL-1$^+$ CPCs differentiate into pacemaker cells [81], as confirmed by the co-expression of marker genes HCN4 and CACNA1G in the present study (1.6 ± 0.4%). Therefore, the occurrence of CPCs-induced spontaneous beating and pacing is unavoidable in current cardiac regeneration therapy. The primary concern is that additional and uncontrolled spontaneous pacing may disrupt normal heart rhythm, potentially leading to unnecessary arrhythmias and ectopic foci [82, 83]. Previous study indicates that ESCs-derived cardiomyocytes respond rapidly to electromechanical surroundings and yield persistent frequency adaptations to exogenous electrical stimulation, which may be related to the promotion of rapid depolarization and the induced expression of hERG by electrical stimulation. When stimulation frequency was set to 0.5 Hz, the spontaneous pacing rate was observed to be lower than that of the electrically induced pacing rate, which is consistent with our findings [84]. Furthermore, we observed that the downregulation of spontaneous pacing is more pronounced during the advanced maturation. Nevertheless, CPCs retain their pacing properties and autonomously adapt to the stimulation frequency in the host myocardial microenvironment. Unexpectedly, the spontaneous pacing did not significantly affect regular pacing. In most instances, they interfered primarily with ultra-low frequencies or even non-existent interference. This indicates that regular pacing exerts an inhibitory influence on the spontaneous pacing, which is the combined outcome of frequency adaptation and intrinsic automaticity in CPCs. The fact that the autonomic activity of CPC-CMs is overridden at any physiological pacing rate indicates a low risk for the induction of arrhythmias, supporting the feasibility of CPCs-based therapy for heart failure via intramyocardial injection [85]. Another critical concern is that the aberrant electrical conduction caused by CPCs prior to their differentiation into mature cardiomyocytes may lead to electrical uncoupling, potentially resulting in ventricular arrhythmias [86]. However, no evidence of such electrical uncoupling between CPCs and the host myocardium was observed in coculture.

Functional integration of CPCs-cocultured myocardium is predominantly manifested as functional neutralization and adaption between mature hfCMs and incompletely differentiated CPC-CMs. Of particular interest is that hfCMs exhibited differentiation potential after CPCs transplantation. Gene enrichment of failing myocardium reveals significant transcriptional alterations with relevance for cardiac development and myocardial contraction in cocultured hfCMs. The significantly increased expression of cardiac development-related genes (TBX5, TBX20, FHL2, CORIN, ERBB4, and FGF12) further supports the evidence of de-differentiation-redifferentiation cycle in cocultured hfCMs. However, the upregulated G0S2 implies that hfCMs reinforced their non-proliferative state and decreased their propensity to re-enter the cell cycle. These changes may contribute to the maintenance of the mature differentiated state and to the reversal of the functional deterioration of failing cardiomyocytes [87, 88]. Moreover, these changes may also lead to altered gene expression patterns in hfCMs and promote functional adaptive remodeling subsequent to CPCs introduction, thereby facilitating integration [89].

4.2 Migration and tissue integration of CPCs into deep failing myocardium

As an inherent characteristic of CPCs, their migratory capability disappears once they differentiate into mature cardiomyocytes [90]. During early embryonic heart development, the movement trajectories mediated by the Wnt3a signaling pathway guide cardiac precursor cells to migrate from the primitive streak along its sides, and then return to the midline, thereby facilitating the formation of the heart primordium [91, 92]. The autonomous migration of CPCs indicates their significant potential in regeneration and repair of cardiac tissue. Previous studies have demonstrated that CPCs possess chemotactic migratory capabilities mediated by CXCL12/CXCR4, and they autonomously migrate to areas of inflammation and fibrosis [93, 94]. This spontaneous migration was confirmed in our ex-vivo model of human failing myocardium. We found a high capacity of CPCs to deeply migrate and home into failing myocardium, particularly into damaged or necrotic cardiac tissue and fibrosis regions. The concentration gradient of chemotactic factors formed on the surface and deeper layers of myocardium may drive CPCs to migrate and invade to the deep damaged regions of failing myocardium.

This contributes to the effective integration of CPCs with failing myocardial tissue, and the repair of damaged areas. In the therapeutic situation, preserved migratory capacity may reduce the aggregation of CPCs in non-target tissues, and thus lower potential side effects [95].

In heart failure, the precise three-dimensional arrangement of cells is disrupted, leading to the remodeling of myocardial structure. The spatial vacancies created by necrotic myocardial cells are often filled by fibrosis, which hinders the propagation of excitatory signals between cardiomyocytes [96]. However, the formation of uniform distribution and network structure indicates that CPC-CMs effectively integrate and reconstruct myocardial tissue in the heart failure environment. This network structure may mimic the arrangement of normal myocardial cells, which facilitates the restoration of structural and functional integrity within myocardium. In addition, CPC-CMs establish direct tissue mechanical attachment and connection with adjacent host cardiomyocytes in a time- and space-dependent manner during coculture. It also reflects their adaptability to complex microenvironments, which may include responses to fibrosis, hypoxia, and other stress factors [97]. The above behavior contrasts with previous in-vivo cell therapy studies, where injected stem cells either vanish after a few months or form a distinct mass of regenerated tissue [98, 99]. Such isolated islets may have limited capabilities to transmit contraction force and to form couplings with the surrounding ventricle, but they hardly occurred in the current CPCs-cocultured myocardium.

Ventricular fibrosis and remodeling in heart failure lead to the loss and spatial rearrangement of connexin-43, and therefore are primary causes of abnormal electrical coupling in failing myocardium [100]. Impaired gap junctions and disrupted electrical coupling in fibrotic regions exacerbate heart failure [101]. In CPCs-cocultured failing myocardium, the physical connections of connexin-43 between CPC-CMs and hfCMs provide a structural basis for reestablishing of electrical and metabolic coupling and for regenerative repair of host failing myocardium. In addition to connexin-43, N-cadherin (CDH2) is crucial for adherens junctions and homeostasis between cardiomyocytes [102], and plays a significant role in the maturation and functionalization of CPC-CMs [103]. Further evidence in mice indicated that overexpressed CDH2 enhances the survival and functional

integration of implanted cardiomyocytes derived from stem cells [104]. In the present study, immunofluorescence imaging and cellular communication analysis confirmed the direct contact of N-cadherin between them, as well as intense and frequent CDH2-mediated cellular communication. Moreover, NCAM1- and PTPRM- and laminin- and collagen-mediated intercellular communications between them suggest the regulation of cell adhesion and matrix interaction, as well as interrelated adaptation to coculture microenvironments. These firm cell-cell adhesions transmit contractile force more effectively, and enhance electromechanical coupling, and thereby maintain the integrity of host failing myocardium [105]. The above findings demonstrate that deep tissue integration has been achieved in CPCs-implanted failing myocardium.

4.3 Host failing myocardium promotes CPCs maturation

The immature state of stem cell-derived cardiomyocytes is a major obstacle in cardiac regeneration therapy. Their full differentiation and maturation are not the result of a single factor, but rather the outcome of multiple artificial parameters in combination [106]. Unlike anisotropic shapes with cross-striated myofibrils of stem cell-derived cardiomyocytes in 2D culture [107, 108] , most CPC-CMs in host myocardium organized their rod-like structures and regularly arranged myofibrils with elongated sarcomeres. This structural organization may be coordinated by the regulation of mechanical stress of the native extracellular matrix and the surrounding host cardiomyocytes [109]. The above process guides the differentiation of CPCs into rod-shaped structure suitable for myocardial contraction and relaxation, and the morphological maturation also exceeds that of ESC-derived cardiomyocytes (oblong cells measuring 30 μm in length, 10 μm in width) [110].

Cocultured CPC-CMs exhibit more advanced maturity in ultrastructural features. The formation of t-tubules serves as a key indicator of advanced maturation in cardiomyocytes differentiated from stem cells, significantly enhancing the efficiency of ECC, particularly during the calcium-triggered calcium release phase [111]. The formation of t-tubule is rarely seen in stem cell-differentiated cardiomyocytes, but electromechanical stimulation and appropriate culture conditions contribute to t-tube development. It has been previously reported that t-tubule-like structures of in-vivo transplanted CPCs were observed in renal capsule [24].

Various interventions, including hormonal treatments, electro-mechanical stimulation, and cocultivation, have been demonstrated to promote the development of t-tubule-like structures in stem cell-differentiated cardiomyocytes [112-114]. Under optimized coculture conditions in this study, CPC-CMs formed t-tubule-like structures that contribute to the capacity and efficiency of calcium handling, despite being weaker than adult cardiomyocytes, even in failing myocardium, which is in line with previous findings [115, 116].

In terms of advanced maturation, co-expression and pseudotime trajectory demonstrate that most of CPC-CMs achieved functionalization towards adult ventricular myocytes by expressing MYL2 and PLN, whereas they retained an intermediate stage of differentiation characterized by atrial-like MYL7 expression. The coexistence of MLC2v and MLC2a (myosin light chain proteins encoded by genes MYL2 and MYL7) further confirms the functionalized transitions of CPC-CMs. This time-dependent maturation of CPC-CMs follows the sequence of heart development, wherein atrial-specific genes are expressed initially, followed by the expression of ventricular-specific genes at later stages [117, 118].

4.4 Interaction and crosstalk between CPC-CMs and host myocardium

As CPCs gradually differentiate and mature, and as host failing myocardial tissue progressively degenerates, the interaction between them is regarded as dynamically changing, involving continuous adjustments and adaptations. However, the low survival and integration rates of transplanted CPCs in vivo obstruct the investigation of underlying mechanisms [119]. Paracrine pathways have previously been identified as the primary mechanism of functional improvement following stem cell transplantation to host myocardium [120]. In our optimized ex-vivo coculture of CPCs and host myocardium, we indicated the orientated-contraction of CPC-CMs in host myocardium, as well as intercellular paracrine communication between them. The present study demonstrates an abundant presence of differentiated CPC-CMs, which are likely to substantially contribute to contractile force. These observations suggest that the role of CPCs in improving cardiac function may result from a combination of their contractile contribution and paracrine activities. However, the relative proportions of these contributions are still unclear to date [121]. Regarding direct cell-cell contacts, homophilic cell

adhesion (CDH2-CDH2, NCAM1-NCAM1, PTPRM-PTPRM)-mediated cellular communications facilitate the effective integration of CPC-CMs into the host myocardium, improving cell survival and promoting tissue regeneration and repair, which are essential for optimal myocardial recovery following CPCs transplantation. The CPC-CMs-to-hfCMs communication occurred though differentiation-related signaling pathways (NRG3-ERBB4 and BMP5-(BMPR1A + BMPR2)) in coculture. In particular, the BMP5 pathway, triggered by CPC-CMs, may affect the functional differentiation and myocardial remodeling of host myocardium through SMAD-dependent pathway and non-SMAD pathways [122, 123]. In contrast, the effect of hfCMs on CPC-CMs was mainly mediated through myocardial compaction via SEMA3C signaling pathway, contributing to beneficial spatial reorganization and myocardial remodeling in the host myocardium [124, 125]. Interestingly, strong correlation and low-frequency communication probability in the above one-way SEMA3C-(NRP1 + PLXNA4) communication imply that SEMA3C-mediated rearrangement of myocardial compaction mainly occurred at the specific stage of tissue integration. In addition, extracellular matrix-mediated communications via laminin and collagen may promote intercellular adhesion and cytoskeletal reorganization and mechanical coupling between hfCMs and CPC-CMs in coculture [126].

Bidirectional communication between CPC-CMs and hfCMs (CDH2-CDH2, NCAM1-NCAM1, PTPRM-PTPRM) and unidirectional communications from CPC-CMs to hfCMs (NRG3-ERBB4 and BMP5-BMPR1A) suggest that CPC-CMs may improve the cardiac function of host myocardium by the above signal interactions. These signals are transduced to MAPK/ERK, PI3K-Akt, and TGF-β signaling pathways, while the regulatory network of these signaling cascades in heart failure impacts cardiac function improvement [127]. Additionally, it has previously been proven that TGF-β signaling pathway affects electrical remodeling and calcium handling in cardiomyocytes [128]. Moreover, the relevant receptor genes (CDH2, PTPRM, NCAM1, BMPR1A, and ERBB4) involved in signaling of CPC-CMs were co-expressed with the genes related to myocardial excitation-contraction coupling (RYR2, TPM1, CACNA2D1, CACNB2, CAMK2D, SCN5A) and cardiac development (TBX5, GATA6, MEF2A, MEF2C, FOXP1, SMAD2, SMAD5, IGF1R, ZFPM2) in the same regulons (TFs: NFIA, NFIB, and ZBTB20).

This co-expression demonstrates the possibility of synergistic effects on myocardial repair by CPC-CMs.

Overall, our study further substantiates the mechanisms by which CPCs alleviate heart failure, revealing that the therapeutic effects depend not only on an active contractile contribution but also on paracrine signaling by CPC-CMs following the cardiac developmental trajectory (Figure 35).

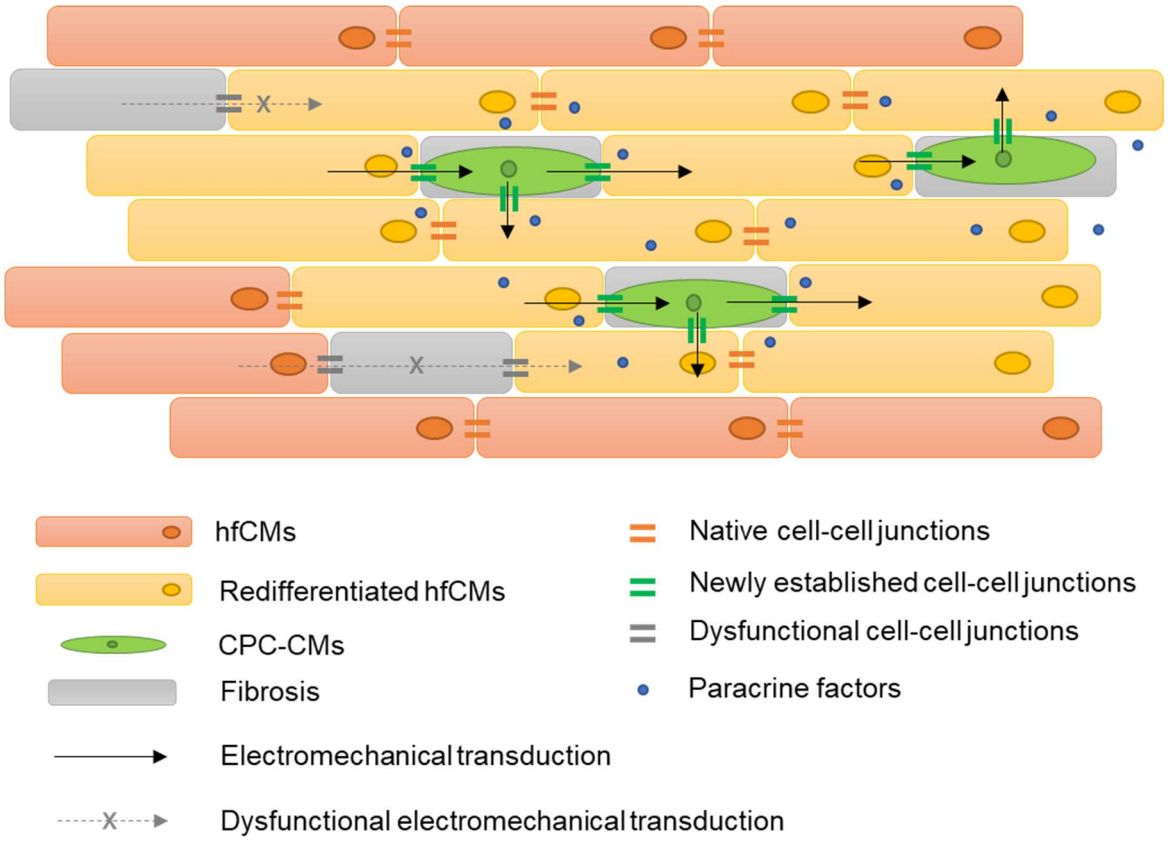

Figure 35. Potential mechanism of tissue integration and functional synchronization between CPC-CMs and host failing myocardium.

CPC-CMs migrate to fibrotic regions within cocultured failing myocardium, and establish electromechanical coupling with hfCMs. In parallel, hfCMs are influenced by both contact-dependent signaling and paracrine communication from CPC-CMs, entering a dedifferentiation-redifferentiation cycle that contributes to cardiac remodeling and repair.

4.5 Limitations

(1) Access to authentic mature cardiomyocytes differentiated from CPCs is currently the focus of attention in cardiac regeneration research and a critical issue to be addressed urgently. By coculturing CPCs with failing myocardium ex vivo and applying a variety of interventions, such as continuous electrical stimulation and preload, we have harvested ventricular-like cardiomyocytes, which are not yet considered to be adult mature cardiomyocytes. Coculture duration-dependent changes in CPCs maturation were not explored. Ultra-long-term coculture (over a year) might further promote further differentiation and maturation of CPCs, however it presents a challenge for the ex-vivo culture model we have developed.

(2) Although the ex-vivo biomimetic myocardial culture adopted in this study has largely replicated the pathophysiological conditions of the failing myocardium in patients, long-term ex-vivo cultures of myocardium inevitably undergo tissue degeneration and adaptation to culture conditions. Therefore, large-scale clinical trials are still required for further validation. The low survival rate of trans-myocardially injected CPCs may be attributed to hypoxia-ischemia injury and immune rejection. Despite the optimized ex-vivo culture conditions in the present study significantly improving CPCs survival and enabling their long-term maintenance, these advancements still need to be established in vivo. Additionally, our ex-vivo model focuses on the functional and molecular changes in the symbiotic relationship between CPCs and human failing myocardium, but it cannot address issues related to organ interactions and tissue specificity in vivo. Further research is necessary to confirm these potential benefits.

(3) The diversity and interaction of cardiac lineage cell populations in the failing myocardium following CPCs transplantation add to the complexity of cardiac regeneration therapy. The mechanism of CPCs therapy for heart failure may involve contributions from exogenous contractile force of CPC-CMs and cellular communication networks in cocultured myocardium. Although we preliminarily explored the tissue integration and functional synchronization of CPCs in the treatment of heart failure and their potential mechanisms, it remains unclear which mechanism predominates. Consequently, the present study focuses on the

interaction between CPC-CMs and hfCMs, while lacking a multi-faceted analysis that involves fibroblasts and macrophages.

4.6 Prospects

The present study highlights the significant potential of CPCs in improving cardiac function of host failing myocardium. The repair and reconstruction of injured myocardium were facilitated through tissue integration and functional synchronization with CPC-CMs. Additionally, CPCs coculture induced the dedifferentiation-redifferentiation of host cardiomyocytes, while the microenvironment of host failing myocardium promoted the differentiation of CPCs into structurally and functionally mature cardiomyocytes. These mutual adaptations between CPCs and host myocardium drive beneficial myocardial remodeling, supporting restoration and regeneration. Multiple mechanisms contribute to the repair of failing myocardium, CPC-CMs not only contribute to total contractility but also improve the cardiac microenvironment by intercellular communication and crosstalk.

Cardiac regenerative therapy based on cardiac embryonic development offers additional possibilities for heart failure treatment. It deepens the understanding of stem cell-mediated cardiac repair mechanisms and provides insights into potential strategies to optimize stem cell therapy for heart failure.

References

1. Ziaeian, B. and G.C. Fonarow, *Epidemiology and aetiology of heart failure.* Nature Reviews. Cardiology, 2016. 13(6): p. 368-378.
2. Martin, S.S., et al., *2024 Heart Disease and Stroke Statistics: A Report of US and Global Data From the American Heart Association.* Circulation, 2024. 149(8): p. e347-e913.
3. Mascolo, A., et al., *Current and future therapeutic perspective in chronic heart failure.* Pharmacological Research, 2022. 175: p. 106035.
4. Miller, L., et al., *Use of Ventricular Assist Devices and Heart Transplantation for Advanced Heart Failure.* Circulation Research, 2019. 124(11): p. 1658-1678.
5. Kim, I.C., J.C. Youn, and J.A. Kobashigawa, *The Past, Present and Future of Heart Transplantation.* Korean Circulation Journal, 2018. 48(7): p. 565-590.
6. Kittleson, M.M. and J.A. Kobashigawa, *Cardiac Transplantation: Current Outcomes and Contemporary Controversies.* JACC. Heart Failure, 2017. 5(12): p. 857-868.
7. Bergmann, O., et al., *Dynamics of Cell Generation and Turnover in the Human Heart.* Cell, 2015. 161(7): p. 1566-1575.
8. Lázár, E., H.A. Sadek, and O. Bergmann, *Cardiomyocyte renewal in the human heart: insights from the fall-out.* European Heart Journal, 2017. 38(30): p. 2333-2342.
9. Wang, L., et al., *Single-cell reconstruction of the adult human heart during heart failure and recovery reveals the cellular landscape underlying cardiac function.* Nature Cell Biology, 2020. 22(1): p. 108-119.
10. Segura, A.M., O.H. Frazier, and L.M. Buja, *Fibrosis and heart failure.* Heart Failure Reviews, 2014. 19(2): p. 173-185.
11. Garbern, J.C. and R.T. Lee, *Heart regeneration: 20 years of progress and renewed optimism.* Developmental Cell, 2022. 57(4): p. 424-439.
12. Chong, J.J., et al., *Human embryonic-stem-cell-derived cardiomyocytes regenerate non-human primate hearts.* Nature, 2014. 510(7504): p. 273-7.
13. Kishino, Y., et al., *Cardiac Regenerative Therapy Using Human Pluripotent Stem Cells for Heart Failure: A State-of-the-Art Review.* Journal of Cardiac

Failure, 2023. 29(4): p. 503-513.

14. Buckingham, M., S. Meilhac, and S. Zaffran, *Building the mammalian heart from two sources of myocardial cells.* Nature Reviews. Genetics, 2005. 6(11): p. 826-835.
15. Moretti, A., et al., *Multipotent embryonic isl1+ progenitor cells lead to cardiac, smooth muscle, and endothelial cell diversification.* Cell, 2006. 127(6): p. 1151-1165.
16. Bu, L., et al., *Human ISL1 heart progenitors generate diverse multipotent cardiovascular cell lineages.* Nature, 2009. 460(7251): p. 113-117.
17. Sepac, A., et al., *Comparison of cardiomyogenic potential among human ESC and iPSC lines.* Cell Transplantation, 2012. 21(11): p. 2523-2530.
18. Pappas, J.J. and P.C. Yang, *Human ESC vs. iPSC-pros and cons.* Journal of Cardiovascular Translational Research, 2008. 1(2): p. 96-99.
19. Shouman, S., et al., *Cardiac Progenitor Cells.* Advances In Experimental Medicine and Biology, 2021. 1312: p. 51-73.
20. Mononen, M.M., et al., *Trajectory mapping of human embryonic stem cell cardiogenesis reveals lineage branch points and an ISL1 progenitor-derived cardiac fibroblast lineage.* Stem Cells, 2020. 38(10): p. 1267-1278.
21. Witman, N., et al., *Cardiac progenitors and paracrine mediators in cardiogenesis and heart regeneration.* Seminars In Cell & Developmental Biology, 2020. 100: p. 29-51.
22. Menasché, P., et al., *Human embryonic stem cell-derived cardiac progenitors for severe heart failure treatment: first clinical case report.* European Heart Journal, 2015. 36(30): p. 2011-2017.
23. Menasché, P., et al., *Transplantation of Human Embryonic Stem Cell-Derived Cardiovascular Progenitors for Severe Ischemic Left Ventricular Dysfunction.* Journal of the American College of Cardiology, 2018. 71(4): p. 429-438.
24. Foo, K.S., et al., *Human ISL1+ Ventricular Progenitors Self-Assemble into an In Vivo Functional Heart Patch and Preserve Cardiac Function Post Infarction.* Molecular Therapy : the Journal of the American Society of Gene Therapy, 2018. 26(7): p. 1644-1659.
25. Poch, C.M., et al., *Migratory and anti-fibrotic programmes define the regenerative potential of human cardiac progenitors.* Nature Cell Biology,

2022. 24(5): p. 659-671.

26. Chong, J.J.H. and C.E. Murry, *Cardiac regeneration using pluripotent stem cells--progression to large animal models.* Stem Cell Research, 2014. 13(3 Pt B): p. 654-665.
27. Blin, G., et al., *A purified population of multipotent cardiovascular progenitors derived from primate pluripotent stem cells engrafts in postmyocardial infarcted nonhuman primates.* J Clin Invest, 2010. 120(4): p. 1125-39.
28. Song, H., et al., *Interrogating functional integration between injected pluripotent stem cell-derived cells and surrogate cardiac tissue.* Proc Natl Acad Sci U S A, 2010. 107(8): p. 3329-34.
29. Li, X., et al., *Improving Cell Engraftment in Cardiac Stem Cell Therapy.* Stem Cells International, 2016. 2016: p. 7168797.
30. Terrovitis, J.V., R.R. Smith, and E. Marbán, *Assessment and optimization of cell engraftment after transplantation into the heart.* Circulation Research, 2010. 106(3): p. 479-494.
31. Kervadec, A., et al., *Cardiovascular progenitor-derived extracellular vesicles recapitulate the beneficial effects of their parent cells in the treatment of chronic heart failure.* The Journal of Heart and Lung Transplantation : the Official Publication of the International Society For Heart Transplantation, 2016. 35(6): p. 795-807.
32. Wu, Q., et al., *Extracellular vesicles from human embryonic stem cell-derived cardiovascular progenitor cells promote cardiac infarct healing through reducing cardiomyocyte death and promoting angiogenesis.* Cell Death & Disease, 2020. 11(5): p. 354.
33. Maring, J.A., et al., *Cardiac Progenitor Cell-Derived Extracellular Vesicles Reduce Infarct Size and Associate with Increased Cardiovascular Cell Proliferation.* Journal of Cardiovascular Translational Research, 2019. 12(1).
34. van Niel, G., G. D'Angelo, and G. Raposo, *Shedding light on the cell biology of extracellular vesicles.* Nature Reviews. Molecular Cell Biology, 2018. 19(4): p. 213-228.
35. Colombo, M., G. Raposo, and C. Théry, *Biogenesis, secretion, and intercellular interactions of exosomes and other extracellular vesicles.*

Annual Review of Cell and Developmental Biology, 2014. 30: p. 255-289.

36. Yang, L., et al., *Stem cell-derived extracellular vesicles for myocardial infarction: a meta-analysis of controlled animal studies.* Aging, 2019. 11(4): p. 1129-1150.
37. Sluijter, J.P.G., et al., *Extracellular vesicles in diagnostics and therapy of the ischaemic heart: Position Paper from the Working Group on Cellular Biology of the Heart of the European Society of Cardiology.* Cardiovascular Research, 2018. 114(1): p. 19-34.
38. El Harane, N., et al., *Acellular therapeutic approach for heart failure: in vitro production of extracellular vesicles from human cardiovascular progenitors.* European Heart Journal, 2018. 39(20): p. 1835-1847.
39. Wang, L., et al., *Role of cardiac progenitor cell-derived exosome-mediated microRNA-210 in cardiovascular disease.* Journal of Cellular and Molecular Medicine, 2019. 23(11): p. 7124-7131.
40. Roefs, M.T., et al., *Cardiac progenitor cell-derived extracellular vesicles promote angiogenesis through both associated- and co-isolated proteins.* Communications Biology, 2023. 6(1): p. 800.
41. Garikipati, V.N.S., et al., *Extracellular Vesicles and the Application of System Biology and Computational Modeling in Cardiac Repair.* Circulation Research, 2018. 123(2): p. 188-204.
42. Bollini, S., et al., *Triggering Endogenous Cardiac Repair and Regeneration via Extracellular Vesicle-Mediated Communication.* Frontiers In Physiology, 2018. 9: p. 1497.
43. Chavakis, E., C. Urbich, and S. Dimmeler, *Homing and engraftment of progenitor cells: a prerequisite for cell therapy.* Journal of Molecular and Cellular Cardiology, 2008. 45(4): p. 514-522.
44. Park, H.J., et al., *Bidirectional relationship between cardiac extracellular matrix and cardiac cells in ischemic heart disease.* Stem Cells, 2021. 39(12): p. 1650-1659.
45. Robert, A.W., et al., *Secretome Analysis Performed During in vitro Cardiac Differentiation: Discovering the Cardiac Microenvironment.* Front Cell Dev Biol, 2020. 8: p. 49.
46. Ontoria-Oviedo, I., et al., *Plasmatic Membrane Expression of Adhesion Molecules in Human Cardiac Progenitor/Stem Cells Might Explain Their*

Superior Cell Engraftment after Cell Transplantation. Stem Cells Int, 2020. 2020: p. 8872009.

47. van Laake, L.W., et al., *Extracellular matrix formation after transplantation of human embryonic stem cell-derived cardiomyocytes.* Cell Mol Life Sci, 2010. 67(2): p. 277-90.
48. Matsushita, T., et al., *Formation of cell junctions between grafted and host cardiomyocytes at the border zone of rat myocardial infarction.* Circulation, 1999. 100(19 Suppl): p. II262-II268.
49. Kofidis, T., et al., *Stimulation of paracrine pathways with growth factors enhances embryonic stem cell engraftment and host-specific differentiation in the heart after ischemic myocardial injury.* Circulation, 2005. 111(19): p. 2486-2493.
50. Han, C., et al., *Extracellular vesicles in cardiovascular disease: Biological functions and therapeutic implications.* Pharmacology & Therapeutics, 2022. 233: p. 108025.
51. Xu, M.-Y., et al., *Differences in the cargos and functions of exosomes derived from six cardiac cell types: a systematic review.* Stem Cell Research & Therapy, 2019. 10(1): p. 194.
52. Besser, R.R., et al., *Engineered Microenvironments for Maturation of Stem Cell Derived Cardiac Myocytes.* Theranostics, 2018. 8(1): p. 124-140.
53. Bolli, R., et al., *Cell therapy in patients with heart failure: a comprehensive review and emerging concepts.* Cardiovascular Research, 2022. 118(4): p. 951-976.
54. Rheault-Henry, M., et al., *Stem cell therapy for heart failure: Medical breakthrough, or dead end?* World Journal of Stem Cells, 2021. 13(4): p. 236-259.
55. Fischer, C., et al., *Long-term functional and structural preservation of precision-cut human myocardium under continuous electromechanical stimulation in vitro.* Nature Communications, 2019. 10(1): p. 117.
56. Endoh, M., *Force-frequency relationship in intact mammalian ventricular myocardium: physiological and pathophysiological relevance.* European Journal of Pharmacology, 2004. 500(1-3): p. 73-86.
57. Valls-Margarit, M., et al., *Engineered Macroscale Cardiac Constructs Elicit Human Myocardial Tissue-like Functionality.* Stem Cell Reports, 2019.

13(1): p. 207-220.

58. Janssen, P.M.L. and M. Periasamy, *Determinants of frequency-dependent contraction and relaxation of mammalian myocardium.* Journal of Molecular and Cellular Cardiology, 2007. 43(5): p. 523-531.
59. Mill, J.G., D.V. Vassallo, and C.M. Leite, *Mechanisms underlying the genesis of post-rest contractions in cardiac muscle.* Brazilian Journal of Medical and Biological Research = Revista Brasileira de Pesquisas Medicas E Biologicas, 1992. 25(4): p. 399-408.
60. Sun, Z., et al., *Synchronous force and Ca2+ measurements for repeated characterization of excitation-contraction coupling in human myocardium.* Communications Biology, 2024. 7(1): p. 220.
61. Fujita, H., et al., *Estimation of crossbridge-state during cardiomyocyte beating using second harmonic generation.* Life Science Alliance, 2023. 6(7).
62. Trapnell, C., et al., *The dynamics and regulators of cell fate decisions are revealed by pseudotemporal ordering of single cells.* Nat Biotechnol, 2014. 32(4): p. 381-386.
63. Jin, S., et al., *Inference and analysis of cell-cell communication using CellChat.* Nature Communications, 2021. 12(1): p. 1088.
64. Aibar, S., et al., *SCENIC: single-cell regulatory network inference and clustering.* Nat Methods, 2017. 14(11): p. 1083-1086.
65. Silva, K.A.S. and C.A. Emter, *Large Animal Models of Heart Failure: A Translational Bridge to Clinical Success.* JACC. Basic To Translational Science, 2020. 5(8): p. 840-856.
66. Gunata, M. and H. Parlakpinar, *Experimental heart failure models in small animals.* Heart Failure Reviews, 2023. 28(2): p. 533-554.
67. Seguret, M., et al., *Cardiac Organoids to Model and Heal Heart Failure and Cardiomyopathies.* Biomedicines, 2021. 9(5).
68. Schwach, V., et al., *Expandable human cardiovascular progenitors from stem cells for regenerating mouse heart after myocardial infarction.* Cardiovasc Res, 2020. 116(3): p. 545-553.
69. Lindsey, S.E., J.T. Butcher, and H.C. Yalcin, *Mechanical regulation of cardiac development.* Front Physiol, 2014. 5: p. 318.
70. England, J. and S. Loughna, *Heavy and light roles: myosin in the*

morphogenesis of the heart. Cellular and Molecular Life Sciences : CMLS, 2013. 70(7): p. 1221-1239.

71. Rubart, M., et al., *Physiological coupling of donor and host cardiomyocytes after cellular transplantation.* Circ Res, 2003. 92(11): p. 1217-24.
72. Bers, D.M., *Cardiac excitation-contraction coupling.* Nature, 2002. 415(6868): p. 198-205.
73. Setterberg, I.E., et al., *The Physiology and Pathophysiology of T-Tubules in the Heart.* Front Physiol, 2021. 12: p. 718404.
74. Synnergren, J., et al., *Global transcriptional profiling reveals similarities and differences between human stem cell-derived cardiomyocyte clusters and heart tissue.* Physiol Genomics, 2012. 44(4): p. 245-58.
75. Marcu, I.C., et al., *Functional Characterization and Comparison of Intercellular Communication in Stem Cell-Derived Cardiomyocytes.* Stem Cells, 2015. 33(7): p. 2208-18.
76. He, J.-Q., et al., *Human embryonic stem cells develop into multiple types of cardiac myocytes: action potential characterization.* Circulation Research, 2003. 93(1): p. 32-39.
77. Pekkanen-Mattila, M., et al., *Human embryonic stem cell-derived cardiomyocytes: demonstration of a portion of cardiac cells with fairly mature electrical phenotype.* Experimental Biology and Medicine (Maywood, N.J.), 2010. 235(4): p. 522-530.
78. Furuta, A., et al., *Pulsatile cardiac tissue grafts using a novel three-dimensional cell sheet manipulation technique functionally integrates with the host heart, in vivo.* Circulation Research, 2006. 98(5): p. 705-712.
79. Halbach, M., et al., *Electrophysiological maturation and integration of murine fetal cardiomyocytes after transplantation.* Circulation Research, 2007. 101(5): p. 484-492.
80. Esfandyari, D., et al., *MicroRNA-365 regulates human cardiac action potential duration.* Nat Commun, 2022. 13(1): p. 220.
81. Sun, Y., et al., *Islet 1 is expressed in distinct cardiovascular lineages, including pacemaker and coronary vascular cells.* Developmental Biology, 2007. 304(1): p. 286-296.
82. Chen, H.-S.V., C. Kim, and M. Mercola, *Electrophysiological challenges of cell-based myocardial repair.* Circulation, 2009. 120(24): p. 2496-2508.

83. Liao, S.-Y., et al., *Proarrhythmic risk of embryonic stem cell-derived cardiomyocyte transplantation in infarcted myocardium.* Heart Rhythm, 2010. 7(12): p. 1852-1859.
84. Eng, G., et al., *Autonomous beating rate adaptation in human stem cell-derived cardiomyocytes.* Nature Communications, 2016. 7: p. 10312.
85. Chen, K., et al., *Arrhythmogenic risks of stem cell replacement therapy for cardiovascular diseases.* J Cell Physiol, 2020. 235(9): p. 6257-6267.
86. Smit, N.W. and R. Coronel, *Stem cells can form gap junctions with cardiac myocytes and exert pro-arrhythmic effects.* Front Physiol, 2014. 5: p. 419.
87. Mensah, I.K. and H. Gowher, *Signaling Pathways Governing Cardiomyocyte Differentiation.* Genes (Basel), 2024. 15(6).
88. Shakked, A., et al., *Redifferentiated cardiomyocytes retain residual dedifferentiation signatures and are protected against ischemic injury.* Nat Cardiovasc Res, 2023. 2(4): p. 383-398.
89. Zhu, Y., et al., *What we know about cardiomyocyte dedifferentiation.* J Mol Cell Cardiol, 2021. 152: p. 80-91.
90. Vincent, S.D. and M.E. Buckingham, *How to make a heart: the origin and regulation of cardiac progenitor cells.* Curr Top Dev Biol, 2010. 90: p. 1-41.
91. Münsterberg, A. and Q. Yue, *Cardiac progenitor migration and specification: The dual function of Wnts.* Cell Adhesion & Migration, 2008. 2(2): p. 74-76.
92. Song, J., et al., *Smad1 transcription factor integrates BMP2 and Wnt3a signals in migrating cardiac progenitor cells.* Proceedings of the National Academy of Sciences of the United States of America, 2014. 111(20): p. 7337-7342.
93. Zakharova, L., et al., *Transplantation of cardiac progenitor cell sheet onto infarcted heart promotes cardiogenesis and improves function.* Cardiovascular Research, 2010. 87(1): p. 40-49.
94. Li, Y., et al., *Clusterin induces CXCR4 expression and migration of cardiac progenitor cells.* Experimental Cell Research, 2010. 316(20): p. 3435-3442.
95. Ghadge, S.K., et al., *SDF-1α as a therapeutic stem cell homing factor in myocardial infarction.* Pharmacol Ther, 2011. 129(1): p. 97-108.
96. Burchfield, J.S., M. Xie, and J.A. Hill, *Pathological ventricular remodeling: mechanisms: part 1 of 2.* Circulation, 2013. 128(4): p. 388-400.

97. Sakaguchi, A., C. Nishiyama, and W. Kimura, *Cardiac regeneration as an environmental adaptation.* Biochim Biophys Acta Mol Cell Res, 2020. 1867(4): p. 118623.
98. Soma, Y., et al., *Pluripotent stem cell-based cardiac regenerative therapy for heart failure.* J Mol Cell Cardiol, 2024. 187: p. 90-100.
99. Liu, C., et al., *The Current Dilemma and Breakthrough of Stem Cell Therapy in Ischemic Heart Disease.* Front Cell Dev Biol, 2021. 9: p. 636136.
100. Michela, P., et al., *Role of connexin 43 in cardiovascular diseases.* European Journal of Pharmacology, 2015. 768: p. 71-76.
101. Schultz, F., et al., *Cardiomyocyte-myofibroblast contact dynamism is modulated by connexin-43.* FASEB Journal : Official Publication of the Federation of American Societies For Experimental Biology, 2019. 33(9): p. 10453-10468.
102. Li, J., et al., *Cardiac-specific loss of N-cadherin leads to alteration in connexins with conduction slowing and arrhythmogenesis.* Circulation Research, 2005. 97(5): p. 474-481.
103. Soh, B.-S., et al., *N-cadherin prevents the premature differentiation of anterior heart field progenitors in the pharyngeal mesodermal microenvironment.* Cell Research, 2014. 24(12): p. 1420-1432.
104. Lou, X., et al., *N-cadherin overexpression enhances the reparative potency of human-induced pluripotent stem cell-derived cardiac myocytes in infarcted mouse hearts.* Cardiovascular Research, 2020. 116(3): p. 671-685.
105. Noorman, M., et al., *Cardiac cell-cell junctions in health and disease: Electrical versus mechanical coupling.* J Mol Cell Cardiol, 2009. 47(1): p. 23-31.
106. Karbassi, E., et al., *Cardiomyocyte maturation: advances in knowledge and implications for regenerative medicine.* Nature Reviews. Cardiology, 2020. 17(6): p. 341-359.
107. Zhang, J., et al., *Functional cardiomyocytes derived from human induced pluripotent stem cells.* Circulation Research, 2009. 104(4): p. e30-e41.
108. Mummery, C., et al., *Differentiation of human embryonic stem cells to cardiomyocytes: role of coculture with visceral endoderm-like cells.*

Circulation, 2003. 107(21): p. 2733-2740.

109. Silva, A.C., et al., *Bearing My Heart: The Role of Extracellular Matrix on Cardiac Development, Homeostasis, and Injury Response.* Front Cell Dev Biol, 2020. 8: p. 621644.
110. Snir, M., et al., *Assessment of the ultrastructural and proliferative properties of human embryonic stem cell-derived cardiomyocytes.* American Journal of Physiology. Heart and Circulatory Physiology, 2003. 285(6): p. H2355-H2363.
111. Ronaldson-Bouchard, K., et al., *Advanced maturation of human cardiac tissue grown from pluripotent stem cells.* Nature, 2018. 556(7700): p. 239-243.
112. Dunn, K.K., et al., *Coculture of Endothelial Cells with Human Pluripotent Stem Cell-Derived Cardiac Progenitors Reveals a Differentiation Stage-Specific Enhancement of Cardiomyocyte Maturation.* Biotechnology Journal, 2019. 14(8): p. e1800725.
113. Parikh, S.S., et al., *Thyroid and Glucocorticoid Hormones Promote Functional T-Tubule Development in Human-Induced Pluripotent Stem Cell-Derived Cardiomyocytes.* Circulation Research, 2017. 121(12): p. 1323-1330.
114. Godier-Furnémont, A.F.G., et al., *Physiologic force-frequency response in engineered heart muscle by electromechanical stimulation.* Biomaterials, 2015. 60: p. 82-91.
115. De La Mata, A., et al., *BIN1 Induces the Formation of T-Tubules and Adult-Like Ca2+ Release Units in Developing Cardiomyocytes.* Stem Cells (Dayton, Ohio), 2019. 37(1): p. 54-64.
116. Ibrahim, M., et al., *The structure and function of cardiac t-tubules in health and disease.* Proc Biol Sci, 2011. 278(1719): p. 2714-23.
117. Asp, M., et al., *A Spatiotemporal Organ-Wide Gene Expression and Cell Atlas of the Developing Human Heart.* Cell, 2019. 179(7).
118. Murphy, S.A., et al., *Maturing heart muscle cells: Mechanisms and transcriptomic insights.* Seminars In Cell & Developmental Biology, 2021. 119: p. 49-60.
119. Zhang, M., et al., *Cardiomyocyte grafting for cardiac repair: graft cell death and anti-death strategies.* Journal of Molecular and Cellular Cardiology,

2001. 33(5): p. 907-921.

120. Matsuura, K., et al., *Transplantation of cardiac progenitor cells ameliorates cardiac dysfunction after myocardial infarction in mice.* The Journal of Clinical Investigation, 2009. 119(8): p. 2204-2217.
121. Yahyazadeh, R., V. Baradaran Rahimi, and V.R. Askari, *Stem cell and exosome therapies for regenerating damaged myocardium in heart failure.* Life Sci, 2024. 351: p. 122858.
122. van Wijk, B., A.F.M. Moorman, and M.J.B. van den Hoff, *Role of bone morphogenetic proteins in cardiac differentiation.* Cardiovascular Research, 2007. 74(2): p. 244-255.
123. Ye, D., et al., *Insights into bone morphogenetic proteins in cardiovascular diseases.* Frontiers In Pharmacology, 2023. 14: p. 1125642.
124. Farah, E.N., et al., *Spatially organized cellular communities form the developing human heart.* Nature, 2024. 627(8005): p. 854-864.
125. Towbin, J.A., A. Lorts, and J.L. Jefferies, *Left ventricular non-compaction cardiomyopathy.* Lancet (London, England), 2015. 386(9995): p. 813-825.
126. Valiente-Alandi, I., A.E. Schafer, and B.C. Blaxall, *Extracellular matrix-mediated cellular communication in the heart.* J Mol Cell Cardiol, 2016. 91: p. 228-37.
127. He, X., et al., *Signaling cascades in the failing heart and emerging therapeutic strategies.* Signal Transduction and Targeted Therapy, 2022. 7(1): p. 134.
128. Ramos-Mondragón, R., C.A. Galindo, and G. Avila, *Role of TGF-beta on cardiac structural and electrical remodeling.* Vascular Health and Risk Management, 2008. 4(6): p. 1289-1300.

Acknowledgements

First and foremost, I would like to express my deepest gratitude to my supervisor, Prof. Dr. Andreas Dendorfer, for his patience, invaluable guidance, and continuous support throughout my research journey. His rigorous academic approach and profound research insights have consistently served as an inspiration and model for my own work. In times of difficulty, his professional advice and encouragement enabled me to overcome challenges and continue progressing.

I am also deeply thankful to PD Dr. Petra Kameritsch, PD Dr. Thomas Seidel, Prof. Dr. Hendrik Milting, and Dr. Magnus Althage for their valuable support and collaboration throughout the research process. I extend my heartfelt thanks to my Thesis Advisory Committee (TAC) members, Prof. Dr. Christian Schulz and Prof. Dr. Daphne Merkus, for their insightful feedback and constructive criticism during TAC meetings, which significantly contributed to the refinement of my thesis and personal development. Additionally, I am grateful for the research funding provided by AstraZeneca Inc. (Gothenburg, Sweden) and the China Scholarship Council (CSC, No.202009210012).

I would like to extend my sincere appreciation to my colleagues, whose support was instrumental in experimental design and data analysis. My special thanks go to Dr. Eric Lars-Helge Lindberg, Dr. Daniel Reichart, and Heike Kartmann for their assistance with single-nucleus RNA sequencing, PD Dr. Steffen Dietzel, Dr. Andreas Thomae, and Mariano Gonzalez Pisfil for their help with confocal and two-photon imaging, and Dr. Kun Lu for assistance with clinical data collection. I also appreciate Matthias Semisch, Mei-Ping Wu, and Claudia Fahney for their support with heart slice culture. The time we shared will always remain a treasured memory for me.

I am immensely grateful to my family, including my parents, my wife, and my daughter, for their unwavering love and support. Their constant encouragement has been a driving force behind my motivation during the more challenging phases of my studies. Without their enduring support, this journey would not have been possible.

Last but not least, I would like to express my sincere gratitude to all my friends who have played a direct or indirect role in supporting me throughout my doctoral

studies. Your encouragement and support have been essential to my progress and success in this academic journey.

Affidavit

Affidavit

Sun, Zhengwu

Surname, first name

Marchioninistr. 68

Street

81377, Munich, Germany

Zip code, town, country

I hereby declare, that the submitted thesis entitled:

Integration and interaction of cardiac progenitor cells with human failing myocardium: An ex-vivo study modeling regenerative therapy in long-term tissue culture

is my own work. I have only used the sources indicated and have not made unauthorised use of services of a third party. Where the work of others has been quoted or reproduced, the source is always given.

I further declare that the dissertation presented here has not been submitted in the same or similar form to any other institution for the purpose of obtaining an academic degree.

Munich, 25.03.2025 Zhengwu Sun

place, date Signature doctoral candidate

Confirmation of congruency

LMU LUDWIG-MAXIMILIANS-UNIVERSITÄT MÜNCHEN

Promotionsbüro
Medizinische Fakultät

MMRS

Confirmation of congruency between printed and electronic version of the doctoral thesis

Sun, Zhengwu
Surname, first name

Marchioninistr. 68
Street

81377, Munich, Germany
Zip code, town, country

I hereby declare, that the submitted thesis entitled:

Integration and interaction of cardiac progenitor cells with human failing myocardium: An ex-vivo study modeling regenerative therapy in long-term tissue culture

is congruent with the printed version both in content and format.

Munich, 25.03.2025
place, date

Zhengwu Sun
Signature doctoral candidate

List of publications

Original articles

1. **Sun Z**, Lu K, Kamla C, Kameritsch P, Seidel T, Dendorfer A. Synchronous force and Ca^{2+} measurements for repeated characterization of excitation-contraction coupling in human myocardium. **Commun Biol**. 2024;7(1):220.

2. Shumliakivska M, Luxán G, Hemmerling I, Scheller M, Li X, Müller-Tidow C, Schuhmacher B, **Sun Z**, Dendorfer A, Debes A, Glaser SF, Muhly-Reinholz M, Kirschbaum K, Hoffmann J, Nagel E, Puntmann VO, Cremer S, Leuschner F, Abplanalp WT, John D, Zeiher AM, Dimmeler S. DNMT3A clonal hematopoiesis-driver mutations induce cardiac fibrosis by paracrine activation of fibroblasts. **Nat Commun**. 2024;15(1):606.

3. Shi R, Reichardt M, Fiegle DJ, Küpfer LK, Czajka T, **Sun Z**, Salditt T, Dendorfer A, Seidel T, Bruegmann T. Contractility measurements for cardiotoxicity screening with ventricular myocardial slices of pigs. **Cardiovasc Res**. 2023;119(14):2469-2481.

Conference contributions

1. **Sun Z**, Lu K, Kamla C, Kameritsch P, Seidel T, Dendorfer A. Synchronous force and calcium transient analyses in human failing myocardium reveal alterations of excitation-contraction coupling. 90th DGK (German Society for Cardiology) Annual Meeting 2024, 03-06.04.2024, Mannheim, Germany.

2. **Sun Z**, Kameritsch P, Milting H, Althage M, Graneli C, Jennbacken K, Wang QD, Dendorfer A. Tissue integration of stem cell-derived cardiac progenitor cells: in vitro studies in long-term cultivated slices of human failing myocardium. 103th DPG (German Physiological Society) Annual Meeting 2024, 19-21.09.2024, Vienna, Austria.

3. **Sun Z**, Dendorfer A, Kameritsch P. Charge-balancing optimizes electrochemical compatibility of biphasic tissue stimulation. 103th DPG (German Physiological Society) Annual Meeting 2024, 19-21.09.2024, Vienna, Austria.